

Aus dem Institute of Experimental Pneumology der
Ludwig-Maximilians-Universität München
Direktor: Prof. Dr. Oliver Eickelberg

Thema der Dissertation:

**Role of CARM1 in regulation of alveolar epithelial
senescence and emphysema susceptibility**

zum Erwerb des Doktorgrades der Humanbiologie an der Medizinischen
Fakultät der Ludwig-Maximilians-Universität zu München

vorgelegt von

Rim Sabrina Jahan Sarker

aus Dhaka, Bangladesh

2014

**Mit Genehmigung der Medizinischen Fakultät der Ludwig-
Maximilians- Universität München**

Berichterstatter: Prof. Dr. Oliver Eickelberg

Mitberichterstatter: Prof. Dr. rer. nat. Alexander Dietrich
Prof. Dr. Andreas Straube

Mitbetreuung durch den
promovierten Mitarbeiter: Dr. Ali Önder Yildirim

Dekan: Prof. Dr. med. Dr. h.c. M. Reiser, FACR,
FRCR

Tag der mündlichen Prüfung: 26.08.2015

TABLE of CONTENTS

	Page
Table of Contents	3
Summary	7
Zusammenfassung	10
Chapter	
1: Introduction	13
1.1 Chronic obstructive pulmonary disease	13
1.2 Pulmonary emphysema: Pathological definition	15
1.2.1 Historical background	16
1.2.2 Risk factors of emphysema	16
1.2.3 Diagnosis of emphysema	17
1.2.4 Current treatment for emphysema	18
1.2.5 Pathogenesis of emphysema	19
1.2.5.1 Proteases/Anti-proteases imbalance	20
1.2.5.2 Apoptosis/proliferation imbalance	22
1.2.5.3 Oxidative stress	23
1.2.5. Inflammation	24
1.2.5.4 Cellular senescence	25
1.2.6 Animal Models of Emphysema	28
1.2.6.1 Elastase-induced emphysema model	28
1.2.6.2 Cigarette smoke-induced emphysema model	29
1.3 Post-translational modification of arginine	30
1.3.1 Protein Arginine Methylation	31
1.3.2 Characteristics and classification of protein arginine methyltransferases (PRMTs)	31
1.3.3 PRMT family members	33
1.3.4 Coactivator Associated Arginine Methyltransferase 1, CARM1	36
1.3.4.1 Structure of CARM1	36
1.3.5 Molecular function of CARM1	38

1.3.5.1 Methyltransferase activity	38
1.3.5.2 Transcriptional coactivator	38
1.3.6 Substrates of CARM1	39
1.3.6.1 Chromatin remodeling proteins	39
1.3.6.2 RNA binding protein and splicing factors	39
1.3.7 Regulation of CARM1	41
1.3.7.1 Phosphorylation	41
1.3.7.2 Auto-methylation	42
1.3.8 Cellular function of CARM1	42
1.3.8.1 Role in Proliferation and Differentiation	42
1.3.8.2 Role in senescence	44
1.3.9 Protein Arginine methylation in COPD	44
1.4 Aim of the study	46
2. Materials and Methods	47
2.1 Materials	47
2.2.1 Antibodies	47
2.2.2 Biochemicals and chemicals	48
2.2.3 Buffers and Solutions	50
2.2.4 Instruments and softwares	51
2.2.5 Kits	52
2.2.6 Enzymes	53
2.2.7 Cell Lines	53
2.2.8 Cell culture media	53
2.2.9 Serum	53
2.2.10 siRNA and transfection reagents	54
2.2.11 Oligodeoxynucleotides/primers	54
2.2 Methods	55
2.2.1 Animal	55
2.2.2 Lung function measurement	56
2.2.3 Bronchoalveolar lavage (BAL) collection and quatification	57
2.2.4 Lung fixation	57
2.2.5 Lung tissue processing: Paraffin embedding	58
2.2.6 Lung tissue sectioning	59
2.2.7 Histological staining: Hematoxylin and eosin (H&E) staining	60

2.2.8 Immunohistochemistry	61
2.2.9 immunofluorescence staining	61
2.2.10 Quantitative stereological analysis	62
2.2.10.1 Quantification of airspace enlargement	62
2.2.10.2 Quantification of CARM1 or SIRT1 positive alveolar epithelial cells	63
2.2.10.3 Quantification p16 positive alveolar epithelial cells	64
2.2.10.4 Quantification of SP-C positive alveolar epithelial cells	64
2.2.11 Quantitative real time RT-PCR ⁶⁴	64
2.2.11.1 Homogenization and lysis ⁶⁴	
2.2.11.2 RNA isolation and concentration determination	65
2.2.11.3 cDNA synthesis	66
2.2.11.4 Amplification of cDNA	67
2.2.12 Western blot	69
2.2.12.1 Protein isolation and concentration determination	69
2.2.12.2 SDS-PAGE run and blotting	70
2.2.12.3 Signal development and quantification	70
2.2.13 Cell culture	71
2.2.13.1 Condition and maintenance	71
2.2.13.2 siRNA transfection	71
2.2.13.3 Wound healing assay	72
2.2.13.4 Senescence-associated β -galactosidase Staining	72
2.2.13.5 Preparation of cigarette smoke extract	72
2.2.14 Alveolar Epithelial Type II Cell isolation and culture	73
2.2.15 Statistical analysis	73
3. Results	74
3.1 Progressive Lung Emphysema Development in Mice Exposed to Porcine Pancreatic Elastase	74
3.1.1 Analysis of lung function	74
3.1.2 Increased airspace enlargement	75
3.1.3 Analysis of bronchoalveolar lavage (BAL) cells	76
3.2 Reduced CARM1 Expression and Activity in Emphysematous Mouse Lungs	78
3.2.1 CARM1 downregulation in lung homogenate	78

3.2.2 Reduction of CARM1 positive alveolar epithelial cells	78
3.2.3 Elevation of CARM1 phosphorylation	80
3.3 CARM1 Haploinsufficiency Leading to Enhanced Elastase-induced Emphysema in Mouse Lungs	81
3.3.1 CARM1 haploinsufficient mice showed significantly reduced level of CARM1	81
3.3.2 Elastase treatment enhanced airspace enlargement and lung function impairment in CARM1 haploinsufficient mice	82
3.4 CARM1 Reduction Inducing Senescence in Alveolar Epithelial Cells	84
3.4.1 Loss of anti-senescence SIRT1 in alveolar epithelial cells	84
3.4.2 Induction of senescence markers in alveolar epithelial cells	86
3.5 CARM1 Knockdown in ATII-like LA-4 Cells Triggering Senescence <i>In Vitro</i>	88
3.5.1 CARM1 knockdown in LA-4 cells downregulating SIRT1 expression	88
3.5.2 Reduced CARM1 inducing senescence markers in LA-4 cells	89
3.5.3 CSE stimulation augmenting senescence in CARM1 deficient LA-4 cells	91
3.6 Reduced CARM1 Hindering Regeneration and Trans-differentiation of ATII Cells	92
3.6.1 Reduced CARM1 impairing wound healing	92
3.6.2 CARM1 reduction inducing aberrant ATII trans-differentiation	93
4. Discussion	96
5. Reference	105
6. Abbreviation	123
7. Appendix	126
7.1 Acknowledgment	126
7.2 Curriculum Vitae	127
7.3 Eidesstattliche Versicherung	131
7.4 List of Publications	132
7.5 Re-print permission	133

Summary

Chronic obstructive pulmonary disease (COPD) is characterized by an irreversible loss of lung function and is one of the most prevalent and severe diseases world-wide. A major feature of COPD is emphysema- a long-term, progressive condition. The hallmark of emphysema includes the destruction of alveolar structures leading to enlarged air spaces and reduced surface area. Experimental evidence suggests that emphysema development is driven by accelerated senescence of lung cells but the underlying mechanism of senescence is yet to be fully elucidated.

Protein arginine methyltransferases (PRMTs) are important for cellular processes, such as the regulation of senescence, cell proliferation, differentiation and apoptosis. The PRMT family includes 11 members classified as type I, II or III enzymes depending on their methylation pattern (asymmetric dimethylation, symmetric dimethylation or monomethylation, respectively). One member of this family is PRMT4, a type I enzyme, which is also called coactivator associated arginine methyltransferase 1 (CARM1). It was originally identified as a coactivator for steroid hormone receptors. CARM1 is known to methylate histone H3 and various non-histone proteins that play essential roles in transcriptional regulation, RNA splicing, and metabolism. Most importantly, complete loss of CARM1 leads to disrupted differentiation and maturation of alveolar epithelial type-II cells (A₂II). Furthermore, CARM1 also plays a role in regulating cellular senescence via CARM1-dependent methylation.

Based on these reports, we hypothesized that CARM1 regulates the development and progression of emphysema. To address this, we investigated the contribution of CARM1 to

alveolar rarefaction using the mouse model of elastase-induced emphysema *in vivo* and siRNA-mediated knockdown in ATII-like LA4 cells *in vitro*.

In vivo experiments:

We monitored emphysema progression for 161 days in mice treated with a single oropharyngeal application of elastase. The progression was manifested by the decline in lung function parameters. The mean chord length (Lm) confirmed a time dependent airspace enlargement and was directly correlated with a significant increase in dynamic lung compliance. We also observed that at later time points (day 56 and 161), emphysema progression was inflammation-independent. We demonstrated that emphysema advancement was associated with a time-dependent downregulation of CARM1, specifically in alveolar epithelial cells. Furthermore, the global CARM1 activity was also reduced as reflected by an elevated level of CARM1 phosphorylation in the lung. Most importantly, elastase-treated CARM1 haploinsufficient mice showed significantly increased airspace enlargement ($52.5 \pm 9.6 \mu\text{m}$ vs. $38.8 \pm 5.5 \mu\text{m}$, $p < 0.01$) and lung compliance ($2.8 \pm 0.32 \mu\text{l/cmH}_2\text{O}$ vs. $2.4 \pm 0.4 \mu\text{l/cmH}_2\text{O}$, $p < 0.04$) compared with wild type controls. Reduced CARM1 contributed to senescence of alveolar epithelial cells evident by the reduction of anti-senescence SIRT1 and the induction of senescence markers p16 and β -galactosidase in alveolar epithelial cells. We further demonstrated that CARM1 haploinsufficiency impaired trans-differentiation of ATII into ATI cells. Elastase treatment in CARM1 deficient mouse lungs led to the accumulation of SP-C positive ATII cell.

In vitro experiment:

In our *in vitro* studies, we detected that the knockdown of CARM1 in the ATII-like cell line LA-4 led to decreased SIRT1 expression (0.034 ± 0.003 vs. 0.022 ± 0.001 , $p < 0.05$), but increased expression of p16 (0.27 ± 0.013 vs. 0.31 ± 0.010 , $p < 0.5$), p21 (0.81 ± 0.088 vs. 1.28 ± 0.063 , $p < 0.01$) and induced a higher number of β -galactosidase-positive senescent cells

(50.57%±7.36 vs. 2.21%±0.34, $p<0.001$), compared with scrambled siRNA. The senescence in CARM1 deficient cells was further augmented after CSE stimulation. Furthermore, we demonstrated that CARM1 deficiency impaired wound healing (32.18%±0.9512 vs. 8.769%±1.967 wound gap closure, $p<0.001$) of alveolar epithelial cells. The data confirmed that CARM1 reduction induced an accelerated senescence in LA-4 cells by attenuating the effect of SIRT1.

Overall, both our *in vivo* and *in vitro* results revealed a novel function of CARM1 in regulating emphysema development and premature lung aging via alveolar senescence, as well as impaired regeneration, repair and differentiation of ATII cells.

Zusammenfassung

Die chronisch obstruktive Lungenerkrankung (COPD) zählt zu den häufigsten schweren Krankheiten weltweit und ist gekennzeichnet durch eine irreversible Abnahme der Lungenfunktion. Ein Hauptcharakteristikum von COPD ist das Emphysem, das sich stetig über einen langen Zeitraum fortschreitend entwickelt, und durch die Zerstörung alveolärer Strukturen, einhergehend mit vergrößerten Lufträumen und verringerter Alveolaroberfläche, gekennzeichnet ist. Ergebnisse aus Studien legen nahe, dass die Entwicklung des Emphysems durch die erhöhte Seneszenz von Zellen der Lunge beschleunigt wird, doch die genauen zugrundeliegenden Mechanismen sind noch nicht aufgeklärt.

Protein-Arginin-Methyltransferasen (PRMTs) spielen eine bedeutende Rolle bei zellulären Prozessen wie Regulation von Seneszenz, Zellproliferation, Differenzierung und Apoptose. Die Familie der PRMTs umfasst 11 Enzyme, die als Typ I, II, oder III klassifiziert werden, abhängig von ihrem Methylierungsmuster (asymmetrische Dimethylierung, symmetrische Dimethylierung oder Monomethylierung). Ein Mitglied der Familie ist PRMT4, ein Typ I Enzym, das auch unter dem Namen Coactivator-assoziierte Arginin-Methyltransferase 1 (CARM1) bekannt ist. Ursprünglich wurde CARM1 als Coactivator für Steroid-Hormon-Rezeptoren beschrieben. CARM1 methyliert Histon 3 und verschiedene weitere Nicht-Histon Proteine, die eine wichtige Rolle für die Transkriptionsregulation, das RNA-Splicing und den Stoffwechsel spielen. Darüberhinaus führt der komplette Verlust von CARM1 zu gestörter Differenzierung und Maturation von Typ II Alveolarepithelzellen (ATII). Weiterhin ist CARM1 von Bedeutung für die Regulation von zellulärer Seneszenz mittels CARM1-abhängiger Methylierung.

Auf Grundlage dieser Arbeiten wurde die Hypothese aufgestellt, dass CARM1 die Entwicklung und das Voranschreiten des Emphysems reguliert. Um dies aufzuklären, wurde die Rolle von CARM1 am Verlust der Alveolen in einem Elastase-induzierten Emphysem-Mausmodell *in vivo* sowie *in vitro* mittels siRNA knockdown in ATII-ähnlichen LA4-Zellen untersucht.

In vivo Experimente:

Die Entwicklung und das Voranschreiten des Emphysems wurden über einen Zeitraum von 161 Tagen beobachtet. Dabei zeigte sich eine progressive Abnahme verschiedener Lungenfunktionsparameter. Die mittlere Alveolarweite bestätigte die zeitabhängige Vergrößerung des Luftraumes und war direkt mit einer signifikanten Zunahme der dynamischen Lungencompliance korreliert. Außerdem wurde an späteren Zeitpunkten (Tag 56 und 161) eine entzündungsabhängige Progression des Emphysems beobachtet. Das Voranschreiten des Emphysems war mit einer zeitabhängigen Herunterregulierung von CARM1 insbesondere in Alveolarepithelzellen assoziiert. Die Gesamtaktivität von CARM1 war ebenso reduziert, erkennbar anhand von erhöhter CARM1-Phosphorylierung in der Lunge. Weiterhin zeigten mit Elastase behandelte CARM1 haploinsuffiziente Mäuse eine signifikant erhöhte Vergrößerung des Luftraumes ($52.5 \pm 9.6 \mu\text{m}$ vs. $38.8 \pm 5.5 \mu\text{m}$, $p < 0.01$) sowie der Lungencompliance ($2.8 \pm 0.32 \mu\text{l/cmH}_2\text{O}$ vs. $2.4 \pm 0.4 \mu\text{l/cmH}_2\text{O}$, $p < 0.04$) verglichen mit Wildtyp-Kontrollmäusen. Das verringerte Level an CARM1 trug zur Seneszenz von Alveolarepithelzellen bei, bestätigt durch eine Reduktion des Anti-Seneszenz-Markers SIRT1 und durch die Induktion der Seneszenz-Marker p16 und β -Galactosidase in Alveolarepithelzellen. Des Weiteren wurde gezeigt, dass CARM1 Haploinsuffizienz die Transdifferenzierung von ATII zu ATI Zellen verhindert. Dabei führte die Elastase-Behandlung von CARM1-defizienten Mäusen zu einer Akkumulation von SP-C-positiven ATII-Zellen in der Lunge.

In vitro Experimente:

Die in vitro Experimente haben gezeigt, dass der knockdown von CARM1 in ATII-ähnlichen LA4-Zellen zu einer verringerten SIRT1-Expression (0.034 ± 0.003 vs. 0.022 ± 0.001 , $p < 0.05$), und gleichzeitig zu einer erhöhten Expression von p16 (0.27 ± 0.013 vs. 0.31 ± 0.010 , $p < 0.5$), p21 (0.81 ± 0.088 vs. 1.28 ± 0.063 , $p < 0.01$) führte. Weiterhin verursachte der CARM1 knockdown eine erhöhte Anzahl an β -Galactosidase-positiven seneszenten Zellen verglichen mit Kontroll-siRNA-behandelten Zellen ($50.57\% \pm 7.36$ vs. $2.21\% \pm 0.34$, $p < 0.001$). Die erhöhte Seneszenz in CARM1-defizienten Zellen wurde durch Stimulation mit Zigarettenrauchextrakt noch verstärkt. Weiterhin zeigte sich in den Alveolarepithelzellen eine verminderte Wundheilung aufgrund CARM1-Defizienz ($32.18\% \pm 0.9512$ vs. $8.769\% \pm 1.967$ Wundschließung, $p < 0.001$). Diese Daten bestätigten, dass die Reduzierung von CARM1 eine beschleunigte Seneszenz in LA4-Zellen mittels Abschwächung von SIRT1-Effekten verursachte.

Zusammenfassend zeigen die in vivo und vitro Ergebnisse eine neue Rolle von CARM1 bei der Regulierung der Emphysem-Entstehung und der vorzeitigen Lungenalterung, in erster Linie mittels Seneszenz von Alveolarepithelzellen, sowie beeinträchtigter Regenerierung, Reparatur und Differenzierung von ATII-Zellen.

1. INTRODUCTION

1.1 Chronic obstructive pulmonary disease

Chronic obstructive pulmonary disease (COPD) is a life-threatening lung disease worldwide. According to the World Health Organization (WHO), COPD will stand as the third leading cause of death worldwide by the year 2030 (1). The mortality rate of COPD will continue to rise in near future because of a rapidly increasing aging population worldwide. More than 5% of the population over the age of 40 is now affected with COPD (2). It is a major global health problem which is associated with high health-care cost. A stage III COPD patient has an approximate health care cost of \$10,812 per year (3). The staggering socioeconomic burden that comes with COPD treatment and management is currently surpassing any other disease and thus triggers interest in scientific community to better understand the disease (4).

COPD refers to an obstructive disease of lungs manifesting a slow, gradual progression over decades that ultimately leads to mortality from respiratory failure (5). The Global Initiative for Chronic Obstructive Lung Disease (GOLD), collaboration between the National Institutes of Health and the World Health Organization states a standard definition of COPD. According to GOLD COPD is a disease characterized by airflow limitation that is usually progressive and associated with an enhanced chronic inflammatory response in the airways and the lung to noxious particles or gases. Exacerbations and comorbidities contribute to severity of the disease (6). The airflow limitation is the outcome of an increased small conducting airway resistance and an increased lung compliance due to emphysematous destruction (7). The common symptoms that arise in a COPD patient are usually chronic and progressive shortness of breath (dyspnea), chronic cough and sputum production (8). Pathologically, all these symptoms are the outcome of an airflow limitation. COPD is not just a single disease,

rather a group of conditions that includes chronic bronchitis, small airway remodeling and emphysema. All these three conditions can exist in patients separately or in combination.

Chronic bronchitis

The major features of chronic bronchitis are excessive mucus production and chronic infiltration of inflammatory cell at the bronchial wall (9). The pathological changes that cause increased mucus production include goblet cell hyperplasia and submucosal gland hypertrophy associated with loss of ciliated cells. As an outcome, there is reduced mucociliary clearance and increase mucus plug formation (10). If the occurrence of the mucus secretion persists three months a year, for at least two consecutive years without any other pulmonary cause, then it has to be considered as chronic bronchitis (11). As a physiological symptom, the COPD patient suffers from a chronic cough.

Small airway remodeling

The peripheral airways of 2 millimeters or less in diameter is the major site of remodeling (12). In smokers, these airways become even smaller with a diameter less than 0.4 millimeters (13). Airway remodeling is an outcome of the inflammatory response associated with COPD (14). In addition to inflammation, other factors that contribute to airway remodeling are metaplasia of goblet cells and peribronchial fibrosis leading to a thickening of airway walls which narrows the lumen and as a consequence, there is a marked increase in resistance to airflow in the small airways (15, 16).

Emphysema

The hallmark of emphysema is the destruction of alveolar structures leading to enlarged air spaces and reduced surface area (Figure 1) (17). As the focus of this dissertation is emphysema, a detailed overview is discussed in next section.

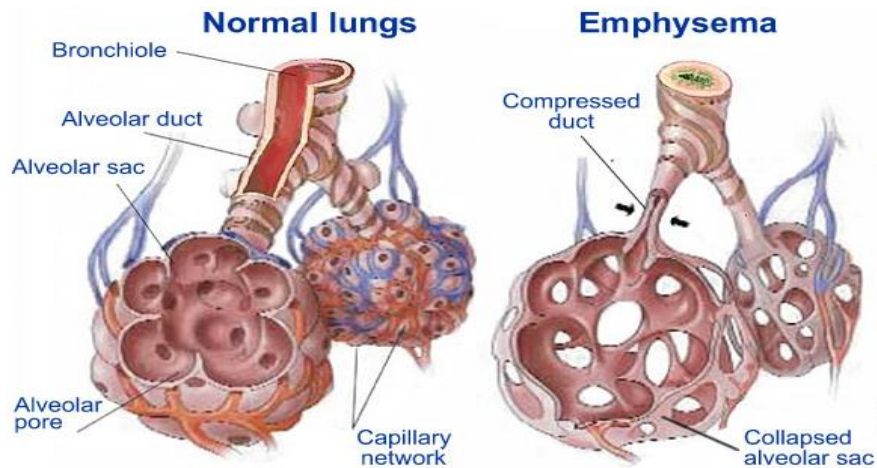


Figure 1. Pulmonary emphysema. Emphysema is a progressive lung disease affecting alveolar sacs, alveoli and disrupts gas exchange capacity leading to less oxygen entrance into the bloodstream. Loss of alveolar elastic recoiling cause them to collapse and trap air every time the patient expels air. Adapted and modified from www.oxygenconcentratordepot.com.

1.2 Pulmonary emphysema: Pathological definition

In lung, respiratory unit is the site where emphysema occurs. It is slowly progressive disease described as a loss of lung elasticity and abnormal enlargement of the air spaces distal to the terminal bronchioles, with destruction of the alveolar walls and capillary beds without obvious fibrosis (18, 19). Previously, pulmonary emphysema used to be considered due to the atrophy of lung tissue resulting from over-inflation (20). Later it was demonstrated that indeed, destruction of the lung parenchyma results in loss of gas exchange area in lung and decrease of elastic recoiling that leads to lung hyperinflation (21). The destruction of the elastic fibers that provide the natural recoil of the lung is actually the early event of emphysema that causes deformation of the alveoli and respiratory bronchioles (22, 23). This leads to a decreased number of functional alveoli and results in shortness of breath (Dyspnea). It is often a strong indicator of emphysema and the most common symptom emphysema patients suffer from (24). Emphysema exists in two subtypes. One is centri-acinar emphysema confined to the apical regions of the lung and characterized by destruction of the central zone of the acinus leading to enlarged respiratory bronchioles. Another subtype is pan-acinar emphysema involved in an uniform destruction of the whole lung acinus and mostly affects the lower lobes of the lung rather than the upper lobes (25).

1.2.1 Historical background

Record of human emphysema was stated back in 1679, when Bonet described of voluminous lungs (26). Later in 1721, the Dutch anatomist, Frederick Ruysch observed expanded air spaces in lung specimens of humans (27). In 1769, Morgagni recorded 19 patient cases where the lungs were turgid or inflated with air (28). However, it was between 1799 and 1807, when Matthew Baillie first pointed out the destructive nature of emphysema and illustrated emphysema as enlarged air spaces (29, 30). In 19th century, a French physician Laënnec noted that there significant variations in the size of air vesicles in lungs ranging from the size smaller than a millet seed to as big as a cherry stone. He hypothesized that the bigger, cherry stone size air vesicles were produced by the collapse of adjacent air spaces following rupture of alveolar walls (31). In 1892, Osler characterized emphysema as enlargement of the lungs due to expansion of the air “cells”, atrophy of their walls and imperfect aeration of the blood resulting in dyspnea (32). In 1956, McLean marked emphysema as a chronic destructive lung disease noting that there is an enlargement of existing airspaces in the lung parenchyma (33). In 1960s, both the World Health Organization (WHO) and the American Thoracic Society (ATS) defined emphysema as destruction of respiratory tissue manifested by a permanent enlargement of airspaces distal to the terminal non-respiratory bronchiole (34, 35).

1.2.2 Risk factors of emphysema

Emphysema is primarily caused by cigarette smoke, air pollution, environmental factors, aging as well as epigenetic modification.

Smoking: Cigarette smoke is considered as the most widely accepted causative factor for emphysema (6). Smoking causes approximately 80 to 90 percent of COPD deaths (36). Compared to the non-smokers, the smokers experience a substantially significant annual decline in FEV1 and rate of mortality (37). Women are even more susceptible to smoking as

studies showed that smoking during pregnancy can potentially affect lung growth of the fetus by dysregulating the immune system (38). Besides active smoking, the passives exposure, also known as second-hand smoking or environmental tobacco smoke can increase the burden of inhaled noxious particles and gasses and thus can also contribute in emphysema development in 20% of cases of non-smokers (39-41). Other forms of smoking such as pipe, cigar, and marijuana also pose as risk factor for emphysema (42-45).

Others: Occupational exposure to dust and chemical fumes are a major risk of COPD for both smokers and nonsmokers (46). In the developing countries, exposure to biomass fuel for cooking also believed to be a strong etiologic agent of emphysema (47). In addition, genetics is likely to play a role. An inherited deficiency of Alpha-1 antitrypsin, a protein that protects the elastic tissue in the lungs contributes in the development and progression of the emphysema (6, 48).

1.2.3 Diagnosis of emphysema

In 1846 the spirometer invented by John Hutchinson was the key diagnostic tool for COPD (49). The spirometry is the measurement of air moving in and out of lungs during different respiratory maneuvers and thus allows to determine how much air can be inhaled or exhaled and how fast (50). The pulmonary function testing (PFTs) using spirometer is still used today for diagnosis and regular assessment of COPD. However, Hutchinson's instrument only measured vital capacity. The measurable parameters expanded when Tiffeneau and Pinelli added the concept of timed vital capacity as a measure of airflow (51). The airflow obstruction is defined by spirometric criteria, as a ratio of FEV1/FVC less than 0.7 in the absence of other respiratory symptoms where FEV1 is the Forced Expiratory Volume in 1 second and FVC is the Forced Vital Capacity (52). The classification of severity of COPD, as issued by GOLD, is based upon the FEV1/FVC (6) (Table 1).

Other pulmonary function test tool includes body plethysmography that measures residual volume (RV) to assess changes in lung hyperinflation. Body plethysmography is a routine measurement in clinical pulmonary practice based on Boyle’s law, with reproducible measurements of absolute lung volumes (53). Other commonly used tests include X-rays or computed tomography (CT) scans of the chest to diagnose specific morphologic changes in the lung parenchyma (54). Another diagnostic tool oximetry or the diffusing capacity for carbon monoxide (DLCO) is a measure of the ability of gas to transfer from the alveoli across the alveolar epithelium and the capillary endothelium to the RBCs (55).

Stage of COPD	COPD Severity	FEV₁ %
Stage I	Mild	≥80
Stage II	Moderate	50–79
Stage III	Severe	30–49
Stage IV	Very severe	<30 or chronic respiratory failure

Table 1: GOLD classification in patient with FEV1/FVC <0.70. Adapted from reference (6).

1.2.4 Current treatment for emphysema

Current available treatments only aim to relieve symptoms and prevent further emphysema progression. Besides treatments, quitting smoking is also essential for patients with emphysema, since continuing to use tobacco will only further damage the lungs. Inhaled as aerosol sprays or taken orally, bronchodilator medications may help to relieve symptoms of emphysema by relaxing and opening the air passages in the lungs. Current bronchodilators include β-Agonists, anticholinergics (short-acting ipratropium bromide and long-acting tiotropium) and phosphodiesterase inhibitor (theophylline, roflumilast) (56). Corticosteroid drugs inhaled as aerosol sprays relieves shortness of breath (57). However, prolonged use may weaken bones and increase risk of high blood pressure, cataracts and diabetes (58).

Antibiotics such as erythromycin may be used to help fight respiratory infections common in people with emphysema, such as acute bronchitis, pneumonia and the flu (59). Supplemental oxygen is recommended in those with mildly low oxygen levels (a partial pressure of oxygen of less than 50–55 mmHg or oxygen saturations of less than 88%), as it may improve shortness of breath (6). Lung transplantation is an option for some patients while for others, lung volume reduction surgery to remove small part of damaged lung tissue is a beneficial treatment (60). Patients with emphysema caused by an alpha-1 antitrypsin (AAT) deficiency may be given infusions of AAT to help slow the progression of lung damage (61).

As a future therapeutic approach, the WNT/ β -catenin activation is shown to be promising. Lithium chloride-mediated WNT/ β -catenin activation attenuated experimental emphysema in mice by decreasing airspace enlargement, improving lung function, reducing collagen content and elevating expression of alveolar epithelial cell markers (62).

1.2.5 Pathogenesis of emphysema

Understanding the pathogenesis of emphysema is quite complex and remains relatively poorly understood. Nevertheless, it is known that there are several key mechanisms have been implicated in the development of emphysema. One of them is the imbalance between protease and antiprotease activity in the lung and considered as the major mechanism causing emphysema. Increased alveolar cell death leading to failure in alveolar wall maintenance is also responsible for emphysema development. Besides, chronic inflammation, oxidative stress and accelerated senescence also contribute to increased alveolar destruction as well as impaired lung maintenance and repair (Figure 2) (63).

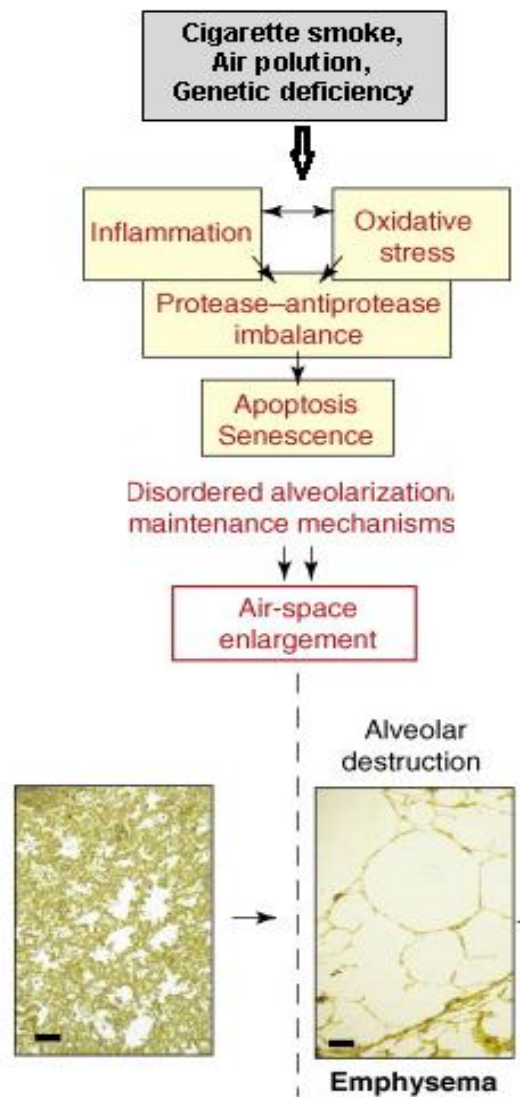


Figure 2. Pathogenesis of emphysema development. The pathophysiology of emphysema include cigarette smoke, air pollution or genetic deficiency of AAT derived oxidative stress, sustained inflammation, protease-anti-protease imbalance, enhanced apoptosis and premature senescence resulting in lung alveolar architecture destruction. Adapted from reference (64).

1.2.5.1 Proteases/anti-proteases imbalance

Proteases are enzymes responsible for breakdown of connective tissue parenchyma in lung and anti-proteases are to inactivate the function of proteases by covalently binding to them. An imbalance between proteases is a widely accepted mechanism behind the development of emphysema (65, 66). The concept of proteases/anti-proteases imbalance originates back in 1960s when subjects deficient in alpha1-antitrypsin (AAT), a major circulating inhibitor of

neutrophil elastase, were shown to be predisposed to an early onset of severe emphysema (67). A study on Pallid mice which are naturally deficient in AAT revealed that they suffered from an early development of emphysema compared to wild type mice with normal level of AAT (68, 69). Indeed, the imbalance may occur either by an unregulated excessive release of proteases or by a deficiency, reduced synthesis or increased breakdown of anti-proteases. The excessive proteolytic load is contributed by infiltrating phagocytic leukocytes, namely neutrophils and macrophages. These cells secrete a wide range of proteases, including serine proteases (neutrophil elastase, proteinase 3, cathepsin G), cysteine proteases (Cathepsins B, H, L, K and S) and a different types of matrix metalloproteases (MMPs) into emphysematous lungs (70-72). Among these, neutrophil elastase is a highly potent elastolytic enzyme and its intra-tracheal injection in experimental animals is capable of inducing emphysema (73). Another study demonstrated that mice lacking neutrophil elastase were 59% protected against emphysema (74). Secretory leukocyte protease inhibitor (SLPI) and elafin secreted by goblet cells, serous cells, Clara cells and alveolar type II (ATII) cells are both potent anti-proteases that can reversibly inhibit neutrophil elastase and in addition, SLPI can inhibit cathepsin G, trypsin, chymotrypsin and chymase while elafin inhibits proteinase-3 (72).

MMPs are released by inflammatory cells as well as lung structural cells. MMPs belong to a large family of zinc-dependent proteases that are able to degrade all components of the extracellular matrix (ECM). According to substrate specificity, MMP-1, MMP-8 and MMP-13 are collagenolytic, MMP-2 and MMP-9 are gelatinolytic, MMP-3, MMP-10 and MMP-11 are stromelysins, while MMP-7 and MMP-12 are elastinolytic (75). The concentration and activity of MMP-1, MMP-2, MMP-8, MMP-9 and MMP-12 are found upregulated in sputum of COPD patients (76-81). The MMPs are inhibited by the tissue inhibitors of metalloproteinases (TIMP). Interestingly, MMP-12 is able to inactivate AAT while neutrophil elastase destroys TIMP-1, thus potentiating the action of each protease (74). Interestingly, MMP-12 is able to

inactivate AAT and thus keep neutrophil elastase active and the neutrophil elastase in turn destroys TIMP-1 to further potentiate the action of each protease (74). TIMP-1 is released at a significantly low level from alveolar macrophages of COPD patients compared to healthy smokers and non-smokers (82). The protective effect of TIMPs is further demonstrated by TIMP-3 knockout mice showing progressive airspace enlargement and collagen degradation (83).

1.2.5.2 Apoptosis/proliferation imbalance

There is increasing evidence suggesting that a disturbance of the balance between apoptosis and proliferation in lung tissue contributes to emphysema development. Imai and colleagues reported increased apoptosis of alveolar epithelial cells, endothelial cells and mesenchymal cells in emphysematous lung tissue associated with an increase in the activated subunits of caspase-3 and pro-apoptotic proteins Bax and Bad compared to control subjects. Interestingly, several studies also reported an increased cell proliferation was found in patients with emphysema (84, 85). Aoshiba and colleagues reported that intra-tracheal administration of active caspase-3 is capable of inducing epithelial apoptosis and results in emphysematous changes in mice (86).

Apoptosis is found to be associated with decreased expression of vascular endothelial growth factor (VEGF), a protein required for cell maintenance (87). VEGF and VEGFR2 level were decreased in emphysema patients compared to healthy controls (88). Animal models demonstrate inactivation of VEGF leads to the early development of emphysema (89). A similar outcome was observed in another study where mice over-expressing placental growth factor (PIGF) showed to develop VEGF deficiency that led to alveolar apoptosis and emphysema (90). Apoptosis can be mediated by elastolytic activity in lung epithelial cells observed in a mouse model of emphysema. Mice double knockout for IL-1 β and TNF receptors gene were treated with elastase showed less severe form of emphysema as well

as fewer apoptotic alveolar cells suggesting that elastase may contribute in alveolar apoptosis through IL-1 β and TNF-dependent mechanism (91). A direct proteolysis of death-inducing signals can also promote apoptosis. It has been shown that Fas ligand produced by epithelial cells can be shed and activated by proteolytic activity of MMP-7 and thereby mediates apoptosis (92). In addition to these mechanisms, an increased number of CD8+T lymphocytes in the lungs of COPD patients is reported to induce alveolar epithelial cell apoptosis through the release of perforins, granzyme-B and TNF- α (93, 94).

1.2.5.3 Oxidative stress

The lung is constantly exposed to either endogenous oxidants produced by metabolic reactions or exogenous air pollutants and cigarette smoke and thus could be highly susceptible to reactive oxygen species (ROS) mediated injury. Cigarette smoke is a complex mixture of >4,700 chemical compounds and each puff is considered to contain approximately 10^{14} oxidative free radicals (95, 96). Among them superoxide radical ($O_2^{\cdot-}$) and nitric oxide (NO) are quite short-lived while tar-semiquinone persist in the lung for longer time periods (95) and react with oxygen to produce superoxide anion (O_2^-), the hydroxyl radical, and hydrogen peroxide that are abundantly found in smoker's lung (97). Endogenously, activated macrophages and neutrophils and also epithelial cells are known to release high levels of ROS via NADPH oxidase (98). Oxidative stress is able to activate transcription factors such as NF- κ B and transcription factor activator protein-1 (AP-1) leading to increased release of inflammatory mediators including cytokines such as IL-8, TNF- α and nitric oxide (NO) (99).

Endogenous oxidative stress contributing in emphysema has been demonstrated in several animal models. Most of these studies have investigated genes that are related to the cellular antioxidant response, such as Nrf2, thioredoxin 1 and SOD3 (extracellular superoxide dismutase or ECSOD). Nrf2 (NF-E2-related factor 2), is a basic leucine zipper type transcription factors that has been shown to bind to the antioxidant response element (ARE)

(100). Nrf2-knockout mice treated with elastase showed markedly exacerbated emphysema compared to wild-type mice. The emphysema severity correlated with the higher recruitment lung inflammatory cells in the initial stage of elastase treatment. The highly inducible expression of anti-oxidant and anti-protease genes observed in wild type alveolar macrophages was significantly attenuated in the lungs of Nrf2-KO mice (101). Thioredoxin-1 (TRX) is a small protein with anti-oxidative effect shown to ameliorate lung inflammation and emphysema in mice model (102). A study on Superoxide dismutase (SOD3)--null mice exposed to cigarette smoke exposure or treated with elastase demonstrated airspace enlargement as well as impaired lung function and exercise capacity which were improved in mice overexpressing SOD3 or mice treated with pharmacological SOD analog. The improvement resulted from binding the analog with oxidative fragmentation of ECM such as heparin sulfate and elastin and thus attenuating their induction on inflammatory response (103). Lately, a study on mouse model of emphysema demonstrated that mice deficient in inducible nitric oxide synthase (iNOS) were protected against emphysema. Furthermore, treatment of wild-type mice with an iNOS inhibitor prevented as well as reversed already established emphysema demonstrating the pathophysiological role of oxidative stress in emphysema COPD (104).

1.2.5.4 Inflammation

It is widely accepted that inflammation is central to the development of COPD. Lung epithelial cells and inflammatory cells such as neutrophils, macrophages, CD8+T lymphocytes and dendritic cells release potent inflammatory mediators and proteinases which play a role in the progressive lung destruction in emphysema.

The airway epithelium acts as a barrier between external environment and host. It is crucial for the maintenance of lung homeostasis by mucus production, ciliary movement, secretion of anti-microbial agents and immune response to noxious stimuli. Cigarette smoke exposure

triggers epithelial cells to release inflammatory mediators and proteases, such as CXCL8, TNF- α , TGF- β and IL-1 β which in turn initiates and maintains chronic inflammation and airway remodeling (105-107). Cigarette smoke can also induce inflammatory responses in alveolar epithelial cells (108). Among inflammatory cells, macrophages are the key players in the inflammatory process in COPD. In smokers as well as in COPD patients, there is evidence demonstrating elevated levels of macrophages in airways, lung parenchyma, sputum and bronchoalveolar lavage (BAL) fluid. Cigarette smoke activates macrophages to induce the release of inflammatory mediators and matrix metalloproteinases (MMPs) which contribute to sustained inflammation and alveolar wall destruction (65, 109-111). Besides macrophages, numerous evidence have confirmed neutrophil as another a crucial inflammatory cell in COPD pathogenesis. Substantial numbers of activated neutrophils are quantified in sputum and BAL fluid of COPD patients (112-114). Neutrophils secrete a wide range of inflammatory mediators including neutrophil elastases, proteinase-3, cathepsin G as well as matrix metalloproteinase (MMP)-8 and MMP-9 contributing to alveolar destruction (115). In addition, in COPD patients, the airways harbor elevated numbers of lymphocytes, particularly the CD8+ T-cells (116). In animal models, exposure to cigarette smoke induced a surge in the number of dendritic cells (117). In accordance with this evidence, abundant dendritic cells are also observed in the airways and alveolar walls of smokers indicating the contribution of these cells in emphysema progression (118, 119).

1.2.5.5 Cellular senescence

Senescence is described as a permanent cell cycle arrest induced by cellular stress (premature senescence) or by exhaustion of cell's replicative capacity (120). Most recently, accelerated senescence or cellular aging has emerged as a strong hypothesis of COPD and it is now considered to be a disease of premature lung aging (121, 122). As alveolar cell loss and reduced alveolar surface area contribute to lung structure destruction that is characteristics of emphysema, senescence could play a role in pathogenic alteration that

takes place during emphysema development and progression. In emphysematous lung, the repeated cell cycles of alveolar cell to compensate cells lost by apoptosis may shorten telomere length leading to replicative senescence (85, 123). However, the cigarette smoke exposure along with other stress factors associated with emphysema might also induce premature alveolar senescence without telomere shortening (124). Lately, a broad range of investigations has accumulated valid evidence on senescence being involved in COPD development (125). Telomere length in alveolar type II cells and endothelial cells *in situ* has been found to be significantly reduced in emphysema patients compared to control subjects (126).

There have been experimental demonstrations that indeed various senescence markers are expressed in emphysematous lungs of COPD patients (121, 127). Senescence-associated β -galactosidase, a common marker of cellular senescence, is regularly expressed in senescent cells (128). An increased expression of senescence-associated β -galactosidase was observed when lung fibroblasts of emphysema patients were cultured *in vitro* and compared to healthy smokers (124, 129). Exposing human lung epithelial cells to cigarette smoke extract also induced an enhanced expression of β -galactosidase and senescence-associated changes in cell morphology such as an increase in cell size and lysosomal mass, accumulation of lipofuscin, overexpression of p21 and irreversible growth arrest (127). The cyclin dependent kinase (CDK) inhibitors (p16, p21 etc.) regulating cell cycle progress are widely used markers for cellular senescence and reported to involved in emphysema. Genetic inactivation of p16 in BubR1 progeroid mice demonstrated delayed aging by preventing the formation of p16-positive senescent cells proving its role in senescence induction (130). A study done by Tsuji et al., demonstrated that lung tissue obtained from emphysema patients having significantly greater percentages of p16 and p21 positive alveolar type II cells and endothelial than non-smokers. A tumor suppressor and transcription

factor p53 regulates p21 and thus also plays a major role in the induction of cellular senescence in fibroblasts from COPD patients (131).

In addition to cigarette smoke, aging is reported to be another major risk factor for COPD patients (132). Both aging and cigarette smoke induce p16 expression in lung tissue suggest the possibility that cellular senescence plays a crucial role in both the smoke-related as well as and the age-related pathogenic mechanisms of COPD (125, 133). Besides, telomere length in both of these cell types were greatly reduced compared to healthy controls. In addition, p16 expression level was inversely correlated with PCNA, a proliferation marker expression level. Most importantly, there was a strong correlation between cellular senescence and airflow limitation measured as FEV1% values (126). γ H2AX is a marker for DNA double strand breakage and recent study reported the presence of significantly high number of γ H2AX foci in the alveolar type I and II cells and endothelial cells of the lungs of COPD patients compared to healthy smokers or control subjects. The foci were associated with cellular senescence, apoptosis and pro-inflammatory changes (134).

Sirtuin1 or SIRT1 is an anti-aging and anti-inflammatory protein, is a metabolic NAD(+)-dependent protein/histone deacetylase that regulates pro-inflammatory mediators by deacetylating histone and non-histone proteins (135). Peripheral lungs of smokers and patients with COPD showed decreased levels of nuclear SIRT1, as compared with nonsmokers. *In vitro* study on macrophages treated with cigarette smoke extract showed decreased levels of SIRT1 which was associated with an increased acetylation of RelA/p65 NF- κ B (136). It has been demonstrated SIRT1 protecting against emphysema by FOXO3-regulated reduction of premature senescence (137). Treatment of endothelial cells from COPD patients with a SIRT1 activator (resveratrol) is shown to rescue H₂O₂-induced senescent phenotype back to normal state (138).

1.2.6 Animal Models of Emphysema

1.2.6.1 Elastase-induced emphysema model

The application of elastases such as porcine pancreatic elastase (PPE) is a well-established animal model as it induces irreversible progressive changes in lung structure and function that are typical characteristics of emphysema (139, 140). The first reproducible animal model of emphysema was established by Gross et al in 1965 by intratracheally delivering plant proteinase papain in rats (141). Subsequent studies further confirmed that that only enzymes with the capacity to solubilize the ECM protein elastin can produce both morphological and histological changes that are comparable to pan-acinar emphysema observed in human subjects (25). More recent studies have been applying either porcine pancreatic elastase (PPE) or human neutrophil elastase (HNE) as an emphysema model in animals. Crude extract of human neutrophils and later purified HNE capable of inducing emphysematous changes and these studies led to the proteinase/anti-proteinase hypothesis that emphysema develops as a result of an influx of inflammatory cells into lungs triggering release of excessive proteases that ultimately destroys the lung alveolar architecture (142). Consistent quality human neutrophil elastase is commercially available yet relatively expensive whereas PPE offers the advantages of being cost-effective and easy to obtain. PPE application produces consistent and significant airspace enlargement accompanied with inflammatory cells accumulation within the lungs of rodents, guinea pigs, dogs and primates (25, 143). PPE is a 25.9 kDa globular protein consists of a single polypeptide chain of 240 amino acids cross-linked by four disulfides bridges. Unlike other elastases that hydrolyze a wide range of protein substrates, PPE specifically breaks down elastin (144). Despite its known half-life of a few hours and a turn-over rate of 99% in four days (145, 146) PPE triggers a continuous airspace enlargement and lung function decline even after stimulus cessation (139, 140) which mimics the irreversible structural changes occurring in the lungs of COPD patients even after smoking cessation (147). Most recently, a study monitored and described a PPE-induced emphysema progression in animal model for 12 weeks monitored by morphometry

and micro-computed X-ray tomography (148). However, a shortcoming of elastase model is that cannot be used to study all aspects of COPD as it reflects only one main symptom, e.g. pulmonary emphysema. This model lacks significant inflammatory components, resulting in the lack of chronically persisting inflammatory cells (chronic bronchitis) and absence of small airway remodeling. Nevertheless, as an emphysema model the elastase model remains a useful tool with great advantages: a) it is relatively simple to perform, b) highly reproducible, c) models could be established by a single treatment with an inexpensive reagent in a short period, d) requires less time and less labor as compared to the usual 6-month long cigarette smoke exposure and e) most importantly, emphysema progression could be reliably monitor by lung function tests (149). Despite the pros and cons, elastase-induced emphysema is one of the most common means of establishing emphysematous phenotypes in animal models to better understand the pathomechanism of the disease.

1.2.6.2 Cigarette smoke-induced emphysema model

Given its involvement as the major risk factor of COPD, cigarette smoke (CS)-induced emphysema model would be an important tool as well as an attractive approach to investigate the disease. Unlike elastase model, the CS-induced emphysema is accompanied by a significant amount of inflammation. The first cigarette can trigger neutrophil recruitment which is followed by an influx of macrophages. The early neutrophil influx is associated with enhanced degradation of collagen and elastin fibers (150). A shortcoming of the model is that the severity varies from species to species. CS exposure causes highly prominent emphysema in guinea pigs whereas it induces minimal disease development in rats or causes nonspecific particle overload effect if smoked too heavily (151, 152). The effectivity of CS model is also limited by genetic factors influencing susceptibility. Among commonly used mouse strains in laboratories, the AKR/J strain shows significant emphysema whereas A/J, SJL, and C57BL6/J strains show mild and NZWLac/J strain is resistant to CS induction (153). Besides, the brand and number of cigarettes, exposure time, sex and age of the animals

exposed are also important factors modulating lung's response to CS-induced emphysema development. In addition, there are marked differences between main-stream smoke (the smoke that emerges from the mouth-end of the cigarette while smoking) and side-stream smoke (the smoke that emerges from the lit-end of the cigarette between puffs) which also contributes in varying emphysema severity in animal models (154). A major disadvantage of CS model is that it takes considerably more time to induce significant pathological changes in the lung (starting from 4 months of exposure) (155). Furthermore, CS exposure of animals for up to 6 months only produces a mild disease, probably equivalent to human Global Initiative on Chronic Obstructive Lung Disease (GOLD) stage 1 or 2 (6).

1.3 Post-translational modification of arginine

Post-translational modifications (PTM) refer to the proteolytic cleavage or the addition of a modifying group to one or more amino acids of a protein by covalent bonding. PTMs, such as phosphorylation, ubiquitination, acetylation, SUMOylation and methylation can regulate activity, localization, turn-over and interaction of a protein with other proteins and thus play a pivotal role in functional changes of histone and non-histones proteins (156).

Arginine residues within histones and non-histone proteins are subject to various PTM and have been linked to a variety of important cellular processes like transcriptional regulation, translation, and DNA repair (157). Therefore, here, we focus on post-translational modifications on arginines. Arginine is classified as a semi-essential or conditionally essential amino acid in mammals (158). It is a positively charged amino acid which is involved in formation of hydrogen bond and interaction with protein or nucleic acids. Arginine PTM was first described with the identification of citrullination or deimination in protein that removes an imine group from arginine side chain and converts arginine into neutral, hydrophilic citrulline (159, 160). Till to date, arginine is known to be modified by four types of enzymatic PTMs: methylation, citrullination, phosphorylation, and ADP-ribosylation and two types of non-

enzymatic PTMs such as carbonylation, advanced glycation end-products (161). Of all these modifications of arginine, the methylation has been the most extensively characterized due to its biological role.

1.3.1 Protein Arginine Methylation

About 0.5% of arginine moieties are methylated in mammals (162). Regulation of arginine methylation is associated with crucial cellular processes including transcriptional regulation, translation, and DNA repair (157). The existence of methyl group on arginine in proteins first came into notice back in 1967 (163). Methylation of an arginine moiety results in the addition of one or two methyl groups to its guanidino nitrogen atoms (164). In contrast to citrullination, methylation does not neutralize the positive charge in arginine, but increases the hydrophobicity of proteins (165). In mammals, three kinds of methylated arginine have been discovered so far. These are: ω -N^G-monomethylarginine (MMA), ω -N^G,N^G-asymmetric dimethylarginine (ADMA) and ω -N^G,N^G-symmetric dimethylarginine (SDMA) (164). Among them, ADMA is the most commonly occurring derivative (162). All three derivatives can be found on distinct protein species in the cytoplasm, nucleus, and organelles of mammalian cells (157). One common feature of the majority of methylated arginine residues is that they are often flanked by one or more glycine residues (164).

1.3.2 Characteristics and classification of protein arginine methyltransferases (PRMTs)

Although protein arginine methylation was reported 40 years ago (163), the first gene coding for the arginine methyltransferase enzyme was identified only a decade ago (166, 167). PRMT-encoding genes have been identified from the sequenced genomes of yeasts, worm, fly, plants, and mammals (157). Currently, 11 PRMT members, differing in sequences and substrate specificities is known to exist and already has been characterized (168). All PRMTs contain a conserved core region that includes a methyltransferase (MTase) domain, a β -barrel and a dimerization arm (169).

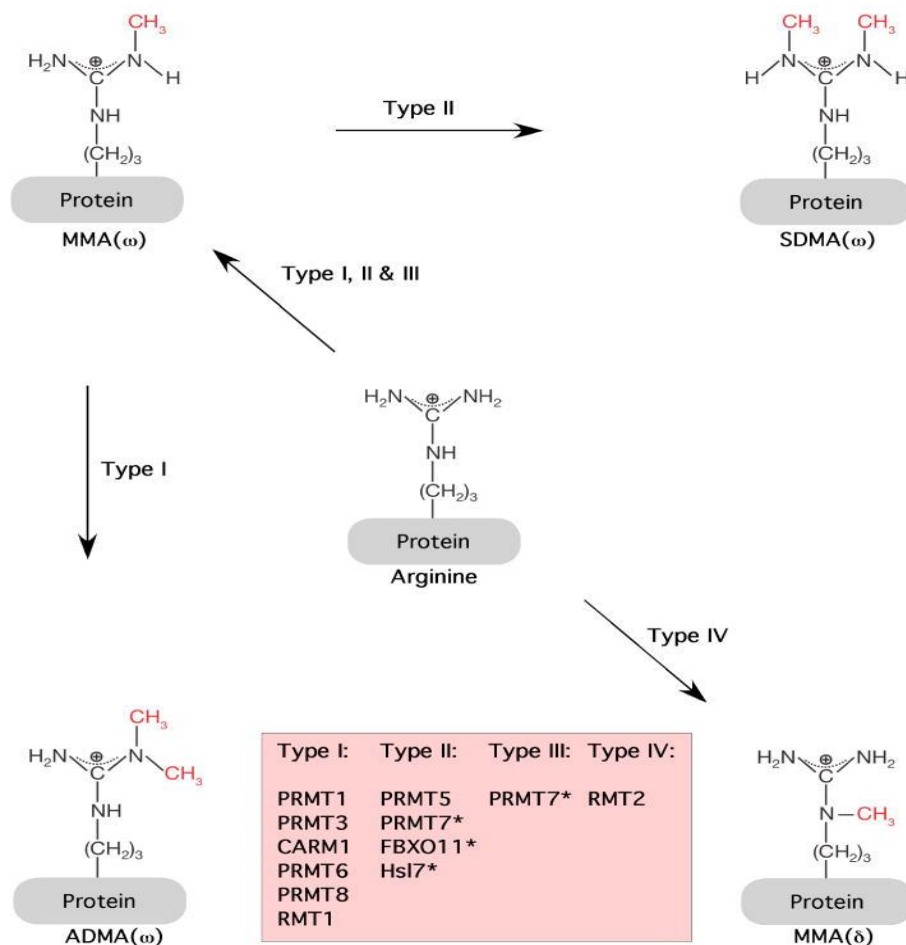


Figure 3: Classification of PRMTs. Types I, II and III PRMTs catalyze the formation of monomethylarginine (MMA) on one of the terminal guanidino nitrogen atoms. Type I enzymes catalyze the subsequent formation of asymmetric dimethylarginine (ADMA) whereas type II enzymes generates symmetric dimethylarginine (SDMA). Type III PRMTs catalyze monomethylation only. Type IV enzyme only described in yeast catalyzes monomethylation of the internal guanidino nitrogen. Adapted from reference (170).

PRMTs are AdoMet-dependent methyltransferases as they catalyze transfer of specific methyl group from the ubiquitous cofactor S-adenosyl-L-methionine (AdoMet) to arginine residues of biologically important target proteins in the cell (171). Initially, PRMTs were reported to methylate histone proteins but more recently, PRMT-mediated methylation of non-histone proteins has been under detail investigation. The non-histone proteins methylated by PRMTs are either RNA binding proteins or those that are involved in transcription (164, 172, 173). Usually, proteins that harbor glycine- and arginine-rich patches (GAR motifs) are often substrates for PRMTs (174). Another prominent methylation site for

PRMTs motifs consists of motifs are proline-, glycine-, methionine-, arginine-rich patches (PGM motifs) (175) that are found in a number of splicing factors (176).

According to the methylarginines derivatives they catalyze, PRMTs can be classified into four types (Figure 3 and 4) (177). All members of PRMT family catalyze the formation of ω -N^G-monomethyl arginine (MMA). In addition, type I PRMTs catalyze the formation of asymmetric ω -N^G, N^G-dimethylarginine (ADMA) and this class includes PRMT1, PRMT2, PRMT3, PRMT4/coactivator-associated arginine methyltransferase 1 (CARM1), PRMT6, PRMT8 and RMT1 (170). Type II PRMTs including PRMT5, PRMT7, FBXO11 and Hsl7 catalyze the formation of symmetric ω -N^G, N^G-dimethylarginine (SDMA) (178). However, it is not well characterized whether PRMT7, FBXO11, and Hsl7 are type II PRMT or a type III PRMT which is only able to form MMA monomethylate arginines (170, 179). Type III PRMTs family consists of *T. brucie* homolog of human PRMT7, TbPRMT7 (180). Type IV enzymes catalyze the formation of monomethylation of the internal guanidino nitrogen of arginine (δ -N^G-monomethyl arginine) and so far RMT2 from *S.cerevisiae* and *C.albicans* have been demonstrated to harbor this activity (181, 182).

1.3.3 PRMT family members

PRMT1: It was first identified as a single gene product by sequence similarity to the yeast arginine methyltransferase Hmt1/Rmt1 and it is reported to be the predominant mammalian type I PRMT as it performs over 80% of PRMT activity in cell (183). It was the first human PRMT isolated and well characterized. In human, there exist 3 major transcript variants of PRMT1 (183). The common substrates of PRMT1 are a number of hnRNP molecules and methylation modulates the shuttling of these proteins between the cytoplasm and the nucleus (184). PRMT1 also methylates histone H4 at arginine 3 that functions as a transcriptional activation marks (185). Gene ablation experiments in mice showing that the PRMT1 null embryos die at embryonic day 6.5 proved PRMT1 to be essential for survival (186).

PRMT2: It is a unique member of PRMT family. It harbors an SH3 domain at its N-terminus (187). Human PRMT2 is reported to methylate histone H4 (188) as well as hnRNP E1B-AP5 (189). It also plays a role of a coactivator for androgen and estrogen receptors (190, 191). Unlike PRMT1, the PRMT2-null mice are viable and physiologically normal (192). Increased expression of PRMT2 in alveolar type II cells is observed in chronic hypoxia, a potent stimulus for COPD (193).

PRMT3: It was discovered by its association with PRMT1 (187, 194). PRMT3 is a ribosomal protein methyltransferase that regulates the cellular levels of ribosomal subunits (195). A distinct feature of this PRMT family member is that it contains a zinc-finger domain at its N-terminus and this domain functions as its substrate-recognition module (194). By methylating its zinc-finger-dependent ribosomal protein subunit S2 (rpS2), PRMT3 inhibits its ubiquitination (196, 197). PRMT3 null mouse embryos are small in size, but the mice survive after birth and grow to a regular healthy size in adulthood. The ribosome protein rpS2 is hypo-methylated in the absence of PRMT3, which demonstrates that it is an *in vivo* PRMT3 substrate (198).

PRMT4: It binds the steroid receptor coactivators (SRC1-3) and has clear transcriptional coactivator activity itself, thus its name-the coactivator associated arginine methyltransferase 1 or CARM1 (199). It was the fourth arginine methyltransferase described. It is also referred to as PRMT4. As PRMT4/CARM1 is the main focus of this dissertation, it is discussed in detail in the following section (1.3.4).

PRMT5: This member was identified as a Janus kinase 2 binding protein in a yeast two hybrid screening and hence was called JBP1 (200). It is shown to methylate myelin basic protein, fibrillarin and histones H2A, H3 and H4 (201, 202). PRMT5-mediated methylation of

sphingomyelin (Sm) and survival of motor neuron (SMN) contributes in spliceosome assembly (203). PRMT5 is also important for facilitating ATP-dependent chromatin remodeling (204).

PRMT6: It is a 41.9 kDa Type I methyltransferase with auto-methylation activity (205). Its substrates include nuclear scaffold protein HMGA1a, DNA polymerase β , the HIV Tat and histone H3 (206-209).

PRMT7: A characteristic of PRMT7 is that it contains two functional AdoMet-binding motifs. Another marked feature is that it mainly catalyzes the formation of MMA but not DMA and thus labeled as a type III enzyme (210). Knockdown of PRMT7 shows upregulation of gene expression regulating DNA repair (211).

PRMT8: It was originally identified through its high degree of sequence similarity (over 80%) to PRMT1. The unique feature of PRMT8 is that it has a unique N-terminus harboring a myristoylation motif which facilitates its association with the plasma membrane (212). It is known to pose auto-methylation activity at R58 and R73 in the N-terminal region (213).

PRMT9: The protein encoded by the gene 4q31 is identified as human PRMT9 (214). With 845 amino acids, it is the largest member in the PRMT family. It also harbors two tetratricopeptide repeats (TPR) motifs contributing in protein-protein interactions (172). PRMT10 and PRMT11 are not fully characterized.

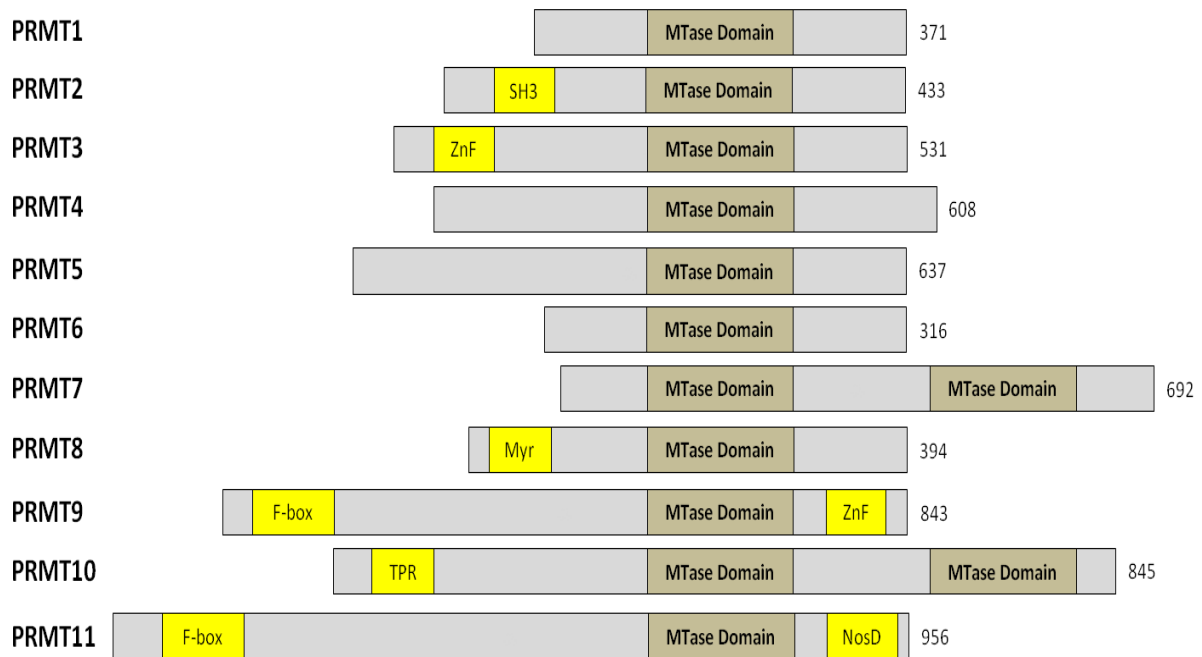


Figure 4: Structural characteristics of PRMT family members. All PRMTs contain at least one methyltransferase (MTase) domain. Additional domains are: Znf (zinc finger), Myr (myristoylation), F-box, TRP (tetratricopeptide) and NosD (nitrous oxidase accessory protein). In addition, PRMT4 has a unique C-terminal region, PRMT7 or PRMT10 has two catalytic domains. Adapted from reference (168).

1.3.4 Coactivator-Associated Arginine Methyltransferase 1, CARM1

PRMT4 or CARM1 was identified in the yeast two-hybrid screening assay in 1999. It was found to be associated with a p160 steroid receptor coactivator, GRIP1 (199). As it binds the steroid receptor coactivators and poses a transcriptional coactivator activity, thus it was named as the coactivator-associated arginine methyltransferase 1 (CARM1).

1.3.4.1 Structure of CARM1

CARM1 harbors 608 amino acids in mouse as well as in human. The CARM1 crystal structure was solved by two groups, providing insight into its mechanism of action (215, 216). Structurally, CARM1 can be divided into three domains. It contains a methyltransferase catalytic core flanked by characteristics pre (N terminal) and post (C terminal)-core segment (215). The catalytic core of other PRMTs such as PRMT1 or PRMT3 shares 49% sequence

similarities whereas, CARM1 shares only 34% sequence similarity (216). The core is folded into two domains that are connected by a conserved cis-proline residue.

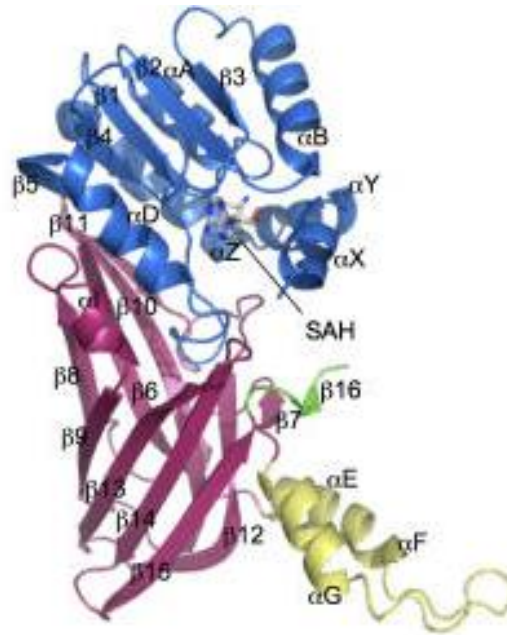


Figure 5: Structural organization of CARM1. The monomer consists of the N-domain (blue), C-domain (red), dimerisation arm (yellow) and C-extension (green). Adapted from reference (216).

The first domain at the N-terminal end contains a typical Rossmann Fold (RF) and two terminal Helices αX and αY was also found in the structure of PRMT3 (215, 217). The RF topology contains the S-Adenosyl methionine (SAM or AdoMet) consensus fold which is conserved in all AdoMet-dependent methyltransferase enzymes (218). The second domain consists of a β -barrel to which an arm harboring a four-helix segment is attached. This arm contributes in the dimerization process of CARM1 as well as other PRMTs (215). Crystal structure of core region reveals the existence of a co-factor-dependent formation of a substrate-binding groove acting as an access channel for arginine to the active site. This groove is supported by the initial 8 residues from the post-core segment called C-extension that is uniquely present only in CARM1 but not in other PRMTs. Deletion of C-extension nullify the methyltransferase activity of CARM1 to Arg17 of histone H3, proving the contribution of this segment to the enzymatic activity of the core domain (216). The N-terminal segment varies in size and poses a Pleckstrin homology (PH) domain (215) (Figure

5, blue region). PH domain is a protein domain of approximately 120 amino acids that occurs in a wide range of proteins involved in intracellular signaling (219). The PH domain in CARM1 can assume different position and acts as a wobbly domain (220). It is connected to the catalytic core by a linker although both domains can behave independently. However, during co-activation of gene expression, they cooperate upon binding to other proteins (215).

1.3.5 Molecular function of CARM1

1.3.5.1 Methyltransferase activity

Enzymatic activity is critical for CARM1 to perform its biological roles. In a recent study on mouse model an enzyme-dead version of CARM1 knock-in embryo and mouse embryonic fibroblasts (MEF) cells were generated to produce enzymatically inactive CARM1. Lack of methyltransferase activity demonstrated embryo lethality, aberrant adipocyte differentiation, impaired T cell development and diminished transcriptional coactivator activity proving that enzymatic activity of CARM1 is essential for all of its cellular functions *in vivo* (221).

1.3.5.2 Transcriptional coactivator

CARM1 is considered as a coactivator for many transcriptional factors. For example, it cooperates with PRMT1 and p300/CBP in ER-dependent transcriptional activation but CARM1 depends on another transcription factor, p160 for its coactivator function, showing that CARM1 is a secondary coactivator rather than acting as the primary transcriptional activator (222, 223). Although CARM1 was initially identified as estrogen and androgen receptor coactivator, it is now emerging as coactivator of large number of transcription factors and thus acts as a molecular switch to control their expression. This includes, p53, p21, p16, SIRT1, NF- κ B, LEF1/TCF4, E2Fs, cyclin E1, PPAR γ , RUNX1, Wnt signaling molecule β -catenin and so on (222-228). This suggests CARM1 plays a role in cell proliferation and cell survival. As a coactivator for PPAR γ , CARM1 promotes preadipocytes to differentiate towards adipocytes (226). The recruitment of CARM1 to NF- κ B target

promoter positively regulates NF- κ B mediated expression of pro-inflammatory genes such as G-CSF, MIP-2, MCP-1, ICAM1 and IP-10 (229).

1.3.6 Substrates of CARM1

Proteins that harbor a glycine and arginine rich motif (GAR motif) are usually the ideal substrate for PRMTs (174). In contrast, CARM1 is shown to be unique in substrate specificity as it does not methylate GAR motif. Actually, there is no particular motif that is recognized by CARM1. This lack of motif specificity makes it difficult to find potential substrate for CARM1 using *in silico* tools that search primary protein sequences. Despite this limitation, CARM1 has been demonstrated to methylate a wide range of proteins crucial for gene expression. The substrates of CARM1 can be classified into two broad classes: chromatin remodeling proteins and RNA binding protein and splicing factors.

1.3.6.1 Chromatin remodeling proteins

The first CARM1 substrate identified was histone H3 (199). It is a major *in vivo* substrate for CARM1. CARM1 catalyzes mono- and asymmetrical dimethylation on R2, R17 and R26 sites in histone H3 which correlates with activation of estrogen-receptor-target gene, pS2 (230). Arginine methylation is reported to take place prior acetylation of H3 by CREB-binding protein (CBP). H3 K18 and K23 acetylation promotes efficient methylation at R17 of H3 and correlates to gene activation (231). Non-histone proteins methylated by CARM1 include CBP/p300, SRC3 and RNA polymerase II (232-235).

1.3.6.2 RNA binding protein and splicing factors

Additional CARM1 substrates have been identified by large-scale enzyme reactions on protein arrays. These include the poly (A)-binding protein 1 (PABP1) and the T cell-specific factor TARPP. PABP1 is by far the most prevalent substrate identified for CARM1 (236). Candidate approaches also identified other RNA-binding proteins, HuR and HuD and

methylation affects their mRNA-stabilizing properties and the half-life of their target mRNAs (237). Splicing factors are another class of transcriptionally important substrates for CARM1. Splicing factors couple transcription with mRNA processing (238). CA150, a splicing factor is methylated by CARM1 and this post translational modification promotes an interaction of CA150 with the methylation mark recognizing Tudor domain of spinal muscular atrophy protein, SMN. The CARM1 dependent methylation of CA150 is suggested to induce exon-skipping. In addition to CA150, other splicing factors methylated by CARM1 include SmB, U1-C and SAP49 (175).

One established mechanism by which CARM1 regulates senescence is via methylation-dependent modulation of its substrate, HuR. It is an RNA binding protein specifically methylated by CARM1 mainly at Arg²¹⁷ of its hinge region (239). HuR methylation determines its binding and stabilization of its target gene transcripts (239, 240).

CARM1-SIRT1 axis

Along with decreasing CARM1, the senescent fibroblasts show a decrease in SIRT1 expression (241). SIRT1 or Sirtuin 1 is a member of SIRT family and is an NAD⁺-dependent lysine deacetylase functioning in multiple cellular events but most importantly in control of lifespan and thus acting as an anti-senescence gene (242). It has been demonstrated that there is a reduction of SIRT1 expression in the lung of smoker and COPD patients (136). In an animal model of COPD, SIRT1 protects against emphysema by reduction of premature senescence (137). CARM1 indirectly regulates SIRT1 expression by methylating HuR and induce its association with SIRT1 mRNA; this association in turn enhances SIRT1 transcript stability by prolonging mRNA half-life (Figure 6) (240).

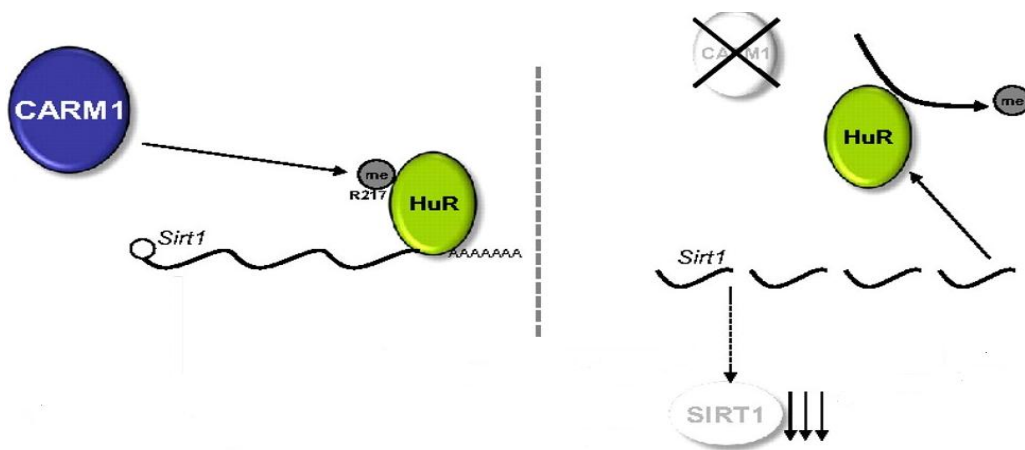


Figure 6 . Regulation of SIRT1 transcript stabilization by CARM1. CARM1 methylation of HuR increases HuR/SIRT1 binding and subsequently stabilizing SIRT1 at mRNA level leading to maintaining a normal level of SIRT1 protein. The decrease in CARM1 is associated with a decrease in HuR methylation and, consequently, of HuR/SIRT1 binding, resulting in less SIRT1 mRNA and protein. Adapted and modified from reference (239).

CARM1-p21/p16/p53 axis

The common senescent phenotypes of cells are characterized by overexpression of CDK inhibitors such as p16 and p21 and checkpoint inhibitor p53 and Rb (243). In contrast to transcript stabilization, CARM1 can also destabilize transcripts for senescence marker genes. CARM1-dependent post-translational methylation of HuR enhances its binding with p16 or p21 mRNA and leading to transcript degradation to protect against senescence (224, 239). CARM1-mediated methylation of HuD, another mRNA binding protein also shown to regulate the half-life of the p21 transcript (237).

1.3.7 Regulation of CARM1

Among all PRMTs, distinct aspects of CARM1 activity have been subjected to be regulated by several post-translational modifications such as phosphorylation and auto-methylation.

1.3.7.1 Phosphorylation

CARM1 is negatively regulated by phosphorylation of its serine residues. Three such sites have been reported to be phosphorylated on sites and two of them contribute in regulation of its enzymatic activity during mitosis (244, 245). Phosphorylation of serine 229 prevents

dimerization of CARM1 and thus abrogates methyltransferase activity of CARM1 (245). Phosphorylation on serine 217 blocks binding of S-Adenosylmethionine (SAM or AdoMet) to the catalytic domain and turns CARM1 into an inactive state. In addition, this modification is also involved in PRMT4/CARM1 trans-location from nucleus to cytoplasm in G2/M transition (244). Recently, a third phosphorylation occurring at serine 448 is identified to facilitate a direct interaction of CARM1 with estrogen receptor (ER α) and leads to ER α -mediated transcription (246).

1.3.7.2 Auto-methylation

Auto-methylation event was first observed in a CARM1 homologue (AgCARM1) in the mosquito model *Anopheles gambiae*, AgCARM1 is dimethylated at arginine 485 in vivo (247). In mouse, the auto-methylation site is at arginine 551 (in exon 15). Mutating this arginine into lysine does not interrupt methyltransferase activity. However, it impairs coactivator function of CARM1 and negatively regulates CARM1-mediated transcription and mRNA splicing (248). Further study on endogenous CARM1 isoforms reveals that alternative splicing serves as the determinant for CARM1 auto-methylation as this modification occurs only in full length CARM1 protein but not in exon 15 deleted isoform (249).

1.3.8 Cellular function of CARM1

1.3.8.1 Role in Proliferation and Differentiation

Proliferation

CARM1-mediated arginine methylation of transcription factor Sox9 prevents its interaction with β -catenin and thus regulating cyclin D1 expression to induce chondrocyte proliferation (250). CARM1 has also been implicated in unregulated cell proliferation. Dysregulated CARM1 is linked to estrogen-induced proliferation of breast cancer cells via playing coactivator role for E2F1 and cyclin E1 expression (251, 252). CARM1 mRNA was found overexpressed in tumors in grade 3 breast cancer patients (252). CARM1-PELP1 axis is also

implicated in breast cancer. PELP1, a proto-oncogene recognizes histone arginine methylation by CARM1 functionally interacts with CARM1 and modulates its coactivator functions. Inhibition of CARM1 expression or blocking its function reduces oncogenic function of PELP1 (253). Elevated CARM1 levels in breast cancer and in prostate cancer is associated with high-levels of an oncogenic coactivator AIB1 as its activity and stability is regulated by CARM1-dependent methylation (234, 252, 254-256). CARM1 is also shown to be overexpressed in human colon cancer cell line (257). In addition, microarray analysis of tissue from colorectal cancers patients confirmed CARM1 to be significantly elevated in the colorectal cancers (258). CARM1 promotes clonal survival and anchorage-independent cell growth via Wnt/ β -catenin signaling. Its methyltransferase domain interacts with β -catenin which then recruits CARM1 to the promoter of Wnt target gene and co-activates transcription (257). More importantly, CARM1 along with PRMT1 are recently found particularly overexpressed in patients with Non-Small Cell Lung Carcinomas (NSCLC) and CARM1 expression is linked to lung tumor differentiation but not to cell survival (259). All these evidence suggest that increased CARM1 expression leads to pathological changes contributing in tumorigenesis. On the contrary, loss of CARM1 leads to hyperproliferation of lung alveolar epithelial cell indicating importance of CARM1 for proper proliferation (251). An explanation of this opposite effect could be the difference in availability of CARM1 target proteins in alveolar versus tumor cells (260).

Differentiation

CARM1 is shown to be crucial for life as CARM1-null mice die from breathing failure immediately after birth. Further analysis revealed that the lung of CARM1 deficient mice showing defective maturation of alveolar epithelial type II (ATII) cells and impaired trans-differentiation evident by an absence of alveolar epithelial type I (ATI) cells (232, 251). Furthermore, CARM1-null embryos shows lack of brown fat showing cells not expressing CARM1 lose the potential to differentiate into mature adipocytes (226). Besides, CARM1 is

also involved in differentiation of chondrocytes and myocytes for skeletal muscle development (204, 250). Loss of CARM1 leads to hypomethylation of cAMP-regulated phospho-protein in thymocytes resulting in defective T cell differentiation (261). Functional CARM1 is also reported to regulate proper fetal hematopoiesis (262). The functional impact of the CARM1-SIRT1 axis is implicated in human embryonic stem cell differentiation (240).

1.3.8.2 Role in Senescence

CARM1 shows significant reduction in explicatively senescent human diploid fibroblast cells (WI-38 fibroblasts) coupled with a marked downregulation of asymmetrically-methylated proteins. Beside replicative senescence, premature senescence induced by H₂O₂ also decreases CARM1 level (263). CARM1-mediated methylation of HuR is reported to suppresses cellular senescence in fibroblasts to regulate the turnover of cyclin A, cyclin B1, c-fos, SIRT1, and p16 mRNAs (224). Reduced level of CARM1 is also observed in testis, thymus and heart of 24-month-old rats compared to 6-month-old rats, suggesting CARM1 is regulated in age-dependent manner (264).

1.3.9 Protein Arginine methylation in COPD

Asymmetric dimethylarginine (ADMA), the catalyzed product of type I PRMTs ADMA has been abundantly detected in urine, plasma, cerebrospinal and most importantly in bronchoalveolar lavage (BAL) fluids (265-268). PRMTs regulate senescence in COPD through ADMA via direct effects on gene expression and protein function, as shown by methylated HuR-mediated stabilization of SIRT1 (137, 240). In addition, PRMTs can also regulate oxidative stress in COPD by regulating nitric oxide (NO) production. It is well known that NO plays critical role in endothelial dysfunction and oxidative stress in COPD (269) and ADMA is a potent inhibitor of nitric oxide synthase (NOS) isoforms (nNOS, iNOS, and eNOS) (270). Therefore, inhibition of NOS and subsequently altered NO generation is may be another way how PRMTs maintain lung homeostasis. However, the lung itself generates a

significant amount of ADMA which suggests that a dysregulated ADMA metabolism in the lung might trigger a chronic lung diseases including COPD (268).

Furthermore, several studies have investigated the relationship between cigarette smoke and ADMA levels although they demonstrate conflicting results. Some studies reported decreased reduced ADMA levels reflecting a decline in PRMT activity in smokers compared with non-smokers while others showed increased ADMA levels in smokers (271, 272). In vitro studies using cigarette smoke extract (CSE)-treated cell also show contrasting data. For example, 10% CSE-treated human endothelial cells lead to decreased intracellular ADMA concentration (272) while others reported upregulation of ADMA levels under such conditions (273). Despite the contrasting results, it can be deduced that cigarette smoke is an important regulator of ADMA and PRMTs. However, more conclusive evidence is necessary to assess whether COPD has a valid association with dysregulated PRMT expression and activity.

A recent analysis of methylarginine metabolism in the mouse lung, heart, liver, and kidney reveals the lung to be a major source of CARM1. The abundance of CARM1 expression in lung in comparison to other organs suggests its possible role in maintaining lung homeostasis (264, 274). Indeed, CARM1 knockdown resulted in the dysregulated proliferation and impaired trans-differentiation of alveolar epithelial cell (251). Thus, abundant pulmonary expression accompanied by its ability to control cell proliferation and differentiation makes CARM1 a potential target for further investigations on COPD development and progression.

1.4 Aim of the study

Emphysema-the major component of COPD is characterized by alveolar damage leading to progressive decline in lung function. Currently, there is no specific treatment for emphysema. There is growing evidence that emphysema is promoted by an accelerated senescence of the lung cells. However, the key regulator of senescence which could be crucial in COPD pathogenesis have not yet been identified. We hypothesized that CARM1 deficiency is involved in emphysema development by modulating cellular senescence in the lung. For our study purpose, we used a porcine pancreatic elastase (PPE)-induced emphysema model in mouse. To test our hypothesis, we aimed:

- a) to assess the contribution of CARM1 expression in a progressive emphysema mouse model
- b) to compare the emphysema susceptibility between CARM1 haploinsufficient mice and wild type mice after elastase treatment
- c) to evaluate the induction of cellular senescence by siRNA-mediated knockdown of CARM1 in ATII-like LA4 cells *in vitro*.

Thus the overall working-hypothesis of this thesis was that CARM1 regulates the development and progression of emphysema.

2. MATERIALS AND METHODS

2.1 MATERIALS

2.2.1 Antibodies

Table 2:

Antibodies (Abs)	Host	Dilution	Suppliers
Anti-CARM1 polyclonal	Rabbit	IHC 1:150, WB 1:750	Abcam, ab87910, Cambridge, UK
Anti-Phospho-CARM1 polyclonal	Rabbit	WB 1:500	Abnova, PAB25896, Taipei, Taiwan.
Anti-SIRT1 polyclonal	Rabbit	IHC 1:100 WB 1:1000	Millipore, 07131, Schwalbach, Germany
Anti-p16 polyclonal	Rabbit	IHC 1:50 WB 1:200	Santa Cruz, sc-1207, Heidelberg, Germany
Anti-p21 polyclonal	Rabbit	WB: 200	Santa Cruz, sc-397 Heidelberg, Germany
Anti-SP-C polyclonal	Rabbit	IF 1:100	Millipore, 3786, Schwalbach, Germany
Anti-SP-C polyclonal	Rabbit	IHC: 1:50	Bioss, bs-2337R, Woburn, MA, USA
Anti- β -galactosidase	Rabbit	IHC 1:50	Life Technologies, A-11132, Darmstadt, Germany
Anti-T1 α polyclonal	Mouse	WB 1:4000	R&D, AF3244, Minneapolis, Minnesota, USA
Anti- β -actin monoclonal HRP conjugated	Rabbit	WB 1:50000	Sigma-Aldrich, Taufkirchen, Germany

Anti-rabbit IgG Alexa Fluor 488 conjugated secondary Ab	Donkey	IF 1:250	Invitrogen, Darmstadt, Germany
Anti-rabbit IgG HRP conjugated secondary Ab	Goat	WB 1:2500	Abcam, Heidelberg, Germany
DAPI, 4',6-diamidino-2-phenylindole	Rabbit	IF 1:2000	Sigma-Aldrich, St.Louis, USA
Anti-goat IgG Alexa Fluor 568 secondary antibody	Donkey	IF 1:250	Invitrogen, Darmstadt, Germany
Anti-rabbit Fab fragment	Goat	IF 1:30	Jackson ImmunoResearch Laboratories, USA

IHC = Immunohistochemistry; WB = Western Blot; IF = Immunofluorescence.

2.2.2 Biochemicals and chemicals

Table 3:

Reagents	Supplier
Absolute ethanol	Sigma-Aldrich, Steinheim, Germany
Agar	Applichem, Dermstadt, Germany
Antibody diluent	Zytomed, Berlin, Germany
β -Mercaptoethanol (98%)	Sigma-Aldrich, St. Luis, MO, USA
Complete Mini Proteinase Inhibitors	Roche Diagnostics, Penzberg, Germany
Dimethylformamide (DMF)	Roth, Karlsruhe, Germany
Giemsa stain	Merck, Dermstadt, Germany
Glycine	Roth, Karlsruhe, Germany
HIER Citrate Buffer, pH 6	Zytomed Systems, Berlin, Germany
Hydrogen peroxide (H ₂ O ₂)	Sigma-Aldrich, St. Louis, MO, USA
Ketamine	CP-Pharma, Burgdorf, Germany
Laemmli sample buffer	Bio-rad, Munich, Germany

Litmus paper	Sigma-Aldrich, St. Luis, MO, USA
May Gruenwald stain	Merck, Darmstadt, Germany
Mayer's hemalum	Merck, Darmstadt, Germany
Methanol	Merck, Darmstadt, Germany
Milk powder	Roth, Karlsruhe, Germany
Mini-PROTEAN pre-cast gel	Bio-rad, Munich, Germany
Natrium-orthovanadate	New England Biolabs, MA, USA
Non-essential amino acids (NEA)	Biochrom, Berlin, Germany
Paraformaldehyde (PFA)	Sigma-Aldrich, Munich, Germany
Penicillin-Streptomycin	Biochrom, Berlin, Germany
Polyvinylidene difluoride (PVDF) membrane	Bio-Rad, Munich, Germany
Phosphate buffered saline (PBS)	Gibco, Life Technologies, Darmstadt, Germany
Precision Plus Protein Standard	Bio-rad, Munich, Germany
Rabbit on rodent Alkaline phosphatase (AP)-Polymer	Biocare Medical, Concord, CA, USA
Rodent block M	Biocare Medical, Concord, CA, USA
3R4F research cigarette	Lexington, KY, USA
Roti-Quick 1	Roth, Karlsruhe, Germany
Roti-Quick 2	Roth, Karlsruhe, Germany
Rox reference dye	Thermo Scientific, Surrey, UK
Sodium chloride (NaCl)	Braun, Germany
Sybr Green	Thermo Scientific, Surrey, UK
Sodium dodecyl sulfate (SDS)	Biorad Laboratories, Hercules, USA
Trypan blue	Fluka, Steinheim, Germany
Tris	Roth, Karlsruhe, Germany

Trypsin-EDTA	Sigma-Aldrich, St. Luis, MO, USA
Vulcan fast red (VFR)	Biocare Medical, Concord, CA, USA
Xylene	Roth, Karlsruhe, Germany
Xylazine (Proxylaz®)	Bela Pharm, Vechta, Germany

2.2.3 Buffers and Solutions

Table 4:

Buffer	Composition
2% Agar	Agar- 2 g, Tap water- 100 ml
Alcoholic eosin	32% Hydrochloric acid- 2 ml, 70% Ethanol- 200 ml
β -galactosidase staining solution	Citric acid/sodium phosphate- 40 mM (pH 6.0) NaCl- 150 mM, MgCl ₂ -2 mM, Potassium ferrocyanide- 5 mM, Potassium ferricyanide- 5 mM, X-gal-1 mg/ml
Fixative solution	Fomaldehyde- 2% and Glutaraldehyde- 0.2% in PBS
H ₂ O ₂ solution 1.8% (v/v)	30% H ₂ O ₂ - 6 ml, dH ₂ O-14 ml, Methanol-80 ml
Ketamine-xylazine solution	Ketamine-14%, Xylazine-3% and NaCl-83%
Laemmli sample buffer 1X	β -mercaptoethanol-100 1 μ l, 4X Laemmli buffer-900 μ l
Paraformaldehyde (PFA) 6%	PFA- 6 g, PBS- 100 ml
PBS-tween buffer stock solution 10X	dH ₂ O- 1 L, Tween 20- 1ml (=0.1%)
Ponceau S solution	Ponceau S-0.1% (w/v), acetic acid- 5% (v/v)
Radioimmunoprecipitation assay (RIPA) buffer	NaCl 150 mM, Tris- 10 mM pH 7.2, SDS- 0.1%, Triton X- 100%, Deoxycholate- 1%, EDTA- 5 mM
Running buffer stock solution 5X	Tris- 15.1 g, 10% SDS- 50 ml, Glycine- 94 g, dH ₂ O- 900 ml
TBS buffer 1X	20X TBS- 50 ml, dH ₂ O-950 ml
Transfer buffer stock solution 20X	Methanol- 200 ml, Tris- 2.42 g (20 mM),

	Glycine- 11.2 g (150 mM), dH ₂ O- 1 L
Vulcan fast red, VFR	VFR buffer- 2.5 ml, VFR- 1 drop

2.2.4 Instruments and softwares

Table 5:

<i>Equipments</i>	<i>Supplier</i>
Automatic tissue processor TP 1020	Leica, Wetzlar, Germany
AxioObserver.Z1 inverted microscope	Zeiss, Göttingen, Germany
Axiovision 4.8 software	Zeiss, Göttingen, Germany
Biosystem XA forced maneuver system	Buxco, Wilmington, USA
Centrifuge apparatus Retina 35R	Hettich, Ebersberg, Germany
Centrifuge apparatus Universal 32R	Hettich, Tuttlingen, Germany
Centrifuge apparatus Minispin Plus	Eppendorf, Hamburg, Germany
Cell counter AC-12	Assistant, Sondheim, Germany
Chemidoc XRS detection system	Bio-Rad, Munich, Germany
Computer Assisted Stereological Toolbox (newCAST) software	Visiopharm, Hoersholm, Denmark
Dakopen	Dako, Glostrup, Denmark
Decloaking chamber	Biocare Medical, Concord, CA, USA
Electrophoresis chamber	Bio-rad, Munich, Germany
Electronic stirrer	IKA, Wilmington, USA
Embedding apparatus Histostar	Thermo Scientific, Germany
FinePointe RC system	Buxco, Wilmington, USA
FlexiVent system	SCIREQ Inc, Montreal, Qc, Canada
GraphPad Prism 5 software	GraphPad Software, La Jolla, USA
Heating-blocks	Haep Labor Consult, Bovenden, Germany

ImageLab 5.0 software	Bio-Rad, Munich, Germany
Imaris 7.6.5 software	Bitplane, Zurich, Switzerland
Micro dismembrator	Sartorius, Göttingen, Germany
Microplate autoreader	Perkin Elmer, Germany
NanoDrop 1000 spectrophotometer	Peqlab, Erlangen, Germany
Nylon meshes	Sefar, Heiden, Switzerland
Primer3	NCBI, USA
Olympus BX51 light microscope	Olympus, Hamburg, Germany
Real-Time PCR System	Applied Biosystems, Carlsbad, CA
Rotary microtome Hyrax M55	Zeiss, München, Germany
Shandon Cytospin 2 centrifuge	Thermo Scientific Shandon, UK
Thermal Cycler PTC 200	Bio-rad, Germany
Thermomixer	Eppendorf, Hamburg, Germany
Trans-blot cassette	Bio-rad, Munich, Germany
Vortex	IKA, Wilmington, USA

2.2.5 Kits

Table 6:

Kits	Supplier
peqGOLD Total RNA kit	Peqlab, Erlangen, Germany
GeneAmp RNA PCR kit	Applied Biosystems, Carlsbad, CA
β-galactosidase assay kit	Cell signaling, Frankfurt, Germany
Pierce BCA Protein Assay kit	Thermo Scientific, Rockford, IL, USA
Amersham ECL Prime Detection kit	(GE Healthcare, Freiburg, Germany).
Platinum SYBR Green qPCR SuperMix kit	Applied Biosystems, Darmstadt, Germany
Vulcan fast red chromogen kit	Zytomed, Berlin, Germany

2.2.6 Enzymes

Table 7:

Enzymes	Supplier
DNase 1	Peqlab, Erlangen, Germany
Dispase	BD Bioscience, San Jose, CA, USA
MuLV Reverse transcriptase	Applied Biosystems, Carlsbad, CA
Porcine pancreatic elastase (PPE)	Sigma-Aldrich, Munich, Germany

2.2.7 Cell Lines

Table 8:

Cell lines	Supplier
Mouse lung epithelial cell (LA4)	American Type Culture Collection (ATCC), Rockville, MD, USA

2.2.8 Cell culture media

Table 9:

Medium	Supplier
Dulbecco's Modified Eagle's Medium, DMEM	PAA Laboratories, Pasching, Austria
Ham's F12K nutrient medium	Biochrom, Berlin, Germany
RPMI 1640 medium	Biochrom, Berlin, Germany

2.2.9 Serum

Table 10:

Serum	Supplier
Fetal bovine serum	Gibco, Life Technologies, Darmstadt, Germany
Bovine serum albumin	Thermo Scientific, Rockford, IL, USA

2.2.10 siRNA and transfection reagents

Table 11:

<i>siRNA/ reagent</i>	<i>Supplier</i>
CARM1-specific siRNA	Qiagen, Hilden, Germany
AllStars negative control siRNA	Qiagen, Hilden, Germany
HiPerfect transfection reagent	Qiagen, Hilden, Germany

2.2.11 Oligodeoxynucleotides/primers

Primers were designed using Primer3 software (<http://www.ncbi.nlm.nih.gov/tools/primer-blast/>).

Table 12:

<i>Gene</i>	<i>Left primer (5´-3´)</i>	<i>Tm</i>	<i>Right primer (5´-3´)</i>	<i>Tm</i>
HPRT1	CCTAAGATGAGCGCAAGTTGAA	59.00	CCACAGGACTAGAACACCTGCTAA	61.84
CARM1	GTGGGCAGACAGTCCTTCAT	59.67	GTCCGCTCACTGAACACAGA	59.97
SIRT1	CCATTAATGAGGAAAGCAATAGGC	58.22	AATACAAGGCTAACACCTTGGG	58.3
p16	TCGTGAACATGTTGTTGAGGC	59.4	CTACGTGAACGTTGCCCATC	59.28
p21	CGGTGTCAGAGTCTAGGGGA	60.03	AGAGACAACGGCACACTTTG	58.7
p53	GTCACGCTTCTCCGAAGACT	59.76	ACAGATCGTCCATGCAGTGAG	60.13
PCNA	CCACATTGGAGATGCTGTTG	57.07	CCGCCTCCTCTTCTTTATCC	57.46
Ki67	TTGACCGCTCCTTTAGGTATGAA	59.48	GGTATCTTGACCTTCCCCATCA	59.22
Cyc E1	GAGCTTGAATACCCTAGGACTG	62	CGTCTCTCTGTGGAGCTTATAGAC	65

2.2 METHODS

2.2.1 Animals

Eight to ten weeks old pathogen-free female C57BL/6 mice were obtained from Charles River Laboratories (Sulzfeld, Germany). The CARM1 haploinsufficient mice (232) were generously provided from Mark Bedford (University of Texas MD Anderson Cancer Center). Briefly, to generate *Carm1*^{+/-} mice, the *Carm1*^{-/-} mice was first generated by gene targeting. The targeting vector was constructed by introducing a neomycin-resistance (*neo*) cassette which was flanked by short flippase recognition target (*frt*) sites into an intronic region. Two exons coding for 71 amino acid-long fragment (amino acids 117–187) were deleted. The deletion of this coding region resulted in a removal of a three-helix segment involved in cofactor binding (*AdoMet*) and formation of Rossmann fold. Using southern blot hybridization, the targeted clones were identified. Targeted embryonic stem (ES) cells were used to generate chimeric mice. Males with a high contribution of ES cells were crossed with Black Swiss females to generate F1 CARM1 haploinsufficient progeny. In our lab, mice were maintained on a C57BL/6N background.

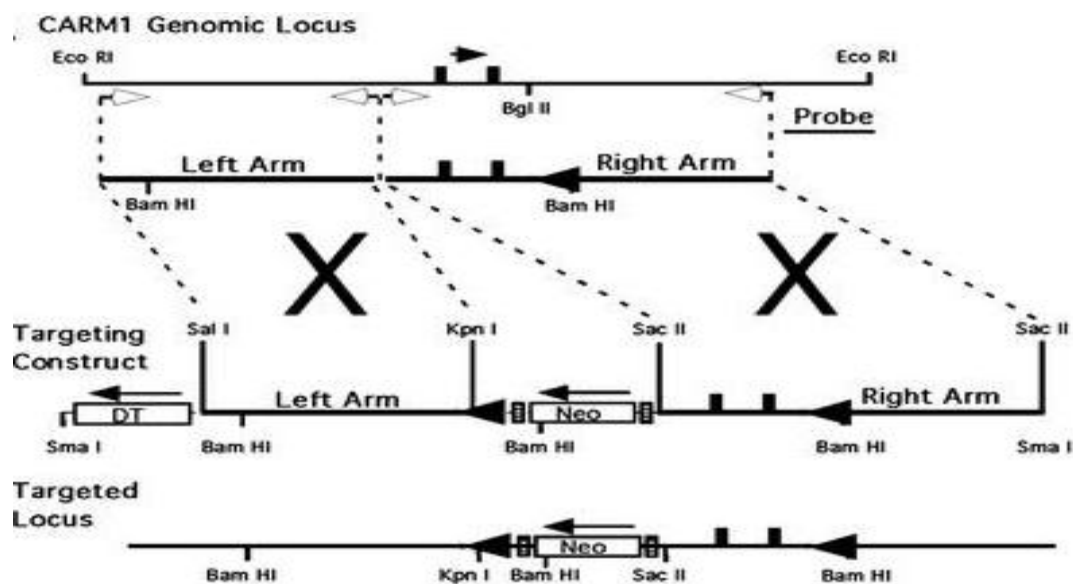


Figure 7: Targeted deletion of *Carm1* exon. A *neo* cassette flanked by *frt* sites was incorporated into the intronic region of *CARM1* gene. Two *Carm1* exons, encoding a segment of the substrate-binding pocket, were floxed. Arrowheads: *loxP* sites, solid boxes: exons, hatched boxes: *frt* sites, filled arrows: direction of transcription and open arrows: position of PCR primers used to generate the arms of the targeting vector construct.

Mice were housed in rooms maintained at constant temperature and humidity with a 12 hour light cycle and were allowed to access rodent laboratory chow and water *ad libitum*. All animal experiments were carried out in strict accordance with the recommendations in the Guide for the Care and Use of Laboratory Animals of the National Institutes of Health. The protocol was approved by the ethics committee of the regional governmental commission of animal protection.

Emphysema was induced by an oropharyngeal application of porcine pancreatic elastase, PPE (Sigma-Aldrich) of 80 U/kg body weight in 80 μ l volume. Control mice (n= 5-6) received 80 μ l sterile phosphate buffered saline, PBS (Gibco). Wild type mice were analyzed on day 2, 28, 56 and 161 and CARM1 haploinsufficient mice were analyzed on day 28. The experiment was repeated twice.

2.2.2 Lung function measurement

Mice were anesthetized with ketamine-xylazine combination solution at the following proportion: 14% Ketamine, 3% xylazine and 83% NaCl by intraperitoneal (i.p.) application at a dosage of 0.1 ml/10 gm body weight of mouse. Once sedated, mice were tracheostomized using an 18 gauge cannula. After intubation, mice were connected to a computer-controlled Biosystem XA forced maneuvers system and a FinePointe RC system (Buxco) or FlexiVent (SCIREQ Inc) to measure lung parameters using a software-generated script. The parameters quantified were Forced Expiratory Volume, (FEV), Functional Residual Capacity (FRC), Total Lung Capacity (TLC), Tiffeneau-index (FEV_{0.1}:FVC ratio), Dynamic compliance/body weight ratio (C_{dyn}/BW) and tissue elastance (E). The analyzed parameters were visible in the software during collection and statistical reporting by treatment group was provided immediately after collection.

2.2.3 Bronchoalveolar lavage (BAL) collection and quantification

BAL was obtained to perform total and differential cell counts for inflammatory cell recruitment of neutrophils, macrophages and lymphocytes. The lungs were lavaged by instilling the lungs with 3 x 0.5 ml aliquots of sterile PBS containing protease inhibitor (Roche). For cytopins, cells were spun down at 400 g and resuspended in RPMI 1640 medium containing 10% (v/v) FBS (both from Gibco). Total cell counts were determined in a hemocytometer via Trypan Blue exclusion using the following equation: Total cells/ml= (Total cells counted / number of square counted) x dilution factor x 10,000 cells/ml.

For cytopin, a volume containing 30,000 cells loaded in a cytofunnel were centrifuged at 400 rpm for 6 minutes in a Shandon Cytospin 2 centrifuge apparatus (Thermo Scientific Shandon). The cytopun cells were stained for 10 minutes in May Gruenwald's eosin-methylene blue solution (Merck). The solution stains the nuclei blue and cytoplasm pinkish-red. Excess stain was removed by placing the slides in tap water for 2 minutes. Subsequently, the slides were incubated in (1:20, vol/vol) Giemsa solution (Merck) 15 minutes. Giemsa solution is a complex consisting of methylene blue chloride, eosin-methylene blue and azure II eosinate. It improves the intensity of nuclear staining and selectively distinguishes cellular structures. Excess stain was removed by incubating the slides in tap water for 2 minutes. Differential cell counts were performed using morphological criteria on stained cytopins (200 cells/sample).

2.2.4 Lung fixation

The lungs were perfused free of blood with PBS through the right ventricle of the heart. The right lung was removed for molecular biology studies whereas the left lung was inflated by an intratracheal instillation of PBS-buffered 6% paraformaldehyde, PFA (Sigma-Aldrich) at a constant pressure of 20 cm fluid column for 10 minutes. For complete fixation, the inflated lungs were stored in PFA at 4°C for at least 24 hours. Afterwards, lungs were embedded in

paraffin for histological and immunohistochemical analysis. Briefly, the lung was placed into 20 ml of 2% (w/v) lukewarm agar and allowed to freeze at 4°C for 1 hour. The lung was sliced into 2 mm thick sections using a cutting apparatus and thinly overlaid with agar in an ice-filled tray. The orientation of lung sections was maintained during the entire cutting procedure. Excess agar was excised once the agar hardened enough. The agar blocks were put in the embedding cassettes and stored in 4% formalin until further processing.

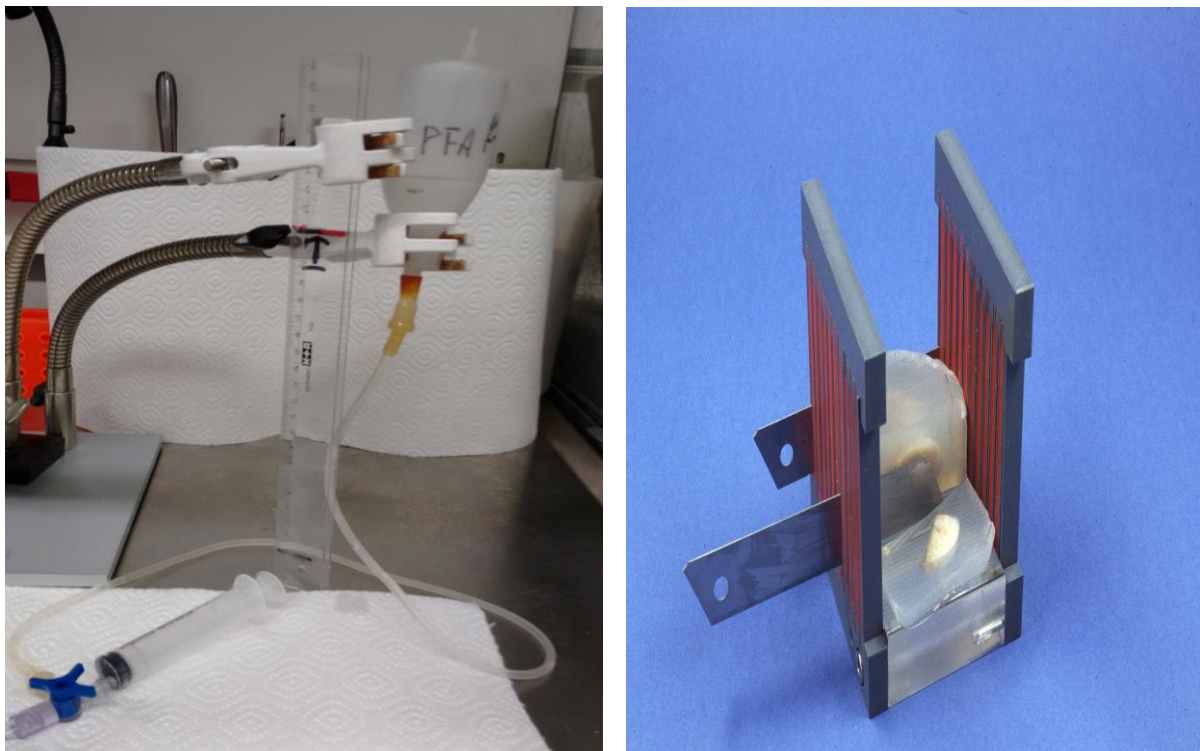


Figure 8: A 20 cm fluid column of PFA (Left) and cutting apparatus for agar block (Right) (Both images adapted from Yildirim lab).

2.2.5 Lung tissue processing: Paraffin embedding

Lungs were embedded in paraffin for histological and immunohistochemical. Briefly, lung sections in individual cassettes were placed in an automatic tissue processor (Leica) for overnight where they undergo serial dehydration through 70%, 80%, 96% (3x), 100% (3x) ethanol. The alcohol was removed by passing the cassettes through Roticlear (2x) (Roth), a less toxic alternative product for xylene. This step rendered the tissue clear. Next, the tissues

were infiltrated by immersion in liquid paraffin wax to saturate the tissue cavities and cells. The lung blocks were embedded again in paraffin in a steel mould and cooled on the cold plate section the embedding apparatus (Thermo Scientific) for 30 minutes for complete solidification before sectioning.



Figure 9: Automatic tissue processor (Left) (Adopted from <http://www.leicabiosystems.com>) and embedding apparatus (right) (Adapted from Yildirim Lab).

2.2.6 Lung tissue sectioning

Before cutting the blocks, they were placed at 4°C for overnight. Lung tissues were manually sectioned using a motorized rotary microtome (Zeiss). Paraffin blocks were placed in the cool block section of a microtome. The cool block maintains temperature at 4°C. The microtome tank was filled with distilled water and the water flow speed was set between 5 and 6 that made the flow suitable for the cut sections to transfer into the water tank. The angle between the paraffin block and the microtome knife was set at 11 degree angle. To access the lung tissue, the blocks were first trimmed by cutting several 10 µm thick sections at speed of 80 mm/sec. Blocks were cut into 3 µm thick sections at the speed of 50 mm/sec. The sections were transferred using a non-charged glass slide into a water bath. There the sections were stretched in hot demineralized water for few seconds. The water temperature was about 10 degrees below the melting point of paraffin (approximately 45°C). Charged slides were used to collect tissue section as the positively charged coating attached to the tissue through

negative charges in the tissue. The slides with sections were placed on a heating plate set at 45°C to dry the slides for at least an hour to ensure adhesion. To evaporate the water and to fix the sections on glass, all slides were kept in incubator at 37°C overnight.

2.2.7 Histological staining: Hematoxylin and eosin (H&E) staining

The H&E staining method involves application of hemalum, which is a complex formed from aluminum ions and hematein, an oxidation product of haematoxylin. Hemalum colors nuclei of cells blue. The nuclear staining is followed by counterstaining with an aqueous or alcoholic solution of eosin, which colors other eosinophilic structures in various shades of red, pink and orange. In the staining protocol, xylene was used as a clearing agent. It is miscible with the embedding medium (paraffin) and the dehydrant (ethanol). Xylene was used at two different stages in H&E staining a) Deparaffinization- removal of paraffin and b) Clearing-displacement of alcohol from the tissue sections with the clearing agent before cover-slipping with mounting media. Firstly, the tissue sections were incubated in xylene for 5 minutes (2x). The sections were passed through an ethanol gradient (ethanol 100% 2x, 90%, 80% and lastly 70%) for 1 minute in each followed by a quick rinse with distilled water to remove ethanol. To stain the nuclei, the tissue sections were stained in Mayer's Hemalaum (Merck) for 5 minutes and rinsed off in running water to get blue in colour. Slides were then stained were dipped in 0,3% HCl-Alcohol (prepared with 70% ethanol) for few seconds to remove excess stain and define nuclei following hematoxylin staining. The step is called the differentiation. The sections were washed in running tap water for 8 minutes and then quickly rinsed in distilled water. Slides were then stained with alcoholic eosin solution for 5 minutes and rinsed off with running water to remove extra staining. A dehydration step was carried out by quickly rinsing the sections in gradient of ethanol (70%, 80%, 90% for few seconds) and in 100% ethanol for 2 minutes (2x). Finally, the slides were cleared in 2 changes of xylene, 5 minutes each. Afterwards tissue sections were manually cover-slipped with 24 x 50 mm cover glasses.

2.2.8 Immunohistochemistry

The paraffin embedded lung sections (3 μ m) were deparaffinized in xylene and rehydrated in alcohol. The tissue was treated with 1.8% (v/v) H₂O₂ solution (Sigma-Aldrich) for 20 minutes to block endogenous peroxidase. Heat induced epitope retrieval was performed in HIER Citrate Buffer (pH 6.0, Zytomed Systems) in a Decloaking chamber (Biocare Medical) set for 30 min at 125°C and 10 min at 90°C. After cooling down, the slides were rinsed in washing buffer, TBS (Zytomed Systems) for 2 minutes each (3x). Nonspecific binding was inhibited with a blocking antibody (Biocare Medical). Tissue sections were incubated overnight at 4°C with primary antibodies against CARM1 (1:150, Abcam), SIRT1 (1:100, Millipore), p16 (1:50, Santa Cruz) and β -galactosidase (1:50, Life Technologies). For negative controls, a rabbit IgG was used instead of primary antibody. The next day following washing steps, tissue sections were incubated afterwards with an alkaline phosphatase-labeled secondary antibody (Biocare Medical) for 1 hour at room temperature. Signals were amplified by a chromogen substrate Vulcan fast red (Biocare Medical). VFR solution was prepared right before incubation (as it is not very stable) by adding 1 drop of Vulcan Fast Red in 2.5 ml of VFR buffer. Tissues were counterstained with hematoxylin for 3 minutes, rinsed in water and incubated in washing buffer for 5 minutes. The sections were dehydrated in ethanol (96% for 1 minute), 100% for 2 minutes (2x) and finally in xylene for 5 minutes (2x).

2.2.9 Immunofluorescence staining

Lung sections were deparaffinized, rehydrated and pressure-cooked in citrate buffer followed by peroxide treatment. After incubation with blocking antibody, the tissue sections were incubated with rabbit polyclonal antibody against Pro-surfactant Protein C (1:100 SP-C, Millipore), CARM1 or SIRT1 followed by 1 hour incubation with donkey anti-rabbit IgG Alexa Fluor 488 labeled secondary antibody (1:250, Invitrogen, Darmstadt, Germany). For nuclear staining, the sections were incubated with 4',6-diamidino-2-phenylindole (DAPI 1:2000, Sigma) in PBS for 1 minute at room temperature.

For the detection of two unlabeled primary antibodies from the same host species (rabbit) we used the following protocol, whereas all incubation steps are at room temperature: the deparaffinized lung sections were blocked with 5% BSA in PBS for 30 min. Then the lung slices were incubated with the primary antibody (Surfactant Protein-C, SP-C) for 2 hours, washed in PBS and then the first antibody was converted into a different host by incubation with a monovalent goat-anti-rabbit Fab fragment (Jackson ImmunoResearch Laboratories, 1:30 in PBS) for 2 hours. The masked antibody complexes were fixed with 4% PFA/PBS for 2 min and subsequently incubated with a donkey anti-goat IgG Alexa Fluor 568 secondary antibody (1:250, Invitrogen, Darmstadt, Germany) for 1 hour. Finally, the lung sections were stained with the rabbit CARM1 or SIRT1 antibodies for 2 hours, washed in PBS, and stained with the secondary donkey-anti-rabbit IgG Alexa Fluor 488 antibody for 1 hour.

2.2.10 Quantitative stereological analysis

2.2.10.1 Quantification of airspace enlargement

An unbiased design-based stereology was used to analyze sections using an Olympus BX51 light microscope equipped with the new Computer Assisted Stereological Toolbox (newCAST, Visiopharm) on HE-stained lung tissue slides as previously described (139). Briefly, a statistical estimate of air space enlargement (the mean free distance in the air spaces) was assessed by quantifying mean linear chord length (L_m) on 30 systemic random fields of view per lung. A line grid was superimposed on lung section images taken using the 20x objective. Intercepts of lines with alveolar septa and points hitting air space were counted to calculate mean chord length, L_m as a measurement of airspace enlargement applying the formula: $L_m = \sum P_{air} \times L(p) / \sum I_{septa} \times 0.5$, where, P_{air} are the points of the grid hitting air spaces referring to the volume of air space, $L(p)$ is the line length per test point (99.3 μm as we measured) and I_{septa} is the sum of intercepts of alveolar septa with grid lines referring to the alveolar surface area.

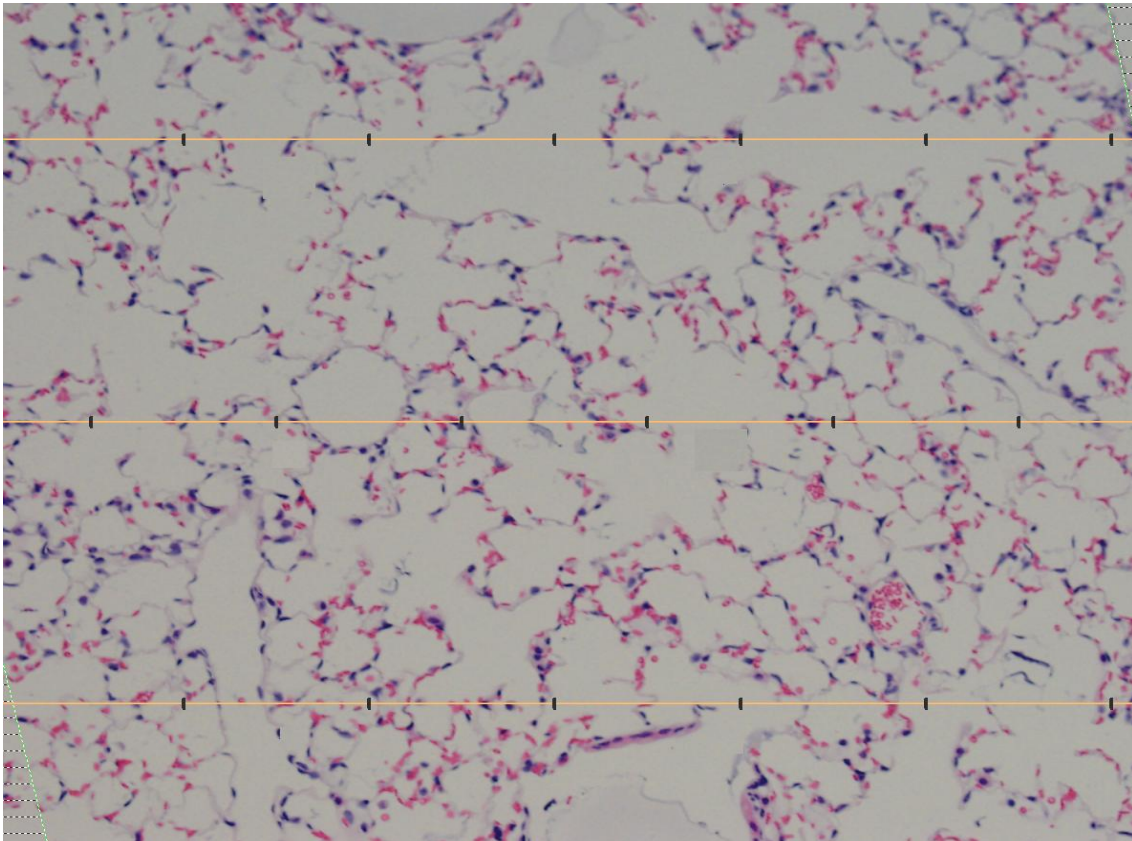


Figure 10: A grid with points and lines was superimposed on each lung tissue section where points (black points on orange line segments) representing alveolar air space volume (ΣP_{air}) were counted. Additionally, the total number of intercepts of the line segments (orange lines) intercepting the alveolar septal surfaces (ΣI_{septa}) were counted. This image is a screenshot of CAST system.

2.2.10.2 Quantification of CARM1 or SIRT1 positive alveolar epithelial cells

To quantify the percentage of CARM1 positive alveolar epithelial cells with newCAST (Visiopharm), 30 systemic random fields of view per lung was chosen. A frame grid was superimposed on lung section images taken using the 40x objective. Within the frame, alveolar epithelial cells either positive or negative for CARM1 staining were counted and the percentage of CARM1 positive alveolar epithelial cells was calculated.

Same method was applied to calculate the percentage of SIRT1 positive alveolar epithelial cells in the lung.

2.2.10.3 Quantification p16 positive alveolar epithelial cells

To quantify p16 positive cells a semi-quantitative manual scoring system was applied. Each lung tissue stained with p16 antibody was scored on a scale from 0–5 where 0 = no positive cells, 1= lowest, 2= moderate, 3= considerable, 4= marked and 5 = highest frequency of p16 positive cells.

2.2.10.4 Quantification of SP-C positive alveolar epithelial cells

Images of SP-C stained lung sections were taken with an AxioObserver.Z1 inverted microscope (Zeiss) using a Plan-Apochromat 20x/0.8 M27 objective. The automated microscopy system was driven by Axiovision 4.8 (Zeiss). For each condition 5 images were taken. The acquired data sets were imported into Imaris 7.6.5 software (Bitplane). Then, the spot detection algorithm of the Imaris software was used to assign a spot for each fluorescent intensity of DAPI stained nuclei and Pro-SPC stained cells. Finally, the number of spots was read out by the Imaris' statistics module.

2.2.11 Quantitative real time RT-PCR

2.2.11.1 Homogenization and lysis

a) Tissue

The right lung tissue was homogenized using a micro dismembrator (Sartorius). Briefly, frozen tissues in cryogenic gyrotubes containing grinding balls were placed in a pre-cooled Teflon shaking device and shaken at 3000 rpm for 1 minute. A major amount of powder was collected and frozen at -80°C for later protein isolation. Roti-Quick 1 (Roth), a tissue lysis buffer was added to the remaining tissue powder and vortexed till the powder dissolved in suspension. The liquid was used for immediate RNA extraction or frozen at -80°C for later extraction. A Phenol-Chloroform extraction step was carried out to eliminate proteins. Briefly, following the addition of Roti-Quick 2 solution (Roth) to each homogenized sample solution,

the tubes were incubated on ice for 10 minutes and vortexed every 2 minutes. The samples were then centrifuged at 13000 rpm at 4°C for 15 minutes.

b) ATII-like LA-4 monolayer cells

For lysis of cells grown in monolayer, the culture medium was completely aspirated. The cells were twice washed with PBS. RNA Lysis Buffer T (PepqLab) was added to the cells and the lysate was transferred in a DNA Removing Column (PepqLab) placed in a 2.0 ml Collection Tube and centrifuged at 12000 rcf for 1 min at room temperature. The flow-through lysate was used for RNA extraction.

2.2.11.2 RNA isolation and concentration determination

The total RNA was isolated from lung tissue homogenate or cell lysate using peqGOLD Total RNA kit (PepqLab, Erlangen, Germany) according to the manufacturer's instructions and all steps were performed at room temperature. Briefly, an equal volume of 70% ethanol was added to the supernatant got from tissue or cells and vortexed. A volume of 750 µl solution was taken in a PerfectBind RNA-binding column placed in collection tube and was centrifuged at 10000 rcf for 1 minute. This step was repeated using the remaining solution. The RNA-binding columns were washed with RNA Wash buffer 1 and centrifuged at 10000 rcf for 15 seconds. To remove DNA a DNase digestion solution was applied onto the membrane of RNA-binding columns, incubated for 15 minutes and then washed again with RNA wash buffer 1. Following 5 minute incubation, the tubes were centrifuged at 10000 rcf for 15 seconds. The columns were washed with RNA Wash Buffer 2 and centrifuged for 15 sec at 10000 rcf. To completely remove ethanol, the RNA column placed in collection tube was centrifuged for 2 min at 10000 rcf. For eluting the extracted RNA, sterile RNase-free dH₂O was added directly onto the membrane of the columns and centrifuged for 1 min at 5000 rcf. The eluted RNA was either taken for concentration determination or kept at -80°C for long term storage.

The RNA concentration was determined using the NanoDrop 1000 (Peqlab). The optimum range of the NanoDrop spectrophotometer is 2-3700 ng/μl. A volume of 1 μl of sample RNA was pipetted onto the pedestal and measured. A blank test was performed with sterile RNase-free water before measuring the RNA concentration. The purity was determined by calculating the ratio of absorbance at 260 nm and 280 nm. Volume needed for 1 μg of RNA was calculated from the determined concentration for cDNA preparation.

2.2.11.3 cDNA synthesis

It is the reverse transcriptase-mediated synthesis of single-stranded DNA (complementary DNA or cDNA) using single-stranded RNA as template. A volume equivalent to 1 μg of RNA was added to DNase-RNase free water to prepare a total of 20 μl volume and denatured at 70°C for 10 minutes on a heating block (Haep Labor Consult). A master mix of 20 μl was prepared from the GeneAmp RNA PCR kit (Applied Biosystems) as following:

Table 13:

<i>Reagents</i>	<i>Volume</i>
10x PCR Buffer II	4.0 μl
25mM MgCl ₂	8.0 μl
10mM each type of dNTPs	2.0 μl
50μM Random Hexamers:	2.0 μl
ddH ₂ O	1.0 μl
10U RNase Inhibitor:	1.0 μl
50U MuLV Reverse Transcriptase	2.0 μl

The 10x PCR Buffer II provided the optimal pH and ionic strength for PCR amplification. A separate MgCl₂ solution was used together with the buffer to optimize the magnesium ion concentration to achieve optimal PCR amplification with any specific set of primers and DNA

template. The dNTPs consisted of dATP, dCTP, dGTP, and dTTP. Random Hexamers used were short oligodeoxyribonucleotides of random sequence [d(N)₆] that annealed to random complementary sites on a target RNA to serve as primers for DNA synthesis by reverse transcriptase. RNase Inhibitor (ribonuclease inhibitor) was a 50 kDa recombinant enzyme used to inhibit RNase activity to prevent the degradation of RNA template. It does not contain DNase or endonuclease activity. MuLV (Murine Leukemia Virus) reverse transcriptase in the master mix was a recombinant RNA-dependent DNA polymerase that used single-stranded RNA as a template in the presence of a primer to synthesize a complementary DNA (cDNA) strand. The reverse transcription was carried out in PCR cycler (Bio-rad) following the thermal conditions in a thermal cycler:

- 10 min at 20°C to extend random primers or oligo (dT) primers; without the incubation primers may dissociate from the template at higher temperature;
- 75 min at 43°C for reverse transcription;
- 5 min at 99°C to terminate the reaction.

The cDNA was cooled down to 4 °C, diluted with ddH₂O to a final volume of 100 µl and stored at -20°C.

2.2.11.4 Amplification of cDNA

Quantitative real-time PCR was performed using Platinum SYBR Green qPCR SuperMix (Applied Biosystems, Darmstadt, Germany) on a StepOnePlus™ 96 well Real-Time PCR System (Applied Biosystems, Carlsbad, CA). HPRT1 (Hypoxanthine-guanine phosphoribosyltransferase) was used as a reference housekeeping gene in all qRT-PCR reactions. The mRNA expression of target genes was determined in comparison to HPRT1. Primers used are listed in Table 10. Relative gene expression presented as $2^{\Delta Ct}$ ($\Delta Ct = Ct_{reference} - Ct_{target}$) and relative change to control as $2^{\Delta\Delta Ct}$ ($\Delta\Delta Ct = \Delta Ct^{control} - \Delta Ct^{treated}$). Primers were generated using NCBI Primer-BLAST software. For PCR master mix, the following reagents were added to cDNA-Template 2 µl to a total volume of 25 µl:

Table 14:

Reagents	Volume
Sybr Green Buffer	13 μ l
MgCl ₂ (50mM)	1 μ l
Primer mix (forward and reverse)	1 μ l (0.5 μ l +0.5 μ l)
dH ₂ O	8 μ l

Sybr Green Buffer mix (Thermo Scientific) contained SYBR Green I fluorescent dye, Platinum Taq DNA polymerase, Magnesium ion, uracil-DNA glycosylase (UDG), proprietary stabilizers, and deoxyribonucleotide triphosphates (dNTPs). SYBR Green I was a fluorescent dye that binded directly to double-stranded DNA (dsDNA). The primer pairs used in the reaction were 20-22 base pair long with melting temperature between 57 to 60°C and with 40-60% GC content. The maximum single nucleotide repeat was 4 base pair long. A negative control that contained all reagents but not the template DNA was used as no template control or NTC. The PCR was performed in Step One plus PCR system using the following thermal profile:

Table 15:

Holding/pre-incubation Stage:	Step 1:	2 min for 50 °C
	Step 2:	5 min for 95 °C
Cycling Stages (44 cycles):	Step 1:	5 sec for 95 °C
	Step 2:	5 sec for 59 °C
	Step 3:	30 sec for 72 °C
Melt Curve Stage:	Step 1:	15 sec for 95 °C
	Step 2:	1 min for 60 °C
	Step 3:	15 sec for 95 °C

2.2.12 Western blot

2.2.12.1 Protein isolation and concentration determination

Protein extraction from lung tissue and cell lines was performed using RIPA buffer containing 1:25 Complete Mini Proteinase Inhibitors (Roche) and 1:100 of 100mM Natrium-orthovanadat (New England Biolabs) and shortly vortexed time to time. The samples were centrifuged for 15 min at 4°C at 13000 rpm. The supernatant was taken to measure protein concentration.

A volume of 10 µl from of each standard or supernatant of unknown sample replicate was pipetted into a 96-well microplate. A total of 200µl substrate solution (reagent A: reagent B = 50:1) from Pierce BCA Protein Assay kit (Thermo Scientific) was added to it. The assay uses the formulation based on bicinchoninic acid (BCA) for the colorimetric detection and quantitation of total protein. BCA is a weak acid composed of two carboxylated quinoline rings. In BCA assay, two molecules of bicinchoninic acid chelate a single Cu⁺ ion, forming a purple water-soluble complex. Reagent A contained sodium carbonate, sodium bicarbonate, BCA and sodium tartrate in 0.1M sodium hydroxide while BCA Reagent B contained 4% cupric sulfate. The protein concentrations were determined using a reference protein such as bovine serum albumin (BSA) as a standard. A series of dilutions of known concentration were prepared from the BSA and assayed alongside the protein sample of unknown concentration before the concentration of each unknown is determined based on the standard curve. The plate was incubated at 37°C for 45 minutes for reactions to take place. In the first reaction, copper was chelated by protein and formed a light blue complex. Secondly, the BCA reacted with the reduced (cuprous) cation formed in step one and resulted in an intense purple-colored product from the chelation of two molecules of BCA with one cuprous ion. The BCA/copper complex showed a linear absorbance at 570 nm with increasing protein concentrations measured using a microplate reader (Perkin Elmer).

2.2.12.2 SDS-PAGE run and blotting

A volume of 20 µg of protein was mixed with Laemmli loading buffer (Biorad) and was boiled at 95°C for 10 minutes at 300 rpm on Thermomixer (Eppendorf). Samples were loaded in a 10% or 12% Mini-PROTEAN pre-cast gel (Biorad) and run at constant electric current (about 40mA per chamber) and at 120V for 1 hour. A ladder, Precision Plus Protein Standard (Biorad) used as a molecular weight marker for identification of protein of interest.

To transfer/blot the gel was assembled in a sandwich in a Transblot cassette (Bio-Rad) and run in 1x transfer buffer for 1 hour at 100V. Following the transfer, the membrane was incubated in blocking buffer (5% milk solution in PBS) for 1 hour at room temperature to block unspecific binding sites. After blocking, the membrane was incubated with antibodies against CARM1 (1:750, Abcam), anti-phospho-CARM1 (1:500, Abnova), anti-SIRT1 (1:1000, Millipore), anti-p16 (1:200, Santa Cruz), anti-p21 (1:200, Santa Cruz) and anti-T1α (1:4000, R&D, Minneapolis, Minnesota, USA) in 1:5 diluted blocking buffer for overnight at 4°C. Next, the membrane was incubated with a horseradish peroxidase (HRP)-linked anti-rabbit secondary antibody for 1 hour at room temp. An anti-β-actin antibody (Sigma-Aldrich) was used as loading control.

2.2.12.3 Signal development and quantification

The signal from protein bands were visualized by developing the membrane using Amersham ECL Prime Western Blotting Detection Reagents (GE Healthcare). The two detection reagents from the kit when mixed in 1:1 proportion functioned as the substrate for horseradish peroxidase (HRP) linked onto the secondary antibody. The signal was detected on a Chemidoc XRS system (Bio-Rad). A densitometric analysis was performed on the developed signals using ImageLab software (Bio-Rad) and the value was normalized to that of β-actin.

2.2.13 Cell culture

2.2.13.1 Condition and maintenance

The mouse lung epithelial cell line LA-4 (ATCC) which exhibits an alveolar epithelial type II like phenotype (275) and adherent in nature was cultured in Ham's F12K medium (Biochrom) containing stable glutamine with 1.176 g/l NaHCO₃ and with 10 mg/l phenol red. The medium was further supplemented with 15% fetal calf serum (Gibco), 1% non-essential amino acids (Biochrom), 1% Penicillin-Streptomycin (Biochrom). The cells were maintained in 75 cm² flasks at 37°C incubator and subcultured in a ratio of 1:3, twice per week. The cells were used for siRNA transfection, wound healing assay and beta-galactosidase assay and cigarette smoke extract treatment.

2.2.13.2 siRNA transfection

For siRNA application, 4x10⁴ cells in 500 µl per well were seeded in 24-well plates 24 hours prior to transfection. 50 nM CARM1-specific siRNA (siCARM1-2 and siCARM1-5) (Qiagen) was mixed with 4.5 µl HiPerFect transfection reagent (1:22) (Qiagen) in a serum-free medium mixed thoroughly by vortexing and incubated for 10 min at room temperature to allow the formation of transfection complexes. HiPerFect is a mixture of cationic and neutral lipids that enables effective siRNA uptake and efficient release of siRNA inside cells. AllStars Negative Control siRNA (Qiagen) was used as the scrambled (Scr) siRNA. This siRNA has no homology to any known mammalian gene. Non-transfected cells were taken as control. The siRNA/HiPerfect complex was added in a drop-wise manner onto the cells and the plate was gently swirled to ensure uniform distribution of the transfection complexes. The cells were incubated at 37°C under their normal growth conditions. The incubation was for 48 hours to allow an effective knockdown of CARM1 expression. The medium was changed as required to avoid cytotoxicity from dead cells.

2.2.13.3 Wound healing assay

The wound healing assay allows studying cell migration and cell proliferation. The assay is compatible with adherent cells. In order to perform a wound healing assay, a scratch wound was induced by applying a scratch using a 200 μ l pipette tip after 48 hours of siRNA transfection. While scratching the pipette tip was kept under an angle of around 30 degree. Images of the wound were taken after 0 and 16 hours after scratch application. The percentage of gap closure was determined by analyzing a defined area of the wound area using Axiovision software (Zeiss).

2.2.13.4 Senescence-associated β -galactosidase (SA- β -gal) Staining

The staining was performed using a kit (Cell signaling) designed to detect β -galactosidase activity at pH 6, a known feature of senescent cells not found in pre-senescent, quiescent or immortal cells. The assay was carried out after 48 hours of transfection with siCARM1-2 or 5 or scrambled siRNA. Cells treated with 100 μ M H₂O₂ (Sigma-Aldrich) for 1 hours were taken as positive control. Low concentration of H₂O₂ is a known inducer of senescence (276). Cells in each well of a 24-well plate were washed with PBS. Cell samples were fixed for 10 minutes at room temperature with a fixative solution. An amount of 20 mg of 5-bromo-4-chloro-3-indolyl- β -D-galactopyranoside (X-gal) powder was dissolved in 1 mL DMF (Roth) to prepare a 20X (20 mg/ml) stock solution. The cells were incubated with β -galactosidase staining solution at 37°C overnight in a dry incubator (no CO₂). While the solution was still on the plate, the senescent cells were identified by a light microscope as blue or bluish green stained cells. For quantification, a total of 300 cells were counted in 10 random fields per well to determine the percentage of SA- β -gal positive cells.

2.2.13.5 Preparation of cigarette smoke extract

Research grade cigarettes 3R4F were obtained from the Kentucky Tobacco Research and Development Center at the University of Kentucky. Cigarette smoke extract (CSE) was

prepared by bubbling smoke from three cigarettes into 30 ml serum-free media at a rate of 1 cigarette per 5 minutes. This stock was considered as 100% CSE extract (155). CSE was freshly prepared for each experiment and immediately diluted to 5% with culture medium Ham's F12K medium (Biochrom) supplemented with 15% FBS.

2.2.14 Alveolar epithelial type II cell isolation and culture

Primary mouse ATII cell isolation was performed as described previously (278). In brief, mouse lungs were lavaged with 500 μ l sterile PBS twice and flushed through the right heart with 0.9% NaCl solution. Lungs were inflated with Dispase (BD Bioscience, San Jose, CA, USA) and incubated in Dispase (BD Bioscience) for 45 min at room temperature. Subsequently lungs were minced and filtered through 100 μ m, 20 μ m and 10 μ m nylon meshes (Sefar) and centrifuged at 200 g for 10 minutes. The cell pellet was resuspended in DMEM cell culture medium (Sigma-Aldrich). Negative selection for macrophages and lymphocytes was performed with antibodies against CD45 and CD16/32 (both BD Bioscience). Non-adherent cells were collected and negative selection was performed for fibroblasts by adherence for 25 minutes on cell culture dishes. Cell purity was assessed by immunofluorescence staining for pro SP-C, panCK, T1 α , CD45, CD31 and α SMA. Cells were resuspended in DMEM containing 10% FCS, 2 mM L-glutamine, 100 U/ml penicillin, and 100 g/ml streptomycin, 3.6 mg/ml glucose, and 10 mM HEPES (PAA Laboratories) and cultured up to 5 days in a humidified atmosphere of 5% CO₂ at 37°C with a medium change at every other day.

2.2.15 Statistical analysis

Mean values \pm SD are given unless stated otherwise. Student's unpaired t-test was used to compare two groups, and one-way ANOVA following Bonferroni post-test was used for studies with more than two groups, if equal variances and normal distribution was given. Analyses were conducted using Prism 5 software (GraphPad).

3. RESULTS

3.1 Progressive Lung Emphysema Development in Mice Exposed to Porcine Pancreatic Elastase

To investigate the underlying mechanism of emphysema development and progression, we first established a mouse model of emphysema using the porcine pancreatic elastase (PPE). Elastase is a well-established tool as it induces irreversible changes in lung structure and function (139, 140). Emphysema was induced in wild type C57BL/6 mice via oropharyngeal application of porcine pancreatic elastase (PPE) of 80 U/kg body weight in 80 μ l volume and analyzed on day 2, 28, 56 and 161.

3.1.1 Analysis of lung function

The pathological changes were monitored using pulmonary function tests. First significant signs of emphysema became detectable by an increased forced vital capacity (FVC) at day 2 (Figure 11A). Significant increases in forced residual capacity (FRC), total lung capacity (TLC) as well as in dynamic compliance (C_{dyn}) represented a time dependent progressive emphysematous phenotype after elastase application (Figure 11B-D). In addition, a decrease in Tiffeneau index (defined by the ratio of forced expiratory volume of 0.1 seconds (FEV_{0.1}) to FVC) and in elastance (E) until day 161 further confirmed further confirmed elastase-induced emphysema progression in mice (Figure 11E-F).

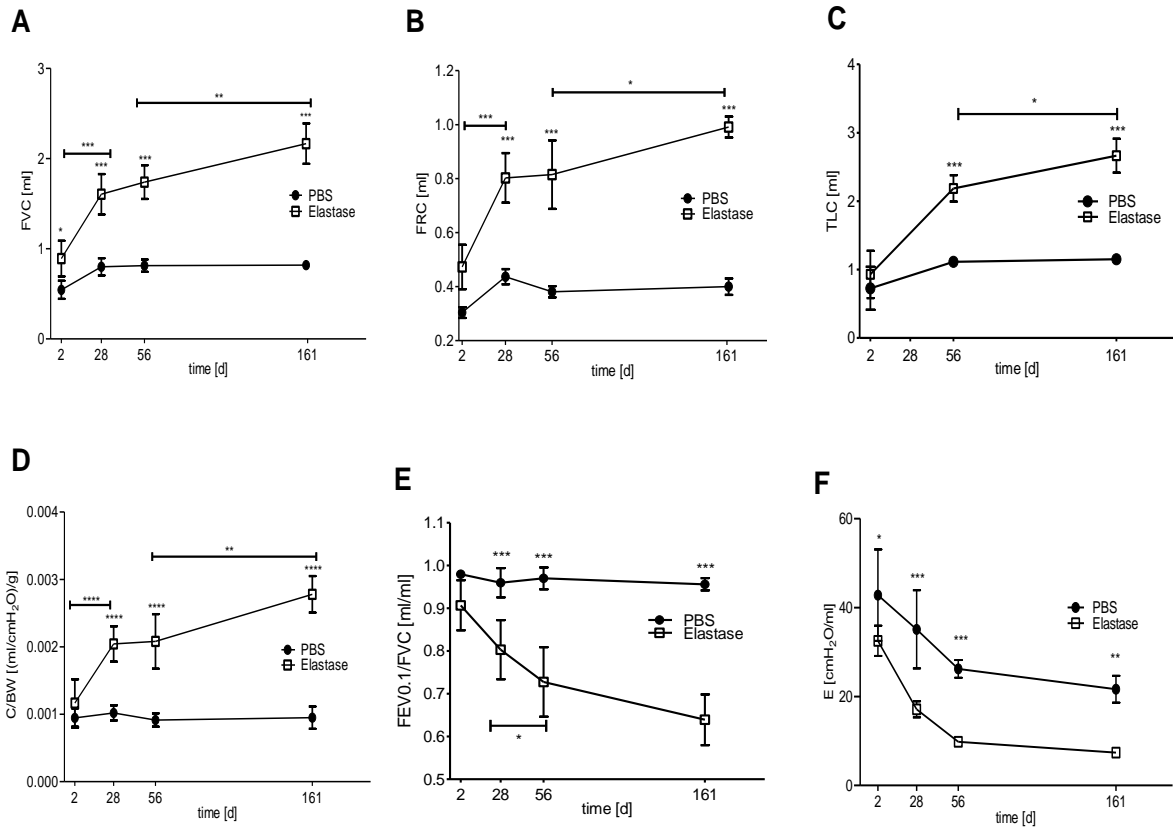


Figure 11. Analysis of elastase-induced impairment of lung function. Pulmonary function tests (A) Forced Expiratory Volume, FVC (B) Functional Residual Capacity, FRC (C) Total Lung Capacity, TLC (D) Dynamic compliance/body weight ratio (Cdyn/BW) (E) Tiffeneau-index, FEV0.1/FVC measured with Buxco forced maneuvers system and (F) Tissue elastance measured with flexiVent by SCIREQ, * $p < 0.05$, ** $p < 0.01$, *** $p < 0.001$, 1-way ANOVA followed by Bonferroni post-test, PBS vs. elastase-treated animals. Data presented are mean \pm SD. The experiments were repeated twice ($n = 5-6$).

3.1.2 Increased airspace enlargement

To confirm that lung function impairment accompanied with early inflammation in BAL were an outcome of lung architecture destruction, next we analyzed lung histology. Hematoxylin and Eosin (H&E) stained lung tissue sections revealed a continuous progression of emphysema in elastase-treated mice compared to control mice (Figure 12A). As a direct measure of emphysema severity, the airspace enlargement was quantified by a quantitative morphometry of mean chord length (Lm) using computer assisted stereology toolbox, newCAST system (Visiopharm) (Figure 12B). The mean chord length (Lm) indeed confirmed a time dependent enhancement of airspace which directly correlated with a significant

increase in dynamic lung compliance following elastase treatment compared to PBS-treated animals (Figure 12C).

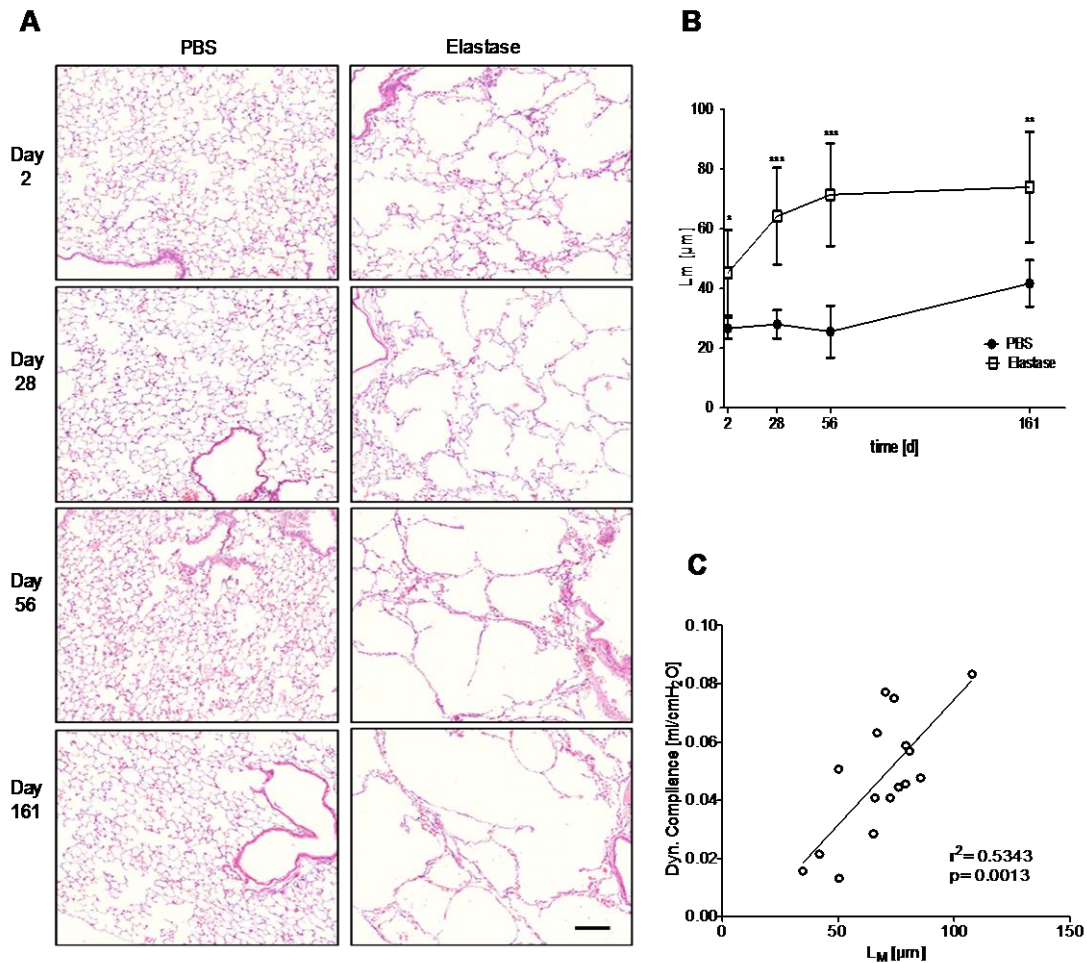


Figure 12. Stereological analysis of elastase induced emphysema progression. (A) Representative histological images from H&E stained lung sections. Scale bar: 200 μm, (B) Mean chord length (L_m) quantified by stereological analysis system, newCAST to determine airspace enlargement, (C) Positive correlation between dynamic compliance and L_m, *p<0.05, **p<0.01, ***p<0.001, 1-way ANOVA followed by Bonferroni post-test, PBS vs. elastase-treated animals. Data presented are mean ± SD. The experiments were repeated twice (n=5-6).

3.1.3 Analysis of bronchoalveolar lavage (BAL) cells

Next, we examined the inflammatory cell profile by performing bronchoalveolar lavage of elastase-treated and PBS-treated mouse lungs. Mice that received elastase showed increased total cell counts in bronchoalveolar lavage (BAL) fluid on days 2 to 28 (Figure 13A), originating mainly from significant increases of macrophages (Figure 13B). Neutrophil

levels substantially significant on day 2 only, while lymphocyte counts were elevated from days 7 to 21 (Figures 13C and D, respectively). No signs of inflammation could be detected in BAL fluid on days 56 or 161. Interestingly, we could not observe lung tissue inflammation at any time suggesting that emphysema progression at later time points was inflammation-independent.

Taken together, the data demonstrated that a single application of elastase induced progressive pulmonary emphysema in mice as evident by the time dependent lung function decline, early inflammatory response and gradual airspace enlargement.

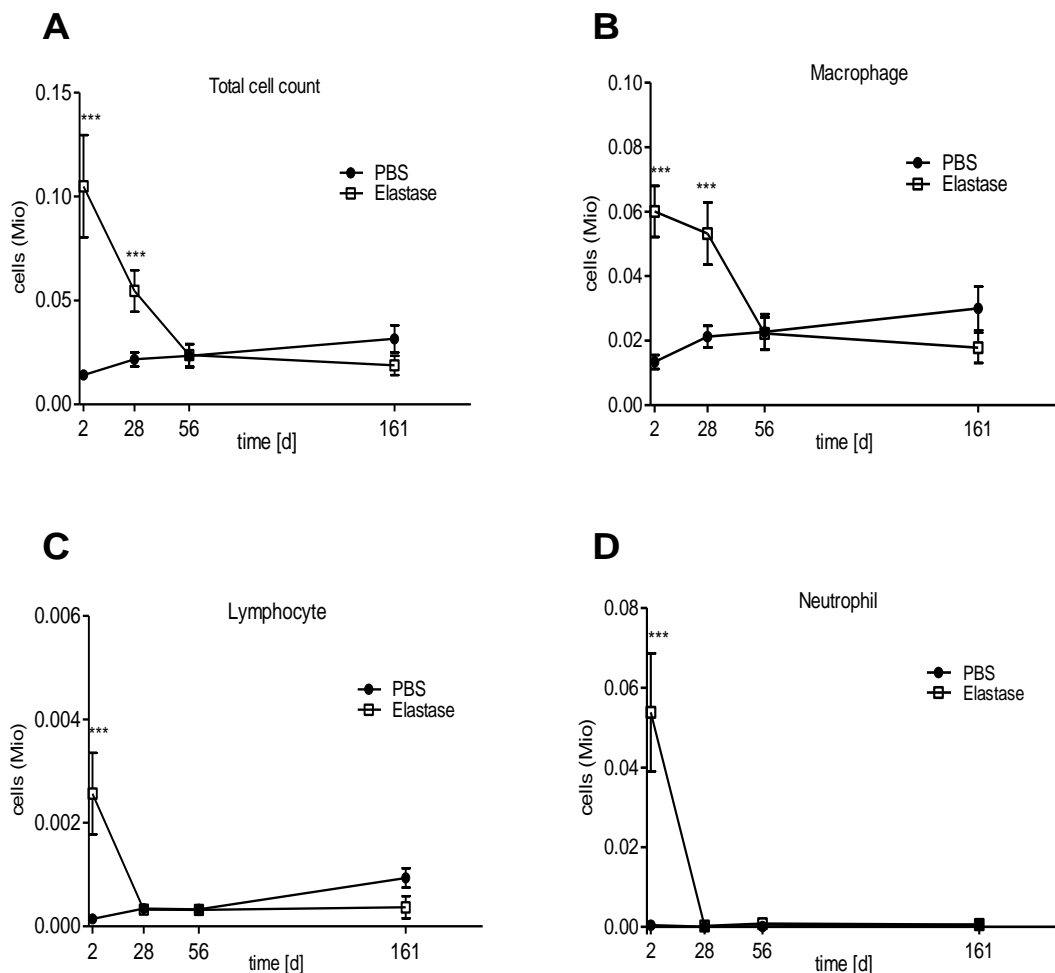


Figure 13. Characterization of elastase induced emphysema mouse model. Mice were lavaged with 2x 500 μ l PBS. (A) Total inflammatory cell counts (B) Number of macrophage, (C) Neutrophils and (D) Lymphocytes, * $p < 0.05$, ** $p < 0.01$, *** $p < 0.001$, 1-way ANOVA followed by Bonferroni post-test, PBS vs. elastase-treated animals. Data presented are mean \pm SD. The experiments were repeated twice ($n = 5-6$).

3.2 Reduced CARM1 Expression and Activity in Emphysematous Lungs

3.2.1 CARM1 downregulation in mouse lung homogenate

There is evidence that the CARM1^{-/-} neonates are unable to inflate the lung with air due to an abnormal alveolar air space demonstrating the involvement of CARM1 in lung morphogenesis (232). Besides, CARM1 is also required for proper regulation of proliferation and differentiation of alveolar epithelial cells during lung development (251). These crucial reports drove us to assess the expression of CARM1 in the elastase-treated emphysematous lungs. We noticed a significant downregulation of CARM1 at mRNA level starting from day 28 (* $p < 0.05$). The expression level showed further decrease till day 161 (** $p < 0.001$) compared to time matched PBS-treated animals (Figure 14).

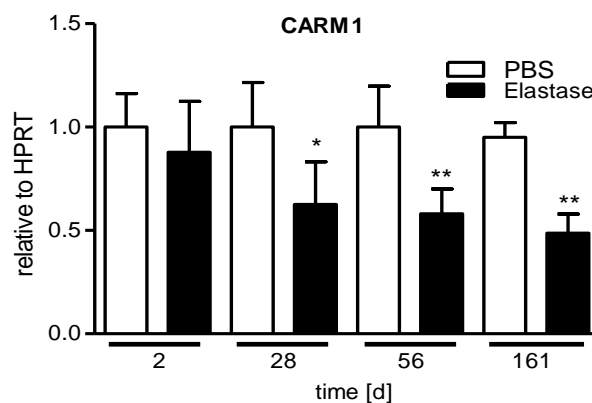


Figure 14. Downregulation of CARM1 expression in emphysematous mouse lung. RNA extracted from whole lung homogenate. Reverse-transcribed cDNA amplified by quantitative real time PCR (qRT-PCR). CARM1 expression at mRNA level in elastase-treated mouse lung compared to PBS treated animals at day 2, 28, 56 and 161, * $p < 0.05$, ** $p < 0.01$, student's *t*-test, PBS vs. elastase treated animals. Data presented are mean \pm SD. The experiments were repeated twice ($n=5-6$).

3.2.2 Reduction of CARM1 positive alveolar epithelial cells

Next, we attempted to identify the cell type that reduces the expression of CARM1 in the emphysematous lung. To address this question, we performed immunohistochemistry using antibody against CARM1 (Figure 15A) and quantified the CARM1-stained lung sections using the newCAST system.

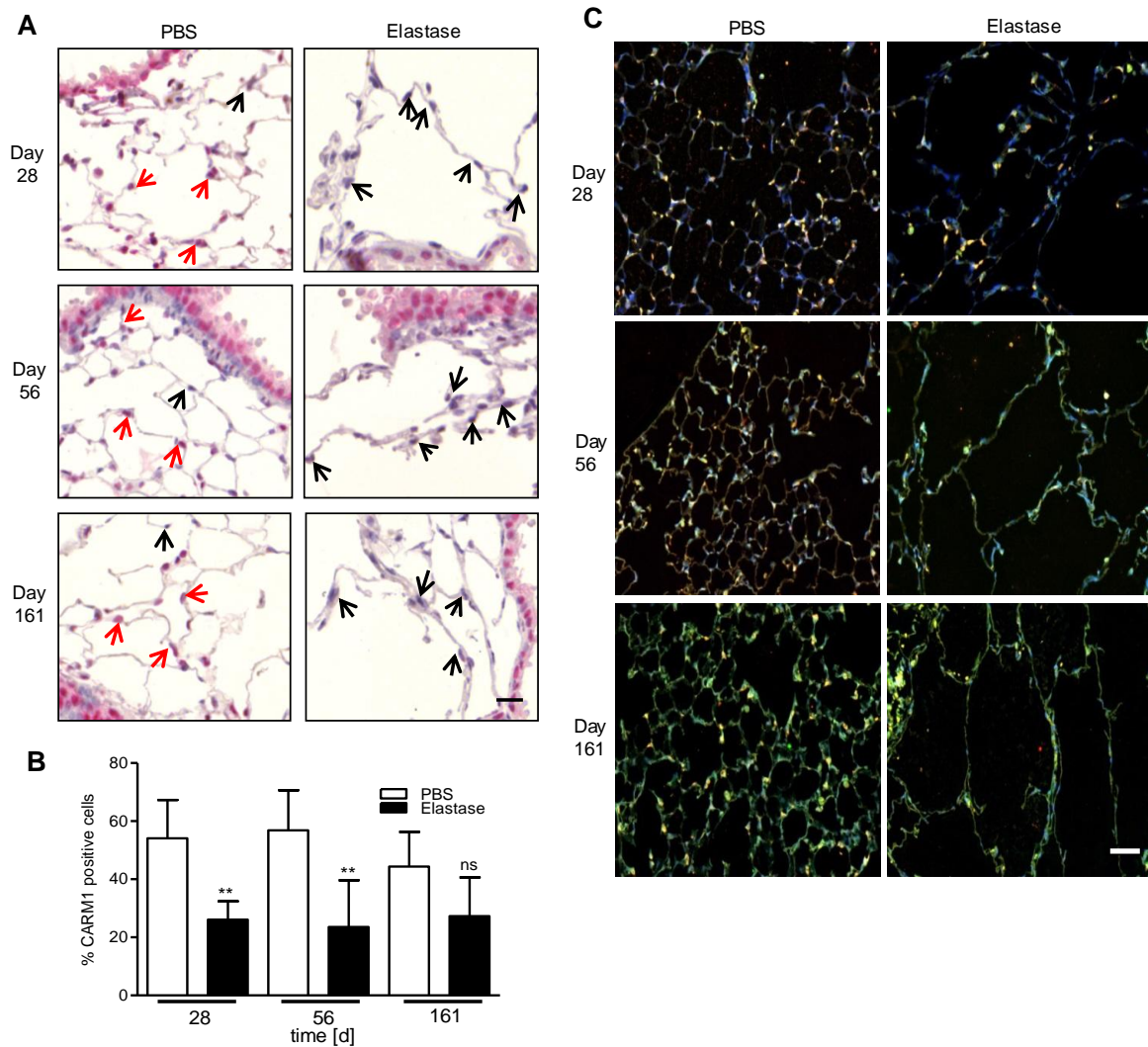


Figure 15. Elastase treatment reduced CARM1 staining in alveolar epithelial cells. (A) Representative images of immunohistochemistry against CARM1 antibody (1:150). Red arrow: positive staining, black arrow: negative staining. Scale bar: 20 μm , (B) Quantification of CARM1 positive alveolar epithelial cells by newCAST stereology system. (C) Representative images from immunofluorescence double staining against CARM1 (1:150) and ATII-specific SP-C (1:100) antibodies. Green: SP-C positive ATII cells, Red: CARM1 positive cells, Yellow (merged): CARM1 and SP-C double positive ATII cells. Scale bar: 10 μm , ** $p < 0.01$, student's *t*-test, PBS vs. elastase treated animals. Data mean \pm SD. Experiments were repeated twice ($n=5-6$).

Quantification revealed a significantly reduced percentage of CARM1 positive alveolar epithelial cells at day 28 and day 56 (** $p < 0.01$) (Figure 15B). In addition, we detected that at day 161, PBS-treated animals showed reduced CARM1 positive SP-C cells, which we speculated as an aging effect in these mice. We did not observe any difference for airway

epithelial cells in elastase-treated mice compared to PBS-treated animals. Furthermore, to confirm that CARM1 was indeed expressed in ATII cells, we conducted a double staining for CARM1 and alveolar epithelial cell type II (ATII) marker SP-C and clearly showed that ATII cells lost CARM1 staining following elastase treatment (Figure 15C).

3.2.3 Elevation of CARM1 phosphorylation

Post-translational modification acts as a molecular switch for controlling CARM1 enzymatic activity as evident by phosphorylation at a specific serine residue inactivating CARM1 (245). Therefore, we analyzed the levels of phosphorylated CARM1 compared to unmodified native CARM1 levels in the lung homogenate of wild type and elastase-treated mice using western blot.

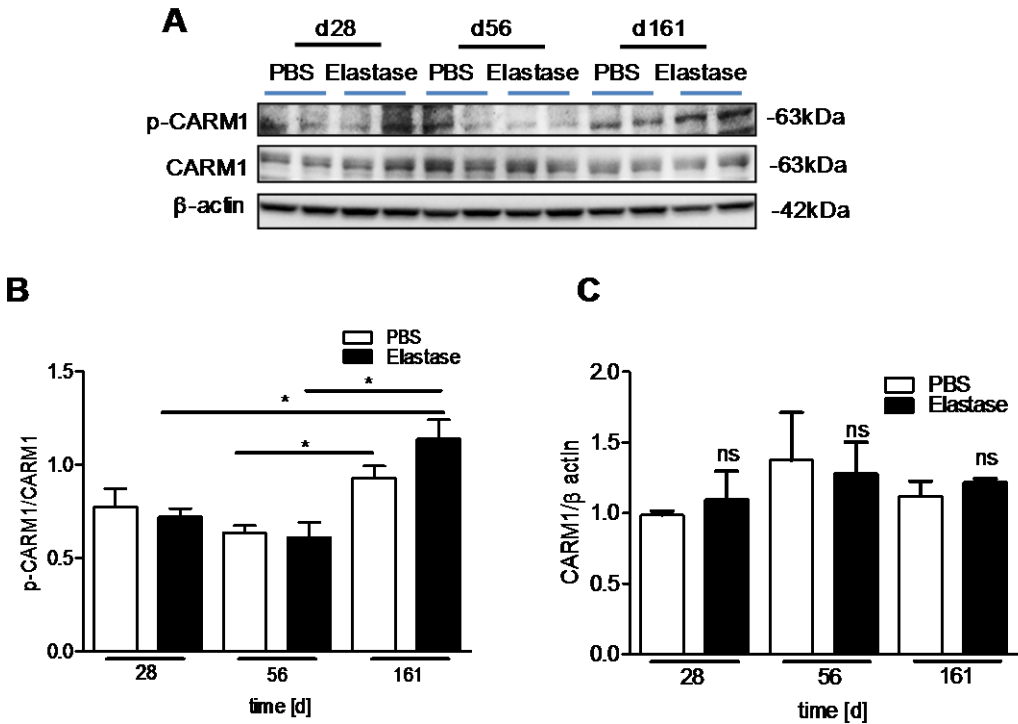


Figure 16. Effect of elastase on CARM1 phosphorylation. (A) Representative western blot for levels of phospho-CARM1 in lung homogenate. β -actin was used as loading control. The size of each band is indicated on the right. (B) Densitometric analysis of western blot for phospho-CARM1, * $p < 0.05$, ** $p < 0.01$, student's *t*-test, PBS vs. elastase-treated animals. Data presented are mean \pm SD. The experiments were repeated twice ($n = 5-6$).

We observed an age-dependent increase in phosphorylation of CARM1 at day 161 in PBS-treated animals. Furthermore, following elastase treatment, we detected a significant increase in phospho-CARM1 levels at day 161 compared to day 28 and day 56 (Figure 16A-B) indicating that the effect of elastase on CARM1 phosphorylation occurs only at later time points. However, we did not observe a regulation of CARM1 protein expression among different time points (Figure 16C).

Taken together, these data demonstrated that emphysema progression is associated with a downregulation of CARM1 expression in lung alveolar epithelial cells and a reduction of global CARM1 activity in lung.

3.3 CARM1 Haploinsufficiency Leading to Enhanced Elastase-induced Emphysema in Mouse Lungs

3.3.1 CARM1 haploinsufficient mice showed significantly reduced level of CARM1

As complete loss of CARM1 exhibits neonatal lethality, we therefore considered CARM1 haploinsufficient mice in order to understand whether a significant deficiency of CARM1 could contribute in emphysema development. For this purpose, we firstly assessed the level of CARM1 in the lung homogenate from haploinsufficient mice. The mRNA expression data by qRT-PCR and the densitometric analysis of western blot displayed that there was a significant 40% reduction of CARM1 level at the mRNA (** $p < 0.001$) (Figure 17A) as well as at the protein level (** $p < 0.01$) (Figure 17B) in the haploinsufficient mice compared to wild type mice (Figure 17B) (please continue to the next page).

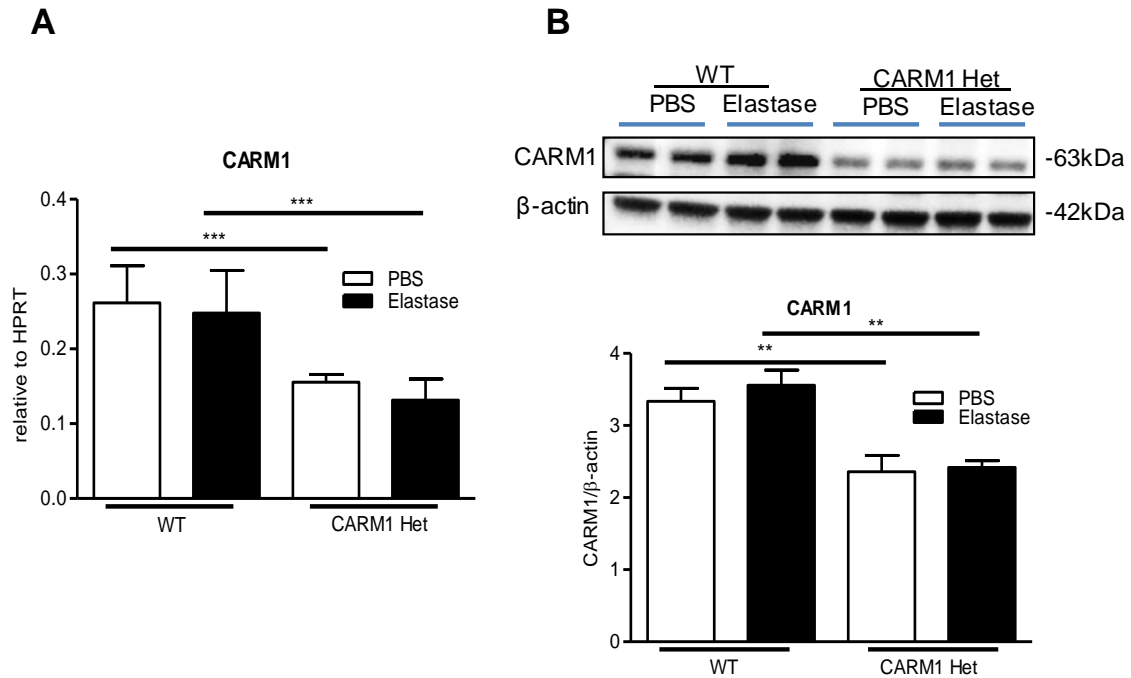


Figure 17. Reduced CARM1 expression in CARM1 haploinsufficient mice. (A) CARM1 expression at mRNA level analyzed by qRT-PCR (B) CARM1 expression at protein level analyzed by western blot and densitometry of the blot, ** $p < 0.01$, *** $p < 0.001$, student's *t*-test, WT vs. CARM1 haploinsufficient animals. WT=Wild type; Het=Heterozygous. Data presented are mean \pm SD. The experiments were repeated twice ($n=4-7$).

3.3.2 Elastase treatment enhanced airspace enlargement and lung function impairment in CARM1 haploinsufficient mice

Next, we asked the question whether the haploinsufficient mice responded differently to elastase treatment in terms of emphysema susceptibility compared to the wild type mice. To answer the question, we measured the mean linear chord length of alveolar airspace by NewCAST stereology system from histological sections of mouse lungs of both genotypes. The stereological quantification revealed a significant airspace enlargement in CARM1 haploinsufficient mouse lungs compared to WT animals after elastase treatment ($52.5 \pm 9.6 \mu\text{m}$ vs. $38.8 \pm 5.5 \mu\text{m}$, ** $p < 0.01$) at day 28 (Figure 18A-B). The higher degree of elastase-induced emphysema was also evident by a significant increase of dynamic lung compliance in CARM1 haploinsufficient mice compared to elastase-treated WT mice ($2.8 \pm 0.32 \mu\text{l/cmH}_2\text{O}$ versus $2.4 \pm 0.4 \mu\text{l/cmH}_2\text{O}$, * $p < 0.05$) (Figure 18C). PBS-treated WT or CARM1

haploinsufficient mice showed no difference in either airspace enlargement (22.28 ± 1.161 vs. 23.37 ± 0.8792) or lung compliance (0.001374 ± 0.00004710 vs. 0.001391 ± 0.0001266). Our data demonstrated for the first time that CARM1 deficiency was capable of predisposing mice to a greater susceptibility of emphysema induced by elastase.

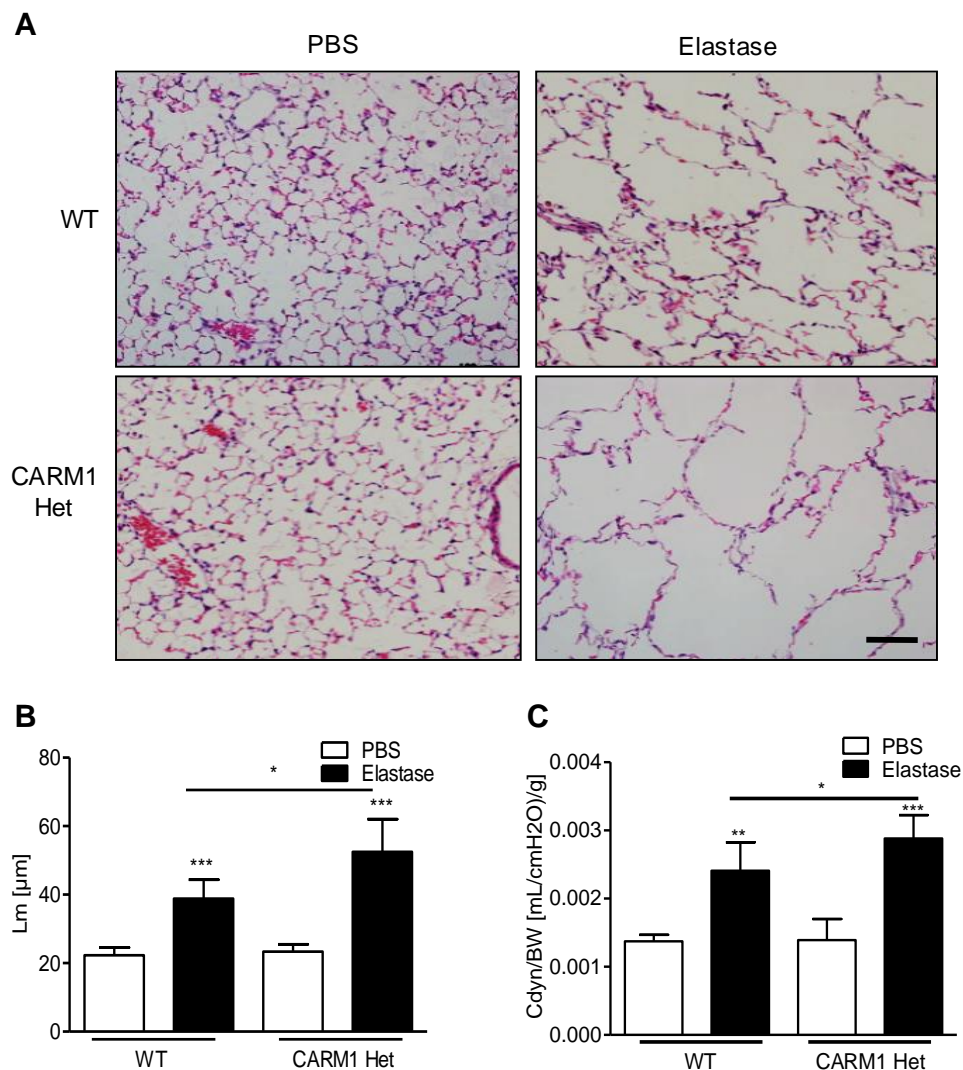


Figure 18. Augmented emphysema in CARM1 haploinsufficient mice. Mice analyzed on day 28 after elastase induction. (A) Representative histological images from H&E stained lung sections. Scale bar: 100 μm . (B) Mean chord length, Lm quantified by newCAST. (C) Lung compliance to body weight ratio, * $p < 0.05$, student's t-test vs. elastase-treated CARM1 haploinsufficient animals. WT=Wild type; Het=Heterozygous. Data presented are mean \pm SD. The experiments were repeated twice ($n=4-7$).

3.4 CARM1 Reduction Inducing Senescence in Alveolar Epithelial Cells

3.4.1 Loss of anti-senescence SIRT1 in alveolar epithelial cells

There are several studies reporting that senescence of lung alveolar epithelial cells contributes in emphysema development (134, 279). However, the underlying causative mechanism remains unsolved. SIRT1, an anti-senescence gene known to defend against elastase-induced emphysema via reduction of premature senescence in mice (137). Interestingly, CARM1 can regulate SIRT1 activity as CARM1-dependent methylated HuR is reported to stabilize SIRT1 transcript (224, 240). Therefore, we investigated whether CARM1 reduction could contribute in inducing alveolar epithelial cell senescence in emphysematous lungs by modulating SIRT1.

Morphological analysis of SIRT1-stained sections (Figure 19A) revealed that elastase treatment significantly reduced the percentage of SIRT1 positive alveolar epithelial cells in wild type animals which was not further decreased in CARM1 haploinsufficient mice (Figure 19B). Most importantly, we detected fewer number of SIRT1 positive ATII cells in PBS-treated CARM1 haploinsufficient mice compared to wild type control mice cells ($69.66\% \pm 4.55$ vs. 56.92 ± 1.99 , $*p < 0.05$). This finding proved our speculation correct that CARM1 deficiency alone could regulate SIRT1 level in ATII. We further confirmed loss of SIRT1 from SP-C positive alveolar epithelial cells (ATII) using immunofluorescence co-staining (Figure 19C).

We also analyzed SIRT1 in the lung homogenate by western blot and observed a downregulation in SIRT1 level in emphysematous lungs (Figure 20A). However, the densitometric analysis detected that among control animals, there was a significant decrease in SIRT1 level in CARM1 haploinsufficient mice compared to wild type animals (Figure 20A-B) although elastase treatment did not show further SIRT1 downregulation in haploinsufficient mice. One possible explanation could be that the SIRT1 alteration in alveolar epithelial cells was masked by other lung cell types expressing SIRT1.

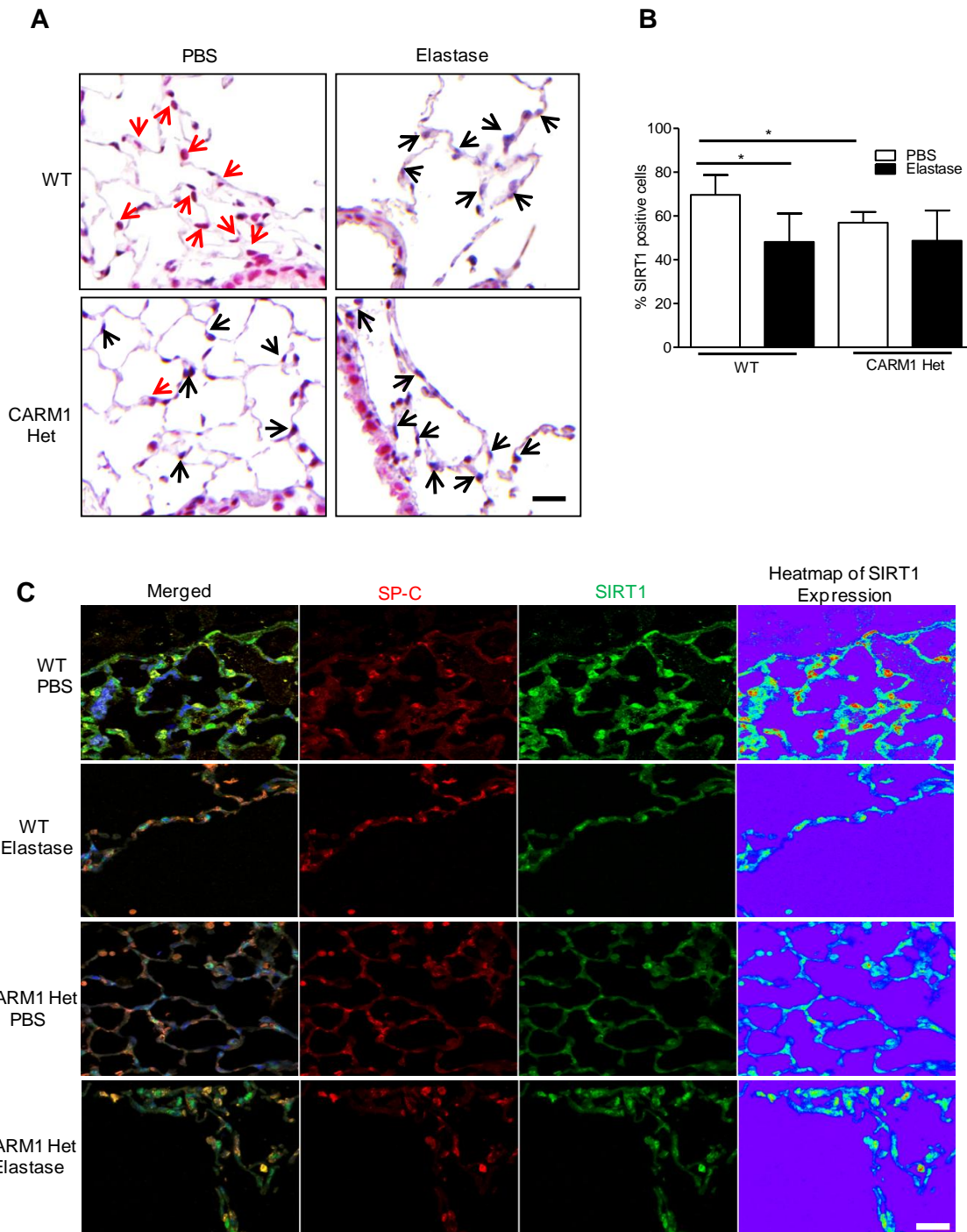


Figure 19. (A) Representative images from Immunohistochemistry using antibody against SIRT1 (1:100). Red: positive stain, black: negative stain. Scale bar: 20 μm (B) Stereological quantification of SIRT1 positive alveolar epithelial cells by newCAST system (C) Representative images from immunofluorescence double staining using antibodies against SIRT1 (1:100) and ATII-specific marker, SP-C. Green: SP-C positive ATII cells, Red: SIRT1 positive cells, Yellow (merged): SIRT1 and SP-C double positive ATII cells. Only the region of interest is shown. Scale bar: 10 μm , * $p < 0.05$, ** $p < 0.01$, student's *t*-test, wild type vs. CARM1 haploinsufficient mice. The experiments were repeated twice ($n = 4-7$).

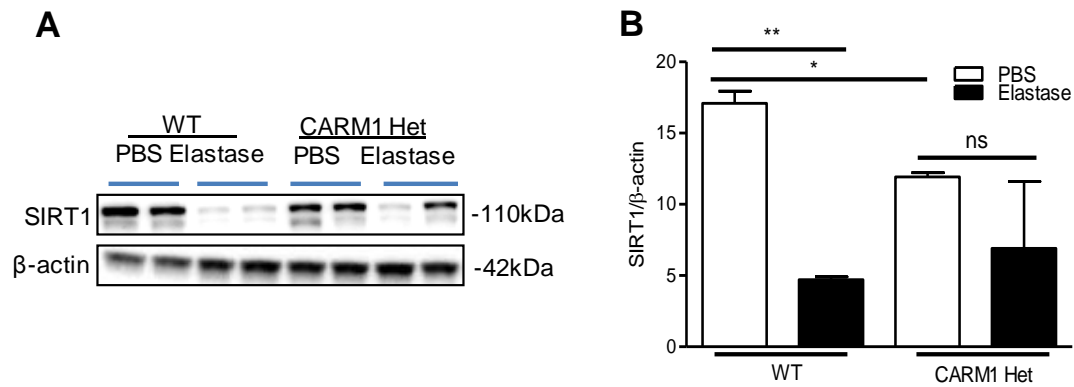


Figure 20. (A) Representative western blot for SIRT1 expression at protein level in lung homogenate. β -actin was used as loading control (B) Densitometry of the blot, * $p < 0.05$, ** $p < 0.01$, student's *t*-test, wild type vs. Data presented are mean \pm SD. The experiments were repeated twice ($n = 4-7$).

3.4.2 Induction of senescence markers in alveolar epithelial cells

Besides stabilizing SIRT1, CARM1-dependent methylation can also destabilize transcripts of p16, which is a hallmark marker for senescence (22, 29, 30). Therefore, we quantified p16 stained sections of mouse lungs of wild type and CARM1 haploinsufficient mice (Figure 21A). The quantification revealed that elastase-treatment induced an increase in p16 positive alveolar epithelial cells in WT as well as in CARM1 haploinsufficient mice. Interestingly, control CARM1 haploinsufficient mice showed a significant 2.5 fold increase in basal numbers of p16 positive alveolar epithelial cells compared to WT control animals (Figure 21B).

In addition, we analyzed protein expression levels of p16 and p21 in lung homogenates by western blot (Figure 21C). Elastase treatment increased expression of p16 in CARM1 haploinsufficient mice although the change was not significant (Figure 21D). For p21, we observed that in PBS-treated control animals, CARM1 deficiency alone significantly induced the level of p21 in haploinsufficient mice compared to wild type animals (Figure 21C and E).

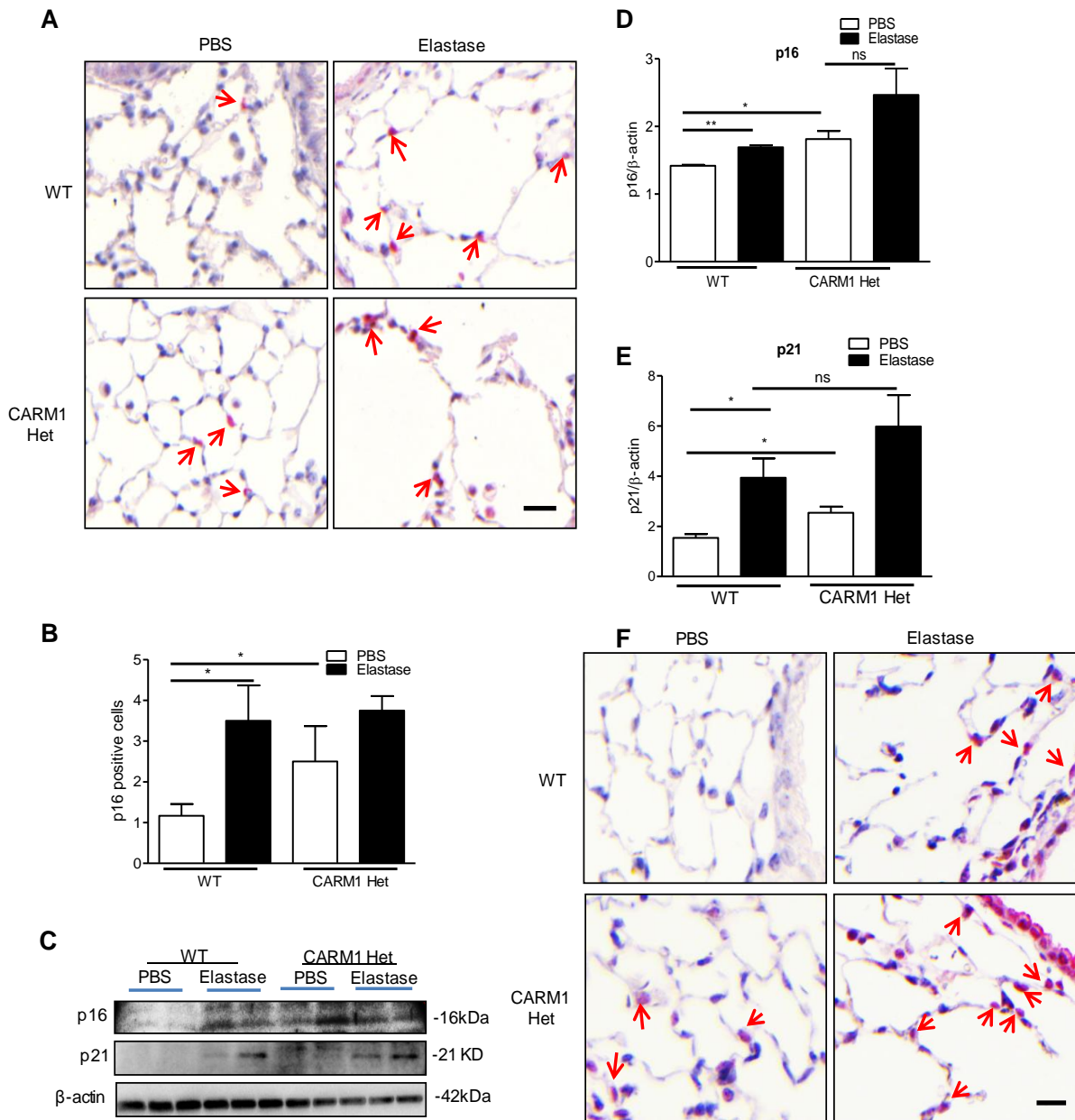


Figure 21. Induction of senescence markers in alveolar epithelial cells (A) Representative lung sections stained with anti-p16 Ab (1:50). Scale bar: 20 μ m (B) Semi-quantitative manual scoring of p16 positive alveolar epithelial cells (C) Representative western blots for p16 (1:200) and p21 (1:200) protein levels in lung homogenate (D) and (E) Densitometric analysis of blot for p16 and p21, respectively (E) Representative lung sections stained with antibody against β -galactosidase (1:50). Scale bar: 20 μ m. Red arrow indicates β -galactosidase positive alveolar epithelial cells, * p <0.05, ** p <0.01, student's t -test, WT vs. CARM1 haploinsufficient mice. Data are mean \pm SD, experiments were repeated twice (n =4-7).

Next, we analyzed β -galactosidase since it is highly expressed and accumulated in senescent cells. We performed immunohistochemistry using antibody against β -galactosidase and demonstrated that PBS-treated CARM1 deficient mice showed a

considerably higher number of β -galactosidase positive alveolar epithelial cells compared to PBS-treated WT animals (Figure 21F). Elastase treatment further increased the number of β -galactosidase positive cells in CARM1 deficient mice compared to wild type animals.

Taken together, these results thus suggested that CARM1 deficiency attenuated the SIRT1-regulated anti-senescence mechanism, which therefore induced senescence markers p16, p21 and increased β -galactosidase activity in alveolar epithelial cells which ultimately accounted for the increased susceptibility of haploinsufficient mice to elastase-induced emphysema.

3.5 CARM1 Knockdown in ATII-like Cells Triggering Senescence *In Vitro*

3.5.1 CARM1 knockdown in LA-4 cells downregulating SIRT1 expression

Previously we and others reported that CARM1 is expressed by airway epithelial cells and by ATII cells in septal regions (193, 251) (Figure 15A). Based on these reports, we considered ATII-like cell line LA-4 to understand the mechanism of CARM1-regulated senescence *in vitro*. With siRNA-mediated gene knockdown technology, we significantly reduced CARM1 expression by 70% as quantified by densitometric analysis of western blot (Figure 22A upper panel, 22B).

Next, we analyzed protein expression of SIRT1 and noticed a significant downregulation in siCARM1 transfected cells (* $p < 0.05$) (Figure 22A middle panel, 22C). The finding was supported by a significant 1.5 fold reduction of SIRT1 at mRNA level compared to scrambled control as analyzed by qRT-PCR (* $p < 0.05$) (Figure 22D) (please continue to the next page).

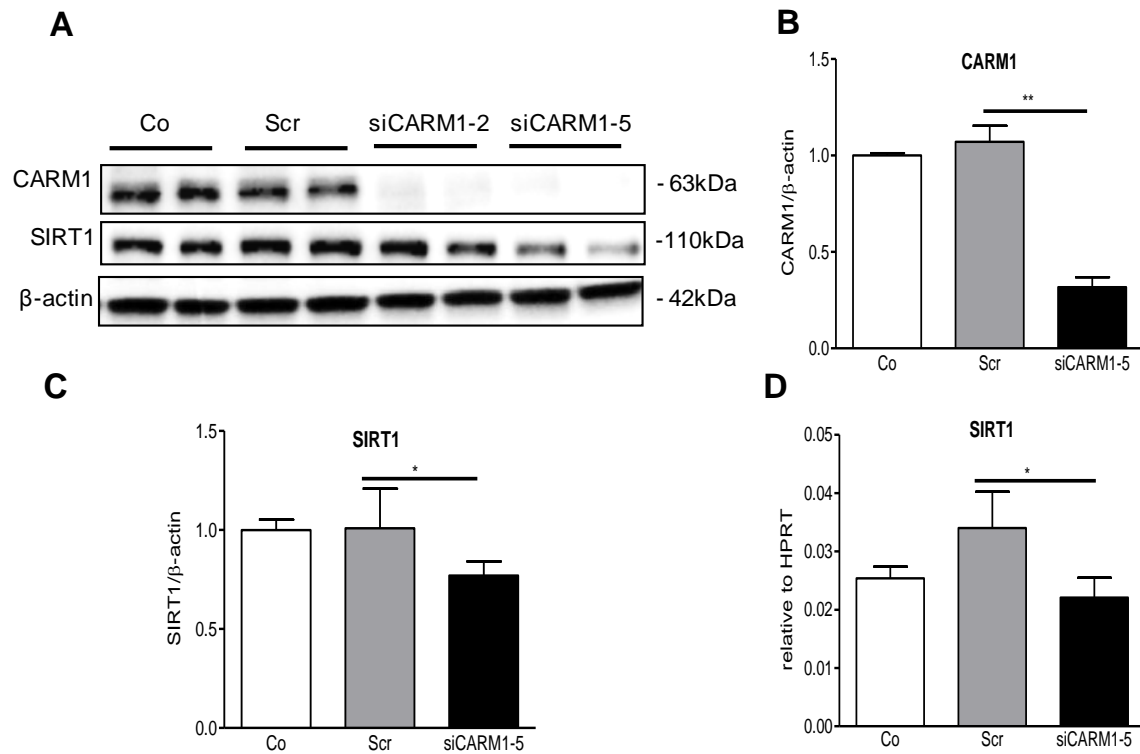


Figure 22. CARM1 reduction cells downregulating SIRT1 in ATII-like cell line LA-4. Cells were transfected with CARM1 specific siRNA (siCARM1-2 or siCARM1-5) or non-specific scrambled siRNA (Scr) for 48 hours and harvested for RNA/protein analysis. Untreated cells were taken as medium control (Co). (A) Representative western blot showing CARM1 (upper lane) and SIRT1 (middle lane) at protein level. β-actin used as loading control (lower lane). (B) Densitometric analysis of the blot for CARM1 (C) Densitometric analysis of the blot for SIRT1, * $p < 0.05$, ** $p < 0.01$, student's *t*-test, siCARM1-5 vs. Scr (D) SIRT1 expression at mRNA level, * $p < 0.05$, 1-way ANOVA. Data as means \pm SD. Data were from two independent experiments.

3.5.2 Reduced CARM1 inducing senescence markers in LA-4 cells

We analyzed senescence markers in siCARM1 transfected LA-4 cells and observed a significant upregulation of p16 and p21 but not p53 mRNA (Figure 23A-C). Furthermore, siCARM1 transfected cells showed a significantly higher percentage of β-galactosidase positive cells compared to the scrambled control (50.57% \pm 7.364 vs. 2.210% \pm 0.3404, *** $p < 0.001$) (Figure 23D-E). The number of positive cells was comparable to a positive control where cells were treated with 100 μ M H₂O₂ (data not shown).

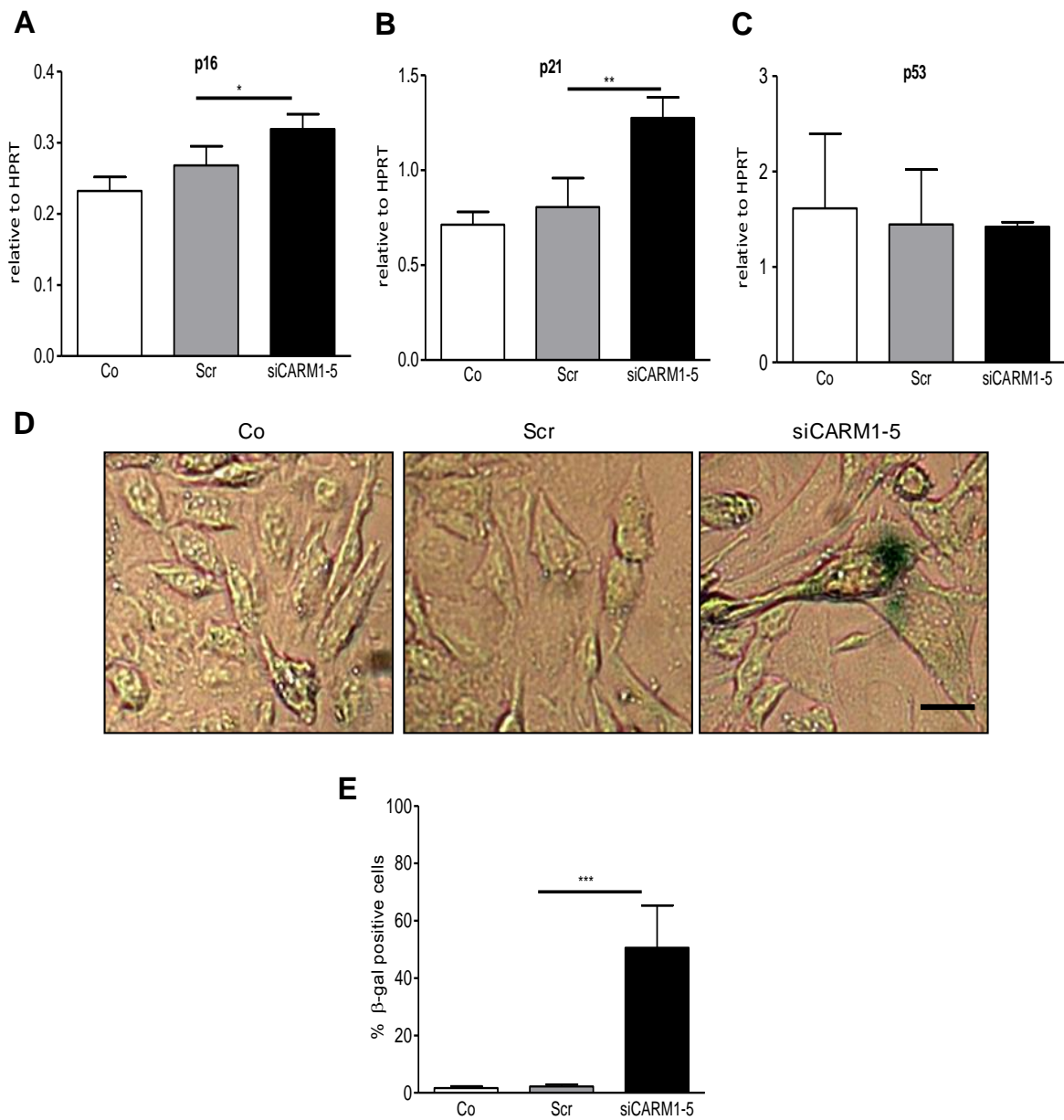


Figure 23. CARM1 reduction accelerated senescence in LA-4. siCARM1 transfected cells were incubated overnight with β -galactosidase staining solution. (A-C) mRNA expression of (A) p16, (B) p21 and (C) p53, $*p < 0.05$, $**p < 0.01$, 1-way ANOVA. (D) Representative images from β -galactosidase assay. Scale bar: 2 μ m (E) Quantification of β -galactosidase positive cells from total 300 cells in 10 random fields/well in 24-well plate, $***p < 0.001$, 1-way ANOVA. Data were from three independent experiments.

3.5.3 CSE stimulation augmenting senescence in CARM1 deficient LA-4 cells

As cigarette smoke is the most common cause of emphysema, we treated LA-4 cells with and without 5% cigarette smoke extract (CSE) in combination with siRNA-mediated knockdown of CARM1. We observed that CSE induced a reduction of CARM1 expression (Figure 24A). Most importantly, in siCARM1-transfected cells stimulated with CSE, the mRNA expression level of p21 was significantly upregulated compared to unstimulated siCARM1-transfected cells (* $p < 0.05$) (Figure 24B).

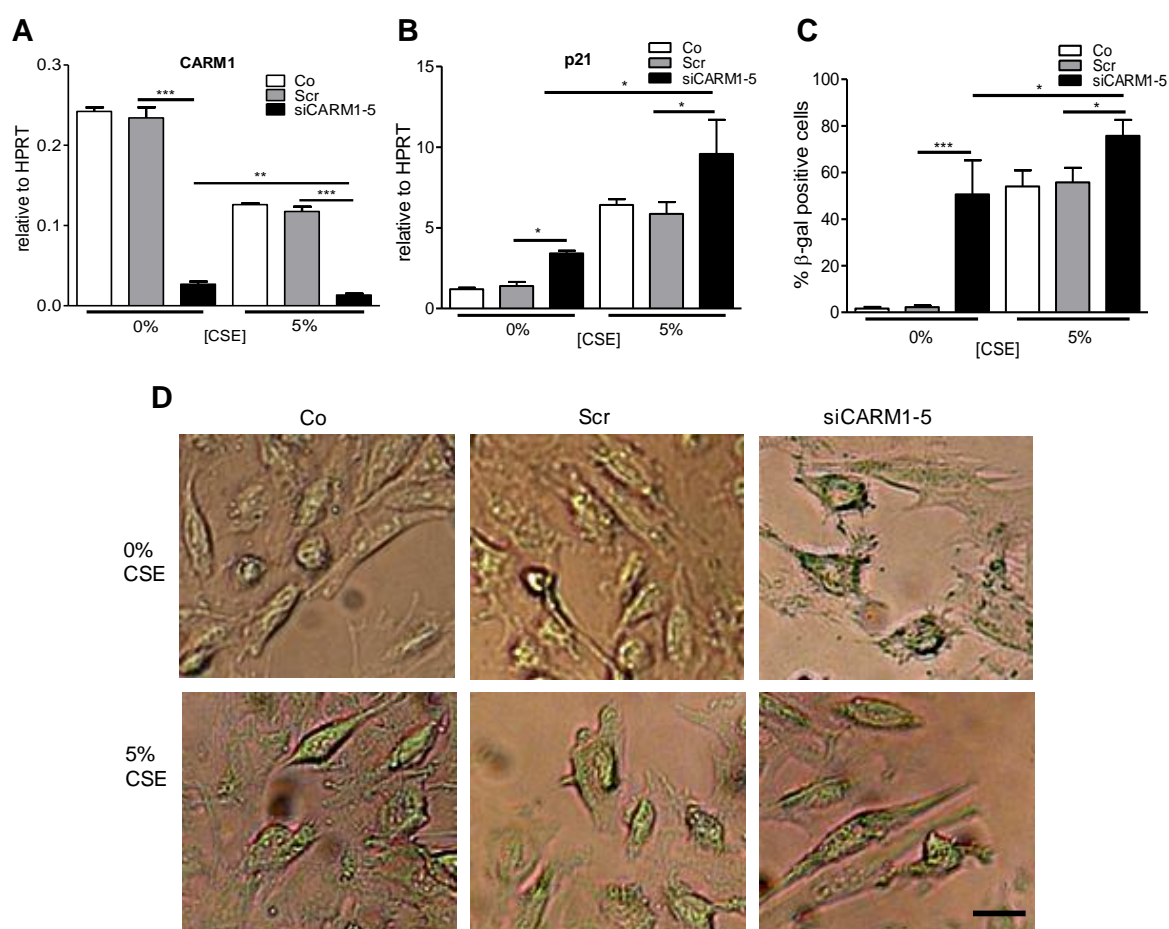


Figure 24. CARM1 reduction accelerated senescence in LA-4. siCARM1-transfected cells were treated with 5% CSE for 6 hours (A) The mRNA expression level of CARM1 and (B) p21 with or without CSE (C) Representative images of β -galactosidase assay (D) Quantification of β -galactosidase positive cells. Scale bar: 2 μ m, * $p < 0.05$, *** $p < 0.001$, student's *t*-test vs. siCARM1-transfected cells treated with 5% CSE. Data represented as means \pm SD. Data were from two independent experiments.

In accordance with this data, we also observed an elevated β -galactosidase activity in siCARM1-transfected cells after CSE stimulation (** $p < 0.05$) (Figure 24C-D) demonstrating that senescence in CARM1 deficient cells was further augmented after CSE stimulation.

These results confirmed that CARM1 reduction triggered an accelerated senescence in LA-4 cells.

3.6 Reduced CARM1 Hindering Regeneration and Trans-differentiation of ATII Cells

3.6.1 Reduced CARM1 impairing wound healing

Given that the reduction of CARM1 induced senescence in ATII cells, we sought to determine the impact of CARM1 on alveolar epithelial cell function and repair capacity. We designed a wound-healing assay using siCARM1-transfected LA-4 cells where the cell monolayer was scratched to induce a wound. CARM1-deficient cells exhibited a significant decrease in proliferation and migratory distance as evidenced by a $72.7\% \pm 12.2$ (** $p < 0.001$) reduction in gap closure compared with scrambled siRNA (Figure 25A-B).

This finding suggested that reduced CARM1 led to impaired wound healing of ATII-like cells. However, we did not observe any downregulation in the expression levels of proliferation markers such as PCNA, Cyclin E1 or ki67 in CARM1 deficient LA-4 cells (Figure 25C-E) (please continue to the next page).

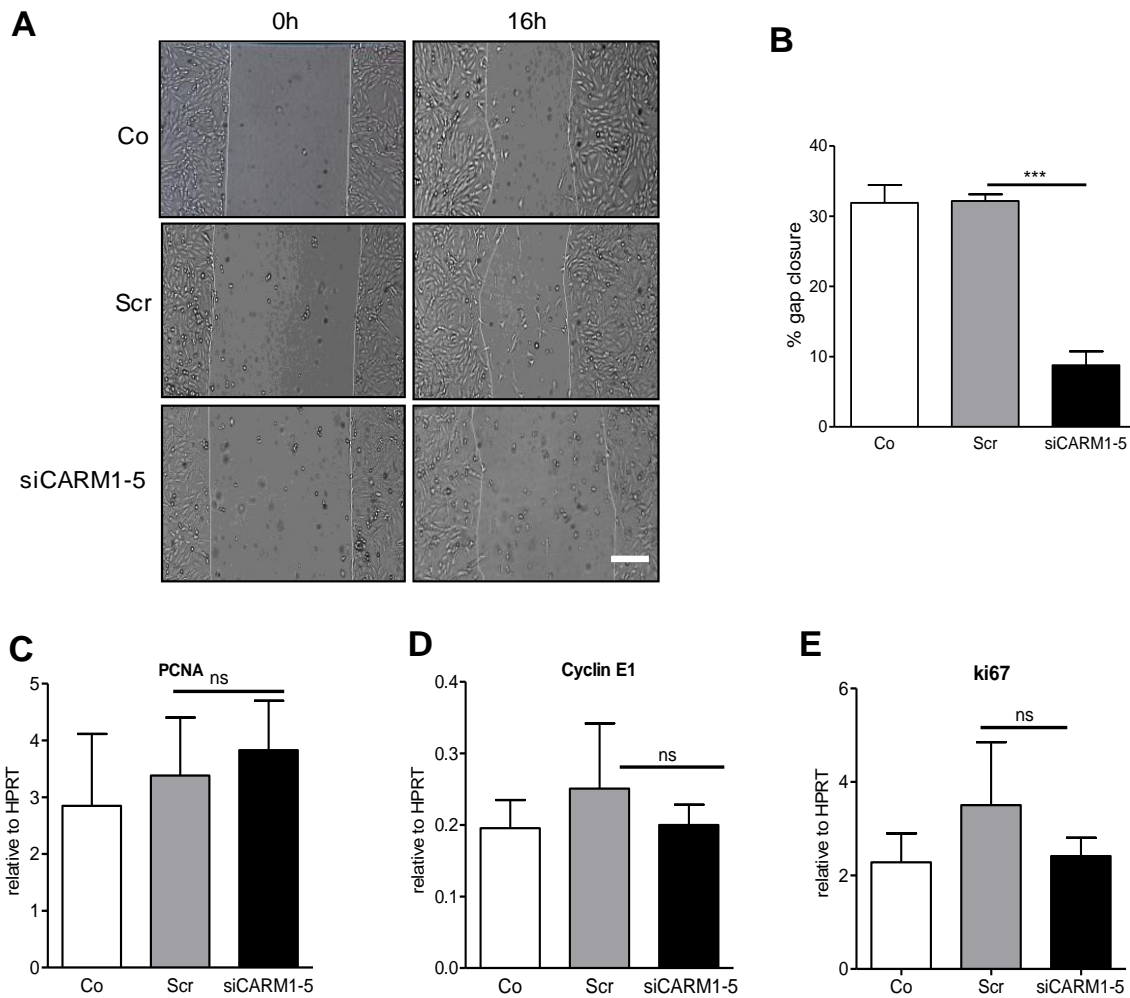


Figure 25. CARM1 reduction impaired wound healing in LA-4 cells. (A) Wound healing assay performed in confluent cultures of siCARM1-5 transfected LA-4 cells using a pipette tip. Scale bar: 200 μ m. (B) Quantification of gap closure determined 16 hours after injury (C) mRNA expression of PCNA, (D) Cyclin E1, (E) ki67, *** p <0.001, 1-ANOVA. Data from three independent experiments.

3.6.2 CARM1 reduction inducing aberrant ATII trans-differentiation

In vivo repair mechanisms consist of cellular regeneration, migration and differentiation. CARM1 is previously reported to regulate the differentiation of ATII into ATI cells, in the embryonic E18.5 mouse lung (251). We explored the role of CARM1 in the differentiation of adult murine cells by culturing primary ATII cells from WT animals, for 5 days under appropriate conditions.

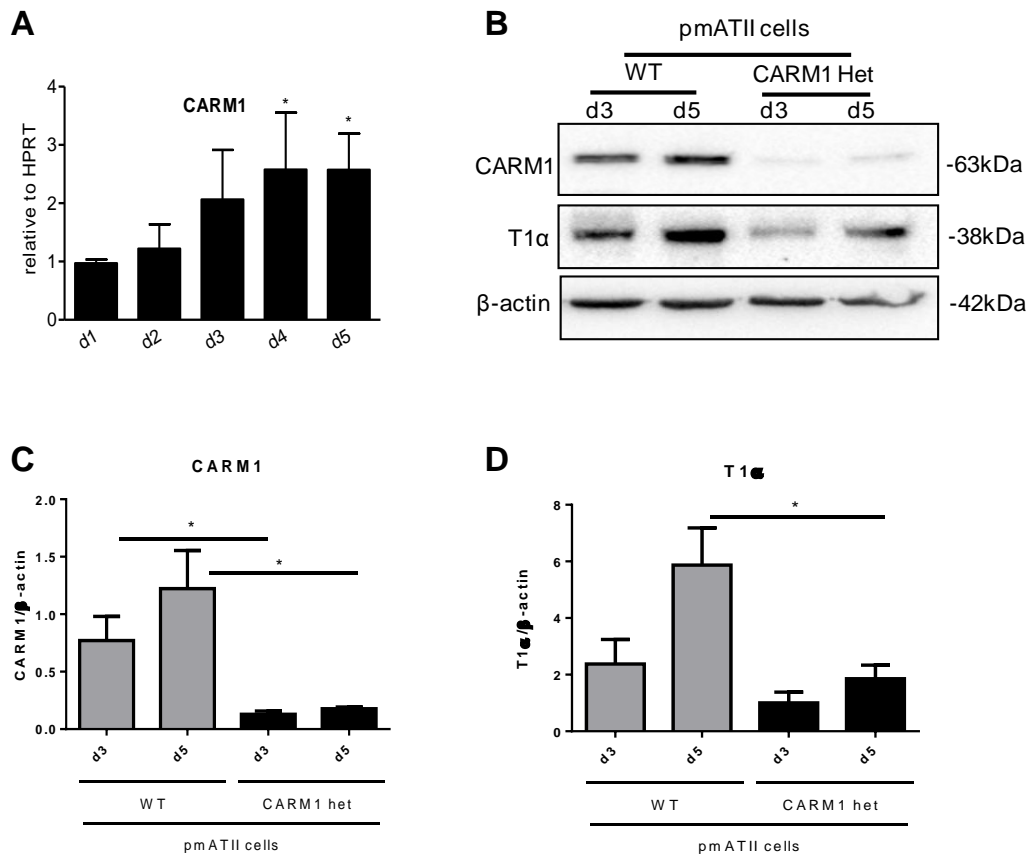


Figure 26. CARM1 reduction impaired trans-differentiation of alveolar epithelial cells. (A) CARM1 mRNA expression during differentiation of isolated primary ATII cells into an ATI-like phenotype in culture at indicated days, * $p < 0.05$, 1-way ANOVA, Dunnett's multiple comparison test vs. d1, $n = 3$ (B) Representative western blot for protein levels of CARM1 and T1α at indicated days of culture of isolated primary ATII cells from WT and CARM1 haploinsufficient animals (C) and (D) Densitometric analyses of western blots for CARM1 and T1α, respectively, the data are normalized to day 1, * $p < 0.05$, student's *t*-test vs. CARM1 haploinsufficient mice. Data represented as means \pm SD. Data from two independent experiments.

From day 3, isolated ATII cells from WT animals started to differentiate into ATI-like cells as demonstrated by expression of the ATI cell marker expression T1alpha. During ATII to ATI cell trans-differentiation CARM1 was significantly upregulated as analyzed by qRT-PCR (Figure 26A).

Similarly, we also isolated and cultured primary ATII cells from CARM1 haploinsufficient mice. We detected a significant downregulation of T1α at protein level at day 5 in these mice compared to WT mice indicating that CARM1 deficiency might lead to impaired differentiation

(Figure 26B-D). This indicates that CARM1 expression is associated with alveolar epithelial cell trans-differentiation processes. Finally, we analyzed the number of SP-C positive cells in emphysematous mouse lungs. We observed an increased ratio of SP-C positive cells to the total cell nuclei in elastase-treated CARM1 haploinsufficient mice compared to PBS-treated haploinsufficient mice (Figure 27A-B) suggesting that the higher number of ATII cells probably resulted from impaired trans-differentiation.

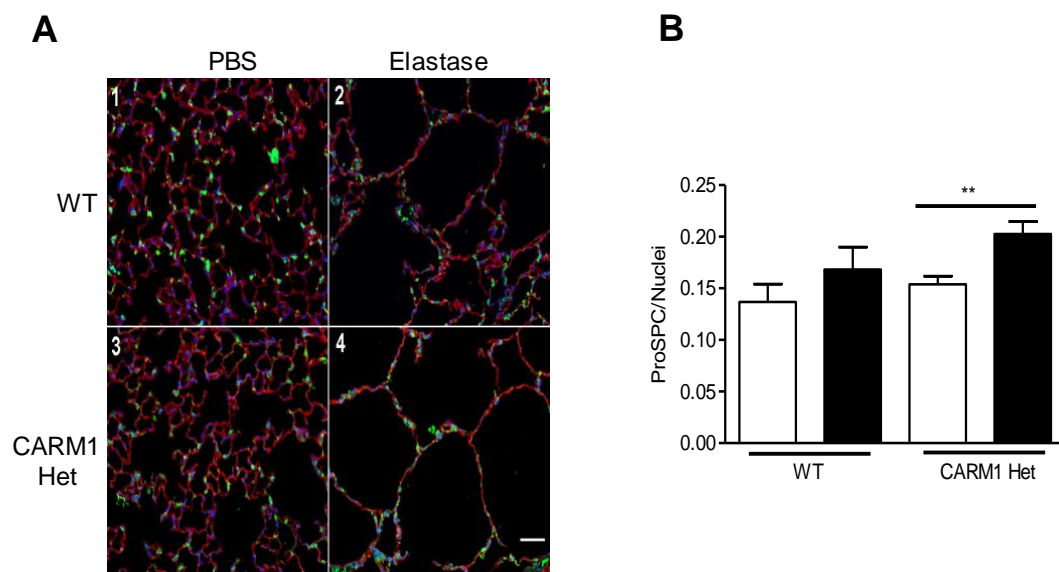


Figure 27. CARM1 reduction accumulated SP-C positive ATII cell in mouse lungs. (A) Representative immunofluorescence images showing SP-C (green) positive alveolar epithelial cells on lung sections from WT or CARM1 haploinsufficient mice treated with either PBS or elastase. DAPI (blue) used as nuclear staining. Scale bar: 50 μ m (B) Stereological quantification of SP-C positive alveolar epithelial cells to total number of nuclei, ** $p < 0.01$, 1-way ANOVA, PBS vs. elastase-treated CARM1 haploinsufficient animals. Data represented as means \pm SD. Data from two independent experiments.

4. DISCUSSION

Emphysema is characterized by enlargement of alveolar spaces accompanied with destruction of alveolar walls in the absence of any obvious fibrosis (6). The progressive and irreversible alveolar destruction results in reduced elastic recoiling and decreasing alveolar capillary exchange area (280). Cigarette smoking is by far the most common cause of pulmonary emphysema. In the lower respiratory tract of the lungs cigarette smoke induces an inflammatory response by recruiting alveolar macrophages and neutrophils (6). The activated inflammatory cells release an array of proteases, oxidants and toxic peptides and trigger damage to the lung structures by apoptosis, oxidative stress, and protease/anti-protease imbalance and premature aging/senescence of lung cells. Taken together, these are believed to be the major causes of the tissue destruction by which emphysema is defined.

Aging is considered as a major risk factor for chronic obstructive pulmonary disease (COPD) (284). It was recently thought that cigarette smoke (CS) and noxious gases trigger accelerated premature aging of the lung via cellular senescence (63, 121). There are evidence demonstrating that cellular senescence of different types of lung cells is accelerated in COPD patients and these cell types include alveolar type II cells, endothelial cells, fibroblasts, and peripheral blood lymphocytes (124, 126, 285, 286). Aging/senescence is a stress response marked by a progressive decline in the function of multiple cells and tissues in lungs (287). Recently, the lungs of smokers with emphysema were associated with overexpression of the cellular senescence marker p16 and telomere shortening in both alveolar epithelial type II (ATII) and endothelial cells (126). Deficiency in the anti-senescence protein (SMP30) in mice also promotes airspace enlargement after cigarette smoke exposure (288). Cellular senescence is a state of irreversible growth arrest. Senescent cells are

presumed to contribute to the pathogenesis of age-related diseases by inhibiting tissue repair, because these cells are viable yet unable to divide and to repair tissue defects (121, 125, 289-291). Therefore, our study aimed at investigating the role of coactivator-associated arginine methyltransferase (CARM1), a PRMT family member regulating cellular senescence via the anti-aging protein/histone deacetylase SIRT1, in elastase-induced emphysema in wild type and CARM1 haploinsufficient mice. We reported for the first time that CARM1 deficiency caused enhanced emphysema by accelerating senescence via SIRT1 leading to impaired regeneration and differentiation of alveolar epithelial cells.

In order to mimic the irreversible structural changes occurring in the lungs of COPD patients even after smoking cessation (147), the elastase-induced emphysema mouse model is a useful and well-established model. Despite its known half-life of a few hours and a turn-over rate of 99% in four days (145, 146), elastase triggers a continuous airspace enlargement and lung function decline even after stimulus cessation (139, 140). We used the porcine pancreatic elastase (PPE)-induced emphysema model as an alternative to the cigarette smoke (CS) model. PPE degrades extracellular matrix components like elastin, collagen and fibronectin. Natural sources of elastases in the lung are neutrophils and macrophages (73). This model can be established by a single treatment inducing progressive emphysema development that can reliably be monitored by lung function tests (140). Protease-induced emphysema is probably the most commonly used emphysema model, since it is easy to establish and reproducible, and the pathological changes develop quickly (292). Studies showed that hamsters or mice treated with PPE develop emphysema within a few days (277). This disease model is therefore very feasible to induce concentration dependent emphysema (139). In contrast cigarette smoke model takes considerably more time to induce significant pathological changes in the lung (starting from 4 months of exposure) (155). Furthermore, CS exposure of animals for up to 6 months only produces a mild disease, probably equivalent to human Global Initiative on Chronic Obstructive Lung Disease

(GOLD) stage 1 or 2 (293). Although elastase model and cigarette smoke model both demonstrate pathologically relevant emphysematous changes, the differences in injury pathway is still not completely known. Furthermore, the onset and duration of lesions differ in both models. To complement our elastase model, we performed an *in vitro* study with cigarette smoke extract (CSE) on siCARM1-treated LA-4 cells to evaluate the effect of CSE on cells with reduced CARM1. In addition, for a future study, we plan to use CS model on SP-C-cre CARM1 mice.

In our current study, we monitored elastase-induced emphysema progression in wild type mice for a period of 161 days. The first evidence of emphysema development was indicated by the impaired pulmonary function two days after elastase application. Further decline was followed till day 161. We demonstrated a significant increase of airspace enlargement in response to elastase treatment, which strongly correlated with increased dynamic lung compliance. Additionally, we found a decreasing Tiffeneau index (FEV_{0.1}/FVC ratio), along with emphysema progression, which is an important characteristic for COPD patients. Most recently, a study monitored and described emphysema progression for 12 weeks by using morphometry and micro-computed X-ray tomography (148). In contrast, in our study, lung function tests reliably monitored emphysema progression until 161 days proving these as useful diagnostic tools.

Inflammatory cells were detectable in bronchoalveolar lavage (BAL) fluid after elastase treatment only during the first four weeks which afterwards resumed to normal levels. As expected, the first early inflammatory responses were neutrophils, which are first recruited to the injured site and release neutrophil elastase, an important emphysema-related enzyme (292). Furthermore, we observed a significant accumulation of macrophages in BAL fluid until day 28, which are known to release macrophage elastase e.g. MMP12, thereby further contributing to emphysema development in addition to elastase-induction (294). This

observation is important because the later time points (day 56 and 161) provided the opportunity to study inflammation-independent progressive emphysema mechanisms, comparable to the situation of reduced inflammation but progressive emphysema after cigarette smoke cessation (295, 296).

Besides regulating senescence, CARM1 was shown to be indispensable for normal lung development, specifically for alveolar proliferation and differentiation. Using electron microscopy, it was observed that the ATII cells in the lungs of the CARM1 homozygote mice did not differentiate normally into alveolar type I (AT1) cells. In addition, many cell-cycle genes and markers of AT1 differentiation were dysregulated in CARM1 homozygote mouse embryos (232, 251). Interestingly, CARM1 was downregulated in ATII cells of emphysematous lungs starting from day 28.

Although we did not observe any change in global level of CARM1 protein expression in lung homogenates among different time points analyzed by western blot but there was a change in the level of phosphorylated CARM1 at day 161. Phosphorylation of CARM1 at a conserved serine residue (Ser-228 in human and Ser-229 in mouse) is known to prevent CARM1 binding with the methyl donor S-adenosylmethionine (AdoMet) thus inhibit its enzymatic activity (244, 245). Phosphorylation at Ser-217 also acts as a molecular switch for controlling CARM1 enzymatic activity during the cell cycle (244, 245). The significant increase in the ratio of phospho-CARM1 to CARM1 level that we observed as a late effect on CARM1 phosphorylation indicated a reduced CARM1 activity after elastase treatment. Most importantly, we demonstrated that CARM1 deficiency leading to pronounced and accelerated emphysema progression at day 28 in response to elastase treatment proving its crucial role in lung architecture maintenance.

Remarkably, CARM1 is reported to be downregulated in testis, thymus and heart of 24-month old aging rats (264). CARM1 reduction is also observed in replicative and H₂O₂-induced premature senescence of human diploid fibroblasts (263). Based on these reports and our initial findings, we hypothesized that diminished CARM1 levels might promote enhanced emphysema by regulating cellular senescence. Therefore, we investigated SIRT1, an NAD⁺-dependent lysine deacetylase functioning in multiple cellular events but most importantly in control of lifespan and thus acting as an anti-senescence gene (242). In the lungs of smokers or COPD patients, SIRT1 is reported to be downregulated (136, 297). In mice, SIRT1 deficiency led to enhanced emphysema in both an elastase- and cigarette smoke-induced models (137).

Indeed, we observed a reduced basal level of SIRT1-positive alveolar epithelial type II cells in CARM1 deficient mice. CARM1 is reported to stabilize SIRT1 transcripts by CARM1-dependent methylation of HuR (240). We presumed that this intrinsic pro-senescent status of alveolar epithelial cells observed in our study resulted from decreased stabilization of SIRT1. However, as there was no significant change in the levels of SIRT1 after elastase treatment in CARM1 haploinsufficient mice, we speculate that further reduction after elastase treatment was masked by other lung cells, especially by airway cells, fibroblasts, endothelial cells and monocytes/macrophages which also express SIRT1 (136, 137, 298, 299). Nevertheless, our *in vitro* study showing SIRT1 downregulation after siRNA-mediated CARM1 knockdown in LA-4 cells further confirmed the presence of a CARM1-SIRT1 axis in regulation of senescence, particularly in ATII cells.

These results were corroborated by an increased basal level of p16 positive alveolar epithelial cells in CARM1 deficient mice and significant upregulation of p16 as well as p21 in CARM1 deficient LA-4 cells. In addition, the global protein levels determined by western blot also revealed that CARM1 deficiency alone significantly induced the protein level of p16 and

p21 in haploinsufficient mice compared to wild type animals. These cyclin-dependent kinase (CDK) inhibitors are two of the widely used senescence markers known to increase with cellular senescence in several rodent and human tissues and most importantly in alveolar epithelial cells of COPD patients (126, 133, 300). Moreover, previous studies showed CARM1-dependent post-translational methylation of HuR enhancing its association with p16 or p21 mRNA and leading to transcript degradation, whereas absence of CARM1 led to transcript stabilization (224, 239, 301).

Another hallmark senescence marker is p53 (302) but in CARM1 homozygote mouse lungs, p53 is downregulated, demonstrating that CARM1 serves as a coactivator for p53 transcription (251). Despite the contradictory, we analyzed p53 expression by qRT-PCR but no significant difference was found between siCARM1 and scramble siRNA transfected cells. As an underlying reason, we speculate that p53 stabilization and activity is regulated by other pathways rather than CARM1-dependent methylation. Another explanation is that the downregulated transactivation of p53 by coactivator function of CARM1 that O'Brien et al., observed is cell type-specific and does not occur in ATII cells.

Besides cyclin-dependent kinase (CDK) inhibitors, another known characteristic of senescent cells is an elevated β -galactosidase activity at pH 6 which is usually absent in pre-senescent, quiescent or immortal cells (305). The impact of CARM1-mediated regulation on senescence was confirmed by increased numbers of β -galactosidase positive alveolar epithelial cells in siCARM1-treated cells which was further augmented after CSE stimulation demonstrating that CARM1 deficiency could further enhance the senescence induction following injury stimulus in ATII cells. Similarly, CARM1 deficiency was capable of inducing senescence in alveolar epithelial cells in mouse lungs which was considerably increased after elastase treatment and thus proved importance of CARM1 to regulate cellular senescence. The impact of CARM1-mediated regulation on senescence was confirmed by increased numbers

of senescence-associated β -galactosidase (SA- β -gal) positive LA-4 cells after siCARM1 transfection.

Exposures to cigarette smoke are reported to turn lung alveolar epithelial cells, fibroblasts and airway cells into an irreversible state of senescence (127, 306, 307). This results in an inability to repair lung injury which is a characteristic feature of emphysema. For our in vitro study, we used cigarette smoke extract (CSE) in combination with siRNA-mediated knockdown of CARM1 in LA-4 cells with twofold purposes. Firstly, to probe its impact on CARM1 expression and secondly, to investigate whether CSE could further augment senescence in CARM1 deficient cells. We used 5% CSE and treated the cells for 6 hours in this experiment, because we have found earlier that this CSE concentration does not induce cell death (unpublished observation). We indeed observed CSE-mediated reduction of CARM1 expression although there were no changes in gene expression for p16, p53 and SIRT1 (data not shown). In contrast, p21 levels as well as SA- β -gal activity were elevated in siCARM1-transfected cells after CSE stimulation. These results demonstrated that reduced CARM1-induced senescence was further enhanced after CSE stimulation.

CARM1-deficient mice are reported to demonstrate hyper-proliferative immature ATII cells that are incapable of trans-differentiating into ATI cells (251). Contrary to the report, we observed a reduced gap closure in CARM1 knockdown LA-4 cells. Our finding suggested that CARM1 was necessary for wound healing after an occurrence of an induced injury. This indicated that CARM1 deficiency delayed the cellular repair mechanism in the lung and impaired repair capacity is a prominent feature of emphysematous lungs.

As proliferation and migration are two principle phases of wound healing, we also considered analyzing proliferation markers, such as PCNA, Ki67 and CyclinE1 by qRT-PCR. However, we did not observe any downregulation in proliferation in CARM1 deficient LA-4 cells. We

would like to point out here that we quantified the gap closure after 16 hours of introducing the wound. One explanation could be that the proliferative phase might have been impaired at an earlier time point in CARM1 deficient cells which resumed to normal level by 16 hour and that were why we did not observe any change in the expression levels of proliferation markers. A time course following wound induction would perhaps provide further information on changes in proliferation in siCARM1-treated cells.

CARM1 has been implicated in differentiation of chondrocytes, myocytes, T cell, human embryonic stem cell and most important alveolar epithelial type II (ATII) cells (204, 240, 250, 251, 261). In accordance with these reports, we also observed an upregulation of CARM1 during trans-differentiation of isolated murine ATII cells into AT1 cells in culture conditions suggesting a direct association of CARM1 in differentiation process. Additionally, we demonstrated that alveolar epithelial senescence resulting from reduced CARM1 could also impair trans-differentiation of ATII cells into ATI cells as manifested by a significant downregulation of T1 α at protein level in cultured ATII cells isolated from CARM1 deficient mice compared to wild type animals on day 3 and 5 when the differentiation process starts to occur.

O'Brien et al. reported hyperproliferation of pro SP-C positive cell in CARM1 deficient mouse lungs. In our study, we showed that elastase-treatment acts as a trigger in CARM1 deficient mouse lungs to stimulate ATII cells hyperproliferation. We speculate that the increase in ProSPC positive cells could be an outcome of dysregulated trans-differentiation of ATII into ATI thereby leading to an accumulation of ATII cells. Wnt signaling pathway might act as an underlying mechanism. It is possible that CARM1 regulates trans-differentiation of ATII cells via the WNT signaling pathway involved in alveolar epithelial trans-differentiation (308). Activation of Wnt/ β -catenin signaling during lung injury promotes alveolar epithelial differentiation toward an ATI-like phenotype (309) and recently, downregulation of WNT/ β -

catenin signaling has been implicated in parenchymal tissue destruction and impaired repair capacity in lungs of COPD patients (62). The methyltransferase domain of CARM1 can specifically interact with β -catenin and thus acts as a bona fide coactivator for Wnt/ β -catenin signaling (257) indicating that CARM1-regulated Wnt pathway might be involved in alveolar epithelial differentiation. However, further study is required to elaborate how CARM1-regulated senescence could lead to impairment of alveolar epithelial trans-differentiation during emphysema development. Especially the upstream pathways regulating CARM1 via post-translational modifications might be a promising target for future investigation.

Collectively, our data support the senescence hypothesis of emphysema development in COPD. Our study demonstrate that indeed the cellular senescence contributed to the pathogenesis of emphysema and this is mediated via a CARM1-SIRT1-axis in ATII cells. We identified CARM1 as the upstream regulator of SIRT1 governing senescence and modulating regeneration, repair and differentiation of ATII to AT1 cells. Most importantly, from a therapeutic approach, our findings also provide an alternative strategy to treat emphysema. As there is no current treatment to reverse the alveolar destruction that is continuously occurring in emphysematous lung, therefore, arresting or slowing down the disease progression is a more realistic goal to achieve. Pharmacological intervention such as targeted drugs or inhibitors might be an effective as well as practical approach to induce CARM1 or to prevent its degradation, respectively in patient with emphysema. Thus, CARM1 may prove to be an effective target to decelerate the premature lung aging process observed in COPD patients.

5. Reference

1. Murray CJ, Lopez AD. Measuring the global burden of disease. *The New England journal of medicine* 2013; 369: 448-457.
2. Buist AS, McBurnie MA, Vollmer WM, Gillespie S, Burney P, Mannino DM, Menezes AM, Sullivan SD, Lee TA, Weiss KB, Jensen RL, Marks GB, Gulsvik A, Nizankowska-Mogilnicka E, Group BCR. International variation in the prevalence of COPD (the BOLD Study): a population-based prevalence study. *Lancet* 2007; 370: 741-750.
3. Hilleman DE, Dewan N, Malesker M, Friedman M. Pharmacoeconomic evaluation of COPD. *Chest* 2000; 118: 1278-1285.
4. Barnes PJ. Chronic obstructive pulmonary disease. *The New England journal of medicine* 2000; 343: 269-280.
5. Barnes PJ. Cellular and molecular mechanisms of chronic obstructive pulmonary disease. *Clinics in chest medicine* 2014; 35: 71-86.
6. Vestbo J, Hurd SS, Agusti AG, Jones PW, Vogelmeier C, Anzueto A, Barnes PJ, Fabbri LM, Martinez FJ, Nishimura M, Stockley RA, Sin DD, Rodriguez-Roisin R. Global strategy for the diagnosis, management, and prevention of chronic obstructive pulmonary disease: GOLD executive summary. *American journal of respiratory and critical care medicine* 2013; 187: 347-365.
7. Hogg JC. Pathophysiology of airflow limitation in chronic obstructive pulmonary disease. *Lancet* 2004; 364: 709-721.
8. Kessler R, Partridge MR, Miravittles M, Cazzola M, Vogelmeier C, Leynaud D, Ostinelli J. Symptom variability in patients with severe COPD: a pan-European cross-sectional study. *The European respiratory journal* 2011; 37: 264-272.
9. Vestbo J, Hogg JC. Convergence of the epidemiology and pathology of COPD. *Thorax* 2006; 61: 86-88.
10. Bhowmik A, Chahal K, Austin G, Chakravorty I. Improving mucociliary clearance in chronic obstructive pulmonary disease. *Respiratory medicine* 2009; 103: 496-502.
11. Siafakas NM, Vermeire P, Pride NB, Paoletti P, Gibson J, Howard P, Yernault JC, Decramer M, Higenbottam T, Postma DS, et al. Optimal assessment and management of chronic obstructive pulmonary disease (COPD). The European Respiratory Society Task Force. *The European respiratory journal* 1995; 8: 1398-1420.
12. Hogg JC, Macklem PT, Thurlbeck WM. Site and nature of airway obstruction in chronic obstructive lung disease. *The New England journal of medicine* 1968; 278: 1355-1360.
13. Cosio MG, Hale KA, Niewoehner DE. Morphologic and morphometric effects of prolonged cigarette smoking on the small airways. *The American review of respiratory disease* 1980; 122: 265-221.
14. Hogg JC, McDonough JE, Gosselink JV, Hayashi S. What drives the peripheral lung-remodeling process in chronic obstructive pulmonary disease? *Proceedings of the American Thoracic Society* 2009; 6: 668-672.
15. Chung KF. The role of airway smooth muscle in the pathogenesis of airway wall remodeling in chronic obstructive pulmonary disease. *Proceedings of the American Thoracic Society* 2005; 2: 347-354; discussion 371-342.
16. Lapperre TS, Sont JK, van Schadewijk A, Gosman MM, Postma DS, Bajema IM, Timens W, Mauad T, Hiemstra PS, Group GS. Smoking cessation and bronchial epithelial remodelling in COPD: a cross-sectional study. *Respiratory research* 2007; 8: 85.
17. McDonough JE, Yuan R, Suzuki M, Seyednejad N, Elliott WM, Sanchez PG, Wright AC, Gefter WB, Litzky L, Coxson HO, Pare PD, Sin DD, Pierce RA, Woods JC, McWilliams AM, Mayo JR, Lam SC,

- Cooper JD, Hogg JC. Small-airway obstruction and emphysema in chronic obstructive pulmonary disease. *The New England journal of medicine* 2011; 365: 1567-1575.
18. The definition of emphysema. Report of a National Heart, Lung, and Blood Institute, Division of Lung Diseases workshop. *The American review of respiratory disease* 1985; 132: 182-185.
 19. Yoshida T, Tuder RM. Pathobiology of cigarette smoke-induced chronic obstructive pulmonary disease. *Physiological reviews* 2007; 87: 1047-1082.
 20. McCallum W. Types of injury: destruction of the respiratory tract. In: A textbook of pathology. 7th ed Philadelphia: WB Saunders 1940: 419-428.
 21. Snider GL. Experimental studies on emphysema and chronic bronchial injury. *European journal of respiratory diseases Supplement* 1986; 146: 17-35.
 22. Saetta M, Ghezzi H, Kim WD, King M, Angus GE, Wang NS, Cosio MG. Loss of alveolar attachments in smokers. A morphometric correlate of lung function impairment. *The American review of respiratory disease* 1985; 132: 894-900.
 23. Shifren A, Mecham RP. The stumbling block in lung repair of emphysema: elastic fiber assembly. *Proceedings of the American Thoracic Society* 2006; 3: 428-433.
 24. Rocker G, Horton R, Currow D, Goodridge D, Young J, Booth S. Palliation of dyspnoea in advanced COPD: revisiting a role for opioids. *Thorax* 2009; 64: 910-915.
 25. Snider GL. Emphysema: the first two centuries--and beyond. A historical overview, with suggestions for future research: Part 2. *The American review of respiratory disease* 1992; 146: 1615-1622.
 26. Bonet T. Sepulchretum sive anatomia pructica ex Cadaveribus Morbo denatis, proponens Histoa's Observations omnium pené humani corporis affectuum, ipsarcomoue Causas recorditas revelans. Geneva. 1679.
 27. Ruysch F. Observationes anatomica-chirurgicae. In: Tractatio anatomica Amsterdam. 1721.
 28. Morgagni G. The seats and causes of disease. Investigated by anatomy; Translated by Alexander B, Miller A, Caldwell T. London: Johnson and Payne 1769.
 29. Baillie M. A series of engravings, accompanied with explanation which are intended to illustrate the morbid anatomy of some of the most important parts of the human body divided into 10 fascicule. London: W Blum R and Co 1799.
 30. Baillie M. The morbid anatomy of some of the most important parts of the human body. London: W Blum R and Co 1807.
 31. Laennec R. A treatise on the diseases of the chest. London: Longman 1834.
 32. Osler W. The principles and practices of medicine: designed for the use of practitioners and students of medicine. 8th ed New York: D Appleton and Co 1892.
 33. McLean KH. The macroscopic anatomy of pulmonary emphysema. *Australasian annals of medicine* 1956; 5: 73-88.
 34. Chronic cor pulmonale. Report of an expert committee. *World Health Organization technical report series* 1961; 213: 35.
 35. American Thoracic Society. Statement on definitions and classification of chronic bronchitis, asthma, and pulmonary emphysema. *The American review of respiratory disease* 1962; 85: 762-768.
 36. . The Health Consequences of Smoking-50 Years of Progress: A Report of the Surgeon General. Atlanta (GA); 2014.
 37. Kohansal R, Martinez-Cambor P, Agusti A, Buist AS, Mannino DM, Soriano JB. The natural history of chronic airflow obstruction revisited: an analysis of the Framingham offspring cohort. *American journal of respiratory and critical care medicine* 2009; 180: 3-10.
 38. Tager IB, Ngo L, Hanrahan JP. Maternal smoking during pregnancy. Effects on lung function during the first 18 months of life. *American journal of respiratory and critical care medicine* 1995; 152: 977-983.

39. Eisner MD, Balmes J, Katz PP, Trupin L, Yelin EH, Blanc PD. Lifetime environmental tobacco smoke exposure and the risk of chronic obstructive pulmonary disease. *Environmental health : a global access science source* 2005; 4: 7.
40. Dayal HH, Khuder S, Sharrar R, Trieff N. Passive smoking in obstructive respiratory disease in an industrialized urban population. *Environmental research* 1994; 65: 161-171.
41. Leuenberger P, Schwartz J, Ackermann-Liebrich U, Blaser K, Bolognini G, Bongard JP, Brandli O, Braun P, Bron C, Brutsche M, et al. Passive smoking exposure in adults and chronic respiratory symptoms (SAPALDIA Study). Swiss Study on Air Pollution and Lung Diseases in Adults, SAPALDIA Team. *American journal of respiratory and critical care medicine* 1994; 150: 1222-1228.
42. Raad D, Gaddam S, Schunemann HJ, Irani J, Abou Jaoude P, Honeine R, Akl EA. Effects of water-pipe smoking on lung function: a systematic review and meta-analysis. *Chest* 2011; 139: 764-774.
43. Tan WC, Lo C, Jong A, Xing L, Fitzgerald MJ, Vollmer WM, Buist SA, Sin DD, Vancouver Burden of Obstructive Lung Disease Research G. Marijuana and chronic obstructive lung disease: a population-based study. *CMAJ : Canadian Medical Association journal = journal de l'Association medicale canadienne* 2009; 180: 814-820.
44. World Health Organization Study Group on Tobacco Product R. WHO Study Group on Tobacco Product Regulation. Report on the scientific basis of tobacco product regulation: fourth report of a WHO study group. *World Health Organization technical report series* 2012: 1-83, 81 p following 83.
45. Tetrault JM, Crothers K, Moore BA, Mehra R, Concato J, Fiellin DA. Effects of marijuana smoking on pulmonary function and respiratory complications: a systematic review. *Archives of internal medicine* 2007; 167: 221-228.
46. Devereux G. ABC of chronic obstructive pulmonary disease. Definition, epidemiology, and risk factors. *Bmj* 2006; 332: 1142-1144.
47. Halbert RJ, Natoli JL, Gano A, Badamgarav E, Buist AS, Mannino DM. Global burden of COPD: systematic review and meta-analysis. *The European respiratory journal* 2006; 28: 523-532.
48. Foreman MG, Campos M, Celedon JC. Genes and chronic obstructive pulmonary disease. *The Medical clinics of North America* 2012; 96: 699-711.
49. Hutchinson J. On the capacity of the lungs, and on the respiratory functions, with a view of establishing a precise and easy method of detecting disease by the spirometer. *Medico-chirurgical transactions* 1846; 29: 137-252.
50. Crapo RO. Pulmonary-function testing. *The New England journal of medicine* 1994; 331: 25-30.
51. Tiffeneau R, Pinelli. [Not Available]. *Paris medical* 1947; 37: 624-628.
52. Qaseem A, Wilt TJ, Weinberger SE, Hanania NA, Criner G, van der Molen T, Marciniuk DD, Denberg T, Schunemann H, Wedzicha W, MacDonald R, Shekelle P, American College of P, American College of Chest P, American Thoracic S, European Respiratory S. Diagnosis and management of stable chronic obstructive pulmonary disease: a clinical practice guideline update from the American College of Physicians, American College of Chest Physicians, American Thoracic Society, and European Respiratory Society. *Annals of internal medicine* 2011; 155: 179-191.
53. Hartman JE, Ten Hacken NH, Klooster K, Boezen HM, de Greef MH, Slebos DJ. The minimal important difference for residual volume in patients with severe emphysema. *The European respiratory journal* 2012; 40: 1137-1141.
54. Newell JD, Jr., Hogg JC, Snider GL. Report of a workshop: quantitative computed tomography scanning in longitudinal studies of emphysema. *The European respiratory journal* 2004; 23: 769-775.
55. Kaminsky DA, Whitman T, Callas PW. DLCO versus DLCO/VA as predictors of pulmonary gas exchange. *Respiratory medicine* 2007; 101: 989-994.

56. Diaz PT, Bruns AS, Ezzie ME, Marchetti N, Thomashow BM. Optimizing bronchodilator therapy in emphysema. *Proceedings of the American Thoracic Society* 2008; 5: 501-505.
57. Shafazand S. ACP Journal Club. Review: inhaled medications vary substantively in their effects on mortality in COPD. *Annals of internal medicine* 2013; 158: JC2.
58. Price D, Yawn B, Brusselle G, Rossi A. Risk-to-benefit ratio of inhaled corticosteroids in patients with COPD. *Primary care respiratory journal : journal of the General Practice Airways Group* 2013; 22: 92-100.
59. Zhou Y, Tan X, Kuang W, Liu L, Wan L. Erythromycin ameliorates cigarette-smoke-induced emphysema and inflammation in rats. *Translational research : the journal of laboratory and clinical medicine* 2012; 159: 464-472.
60. Decramer M, Janssens W, Miravittles M. Chronic obstructive pulmonary disease. *Lancet* 2012; 379: 1341-1351.
61. Sandhaus RA. alpha1-Antitrypsin deficiency . 6: new and emerging treatments for alpha1-antitrypsin deficiency. *Thorax* 2004; 59: 904-909.
62. Kneidinger N, Yildirim AO, Callegari J, Takenaka S, Stein MM, Dumitrascu R, Bohla A, Bracke KR, Morty RE, Brusselle GG, Schermuly RT, Eickelberg O, Konigshoff M. Activation of the WNT/beta-catenin pathway attenuates experimental emphysema. *American journal of respiratory and critical care medicine* 2011; 183: 723-733.
63. MacNee W, Tudor RM. New paradigms in the pathogenesis of chronic obstructive pulmonary disease I. *Proceedings of the American Thoracic Society* 2009; 6: 527-531.
64. Bourbon JR, Boucherat O, Boczkowski J, Crestani B, Delacourt C. Bronchopulmonary dysplasia and emphysema: in search of common therapeutic targets. *Trends in molecular medicine* 2009; 15: 169-179.
65. Barnes PJ. Mediators of chronic obstructive pulmonary disease. *Pharmacological reviews* 2004; 56: 515-548.
66. Barnes PJ. Mechanisms in COPD: differences from asthma. *Chest* 2000; 117: 10S-14S.
67. Laurell CB, Eriksson S. The electrophoretic alpha1-globulin pattern of serum in alpha1-antitrypsin deficiency. 1963. *Copd* 2013; 10 Suppl 1: 3-8.
68. Takubo Y, Guerassimov A, Ghezzi H, Triantafillopoulos A, Bates JH, Hoidal JR, Cosio MG. Alpha1-antitrypsin determines the pattern of emphysema and function in tobacco smoke-exposed mice: parallels with human disease. *American journal of respiratory and critical care medicine* 2002; 166: 1596-1603.
69. Cavarra E, Bartalesi B, Lucattelli M, Fineschi S, Lunghi B, Gambelli F, Ortiz LA, Martorana PA, Lungarella G. Effects of cigarette smoke in mice with different levels of alpha(1)-proteinase inhibitor and sensitivity to oxidants. *American journal of respiratory and critical care medicine* 2001; 164: 886-890.
70. Pham CT. Neutrophil serine proteases: specific regulators of inflammation. *Nature reviews Immunology* 2006; 6: 541-550.
71. Churg A, Zhou S, Wright JL. Series "matrix metalloproteinases in lung health and disease": Matrix metalloproteinases in COPD. *The European respiratory journal* 2012; 39: 197-209.
72. Thorley AJ, Tetley TD. Pulmonary epithelium, cigarette smoke, and chronic obstructive pulmonary disease. *International journal of chronic obstructive pulmonary disease* 2007; 2: 409-428.
73. Abboud RT, Vimalanathan S. Pathogenesis of COPD. Part I. The role of protease-antiprotease imbalance in emphysema. *The international journal of tuberculosis and lung disease : the official journal of the International Union against Tuberculosis and Lung Disease* 2008; 12: 361-367.
74. Shapiro SD, Goldstein NM, Houghton AM, Kobayashi DK, Kelley D, Belaaouaj A. Neutrophil elastase contributes to cigarette smoke-induced emphysema in mice. *The American journal of pathology* 2003; 163: 2329-2335.

75. Stamenkovic I. Extracellular matrix remodelling: the role of matrix metalloproteinases. *The Journal of pathology* 2003; 200: 448-464.
76. Hautamaki RD, Kobayashi DK, Senior RM, Shapiro SD. Requirement for macrophage elastase for cigarette smoke-induced emphysema in mice. *Science* 1997; 277: 2002-2004.
77. Beeh KM, Beier J, Kornmann O, Buhl R. Sputum matrix metalloproteinase-9, tissue inhibitor of metalloproteinase-1, and their molar ratio in patients with chronic obstructive pulmonary disease, idiopathic pulmonary fibrosis and healthy subjects. *Respiratory medicine* 2003; 97: 634-639.
78. Vernooy JH, Lindeman JH, Jacobs JA, Hanemaaijer R, Wouters EF. Increased activity of matrix metalloproteinase-8 and matrix metalloproteinase-9 in induced sputum from patients with COPD. *Chest* 2004; 126: 1802-1810.
79. Culpitt SV, Rogers DF, Traves SL, Barnes PJ, Donnelly LE. Sputum matrix metalloproteinases: comparison between chronic obstructive pulmonary disease and asthma. *Respiratory medicine* 2005; 99: 703-710.
80. Demedts IK, Morel-Montero A, Lebecque S, Pacheco Y, Cataldo D, Joos GF, Pauwels RA, Brusselle GG. Elevated MMP-12 protein levels in induced sputum from patients with COPD. *Thorax* 2006; 61: 196-201.
81. Elkington PT, Friedland JS. Matrix metalloproteinases in destructive pulmonary pathology. *Thorax* 2006; 61: 259-266.
82. Pons AR, Sauleda J, Noguera A, Pons J, Barcelo B, Fuster A, Agusti AG. Decreased macrophage release of TGF-beta and TIMP-1 in chronic obstructive pulmonary disease. *The European respiratory journal* 2005; 26: 60-66.
83. Leco KJ, Waterhouse P, Sanchez OH, Gowing KL, Poole AR, Wakeham A, Mak TW, Khokha R. Spontaneous air space enlargement in the lungs of mice lacking tissue inhibitor of metalloproteinases-3 (TIMP-3). *The Journal of clinical investigation* 2001; 108: 817-829.
84. Imai K, Mercer BA, Schulman LL, Sonett JR, D'Armiento JM. Correlation of lung surface area to apoptosis and proliferation in human emphysema. *The European respiratory journal* 2005; 25: 250-258.
85. Yokohori N, Aoshiba K, Nagai A, Respiratory Failure Research Group in J. Increased levels of cell death and proliferation in alveolar wall cells in patients with pulmonary emphysema. *Chest* 2004; 125: 626-632.
86. Aoshiba K, Yokohori N, Nagai A. Alveolar wall apoptosis causes lung destruction and emphysematous changes. *American journal of respiratory cell and molecular biology* 2003; 28: 555-562.
87. Kanazawa H. Role of vascular endothelial growth factor in the pathogenesis of chronic obstructive pulmonary disease. *Medical science monitor : international medical journal of experimental and clinical research* 2007; 13: RA189-195.
88. Marwick JA, Stevenson CS, Giddings J, MacNee W, Butler K, Rahman I, Kirkham PA. Cigarette smoke disrupts VEGF165-VEGFR-2 receptor signaling complex in rat lungs and patients with COPD: morphological impact of VEGFR-2 inhibition. *American journal of physiology Lung cellular and molecular physiology* 2006; 290: L897-908.
89. Tang K, Rossiter HB, Wagner PD, Breen EC. Lung-targeted VEGF inactivation leads to an emphysema phenotype in mice. *Journal of applied physiology* 2004; 97: 1559-1566; discussion 1549.
90. Tsao PN, Su YN, Li H, Huang PH, Chien CT, Lai YL, Lee CN, Chen CA, Cheng WF, Wei SC, Yu CJ, Hsieh FJ, Hsu SM. Overexpression of placenta growth factor contributes to the pathogenesis of pulmonary emphysema. *American journal of respiratory and critical care medicine* 2004; 169: 505-511.

91. Lucey EC, Keane J, Kuang PP, Snider GL, Goldstein RH. Severity of elastase-induced emphysema is decreased in tumor necrosis factor-alpha and interleukin-1beta receptor-deficient mice. *Laboratory investigation; a journal of technical methods and pathology* 2002; 82: 79-85.
92. Powell WC, Fingleton B, Wilson CL, Boothby M, Matrisian LM. The metalloproteinase matrilysin proteolytically generates active soluble Fas ligand and potentiates epithelial cell apoptosis. *Current biology : CB* 1999; 9: 1441-1447.
93. Barry M, Bleackley RC. Cytotoxic T lymphocytes: all roads lead to death. *Nature reviews Immunology* 2002; 2: 401-409.
94. Liu AN, Mohammed AZ, Rice WR, Fiedeldej DT, Liebermann JS, Whitsett JA, Braciale TJ, Enelow RI. Perforin-independent CD8(+) T-cell-mediated cytotoxicity of alveolar epithelial cells is preferentially mediated by tumor necrosis factor-alpha: relative insensitivity to Fas ligand. *American journal of respiratory cell and molecular biology* 1999; 20: 849-858.
95. Pryor WA, Stone K. Oxidants in cigarette smoke. Radicals, hydrogen peroxide, peroxyxynitrate, and peroxyxynitrite. *Annals of the New York Academy of Sciences* 1993; 686: 12-27; discussion 27-18.
96. Church DF, Pryor WA. Free-radical chemistry of cigarette smoke and its toxicological implications. *Environmental health perspectives* 1985; 64: 111-126.
97. Mateos F, Brock JH, Perez-Arellano JL. Iron metabolism in the lower respiratory tract. *Thorax* 1998; 53: 594-600.
98. Bowler RP, Barnes PJ, Crapo JD. The role of oxidative stress in chronic obstructive pulmonary disease. *Copd* 2004; 1: 255-277.
99. Kode A, Yang SR, Rahman I. Differential effects of cigarette smoke on oxidative stress and proinflammatory cytokine release in primary human airway epithelial cells and in a variety of transformed alveolar epithelial cells. *Respiratory research* 2006; 7: 132.
100. Itoh K, Chiba T, Takahashi S, Ishii T, Igarashi K, Katoh Y, Oyake T, Hayashi N, Satoh K, Hatayama I, Yamamoto M, Nabeshima Y. An Nrf2/small Maf heterodimer mediates the induction of phase II detoxifying enzyme genes through antioxidant response elements. *Biochemical and biophysical research communications* 1997; 236: 313-322.
101. Ishii Y, Itoh K, Morishima Y, Kimura T, Kiwamoto T, Iizuka T, Hegab AE, Hosoya T, Nomura A, Sakamoto T, Yamamoto M, Sekizawa K. Transcription factor Nrf2 plays a pivotal role in protection against elastase-induced pulmonary inflammation and emphysema. *Journal of immunology* 2005; 175: 6968-6975.
102. Tanabe N, Hoshino Y, Marumo S, Kiyokawa H, Sato S, Kinose D, Uno K, Muro S, Hirai T, Yodoi J, Mishima M. Thioredoxin-1 protects against neutrophilic inflammation and emphysema progression in a mouse model of chronic obstructive pulmonary disease exacerbation. *PLoS one* 2013; 8: e79016.
103. Yao H, Arunachalam G, Hwang JW, Chung S, Sundar IK, Kinnula VL, Crapo JD, Rahman I. Extracellular superoxide dismutase protects against pulmonary emphysema by attenuating oxidative fragmentation of ECM. *Proceedings of the National Academy of Sciences of the United States of America* 2010; 107: 15571-15576.
104. Seimetz M, Parajuli N, Pichl A, Veit F, Kwapiszewska G, Weisel FC, Milger K, Egemnazarov B, Turowska A, Fuchs B, Nikam S, Roth M, Sydykov A, Medebach T, Klepetko W, Jaksch P, Dumitrascu R, Garn H, Voswinckel R, Kostin S, Seeger W, Schermuly RT, Grimminger F, Ghofrani HA, Weissmann N. Inducible NOS inhibition reverses tobacco-smoke-induced emphysema and pulmonary hypertension in mice. *Cell* 2011; 147: 293-305.
105. Hellermann GR, Nagy SB, Kong X, Lockey RF, Mohapatra SS. Mechanism of cigarette smoke condensate-induced acute inflammatory response in human bronchial epithelial cells. *Respiratory research* 2002; 3: 22.

106. Mio T, Romberger DJ, Thompson AB, Robbins RA, Heires A, Rennard SI. Cigarette smoke induces interleukin-8 release from human bronchial epithelial cells. *American journal of respiratory and critical care medicine* 1997; 155: 1770-1776.
107. Takizawa H, Tanaka M, Takami K, Ohtoshi T, Ito K, Satoh M, Okada Y, Yamasawa F, Nakahara K, Umeda A. Increased expression of transforming growth factor-beta1 in small airway epithelium from tobacco smokers and patients with chronic obstructive pulmonary disease (COPD). *American journal of respiratory and critical care medicine* 2001; 163: 1476-1483.
108. Li YJ, Yu CH, Li JB, Wu XY. Andrographolide antagonizes cigarette smoke extract-induced inflammatory response and oxidative stress in human alveolar epithelial A549 cells through induction of microRNA-218. *Experimental lung research* 2013; 39: 463-471.
109. Di Stefano A, Capelli A, Lusuardi M, Balbo P, Vecchio C, Maestrelli P, Mapp CE, Fabbri LM, Donner CF, Saetta M. Severity of airflow limitation is associated with severity of airway inflammation in smokers. *American journal of respiratory and critical care medicine* 1998; 158: 1277-1285.
110. Retamales I, Elliott WM, Meshi B, Coxson HO, Pare PD, Sciruba FC, Rogers RM, Hayashi S, Hogg JC. Amplification of inflammation in emphysema and its association with latent adenoviral infection. *American journal of respiratory and critical care medicine* 2001; 164: 469-473.
111. Shapiro SD. The macrophage in chronic obstructive pulmonary disease. *American journal of respiratory and critical care medicine* 1999; 160: S29-32.
112. Lapperre TS, Willems LN, Timens W, Rabe KF, Hiemstra PS, Postma DS, Sterk PJ. Small airways dysfunction and neutrophilic inflammation in bronchial biopsies and BAL in COPD. *Chest* 2007; 131: 53-59.
113. Lacoste JY, Bousquet J, Chanez P, Van Vyve T, Simony-Lafontaine J, Lequeu N, Vic P, Enander I, Godard P, Michel FB. Eosinophilic and neutrophilic inflammation in asthma, chronic bronchitis, and chronic obstructive pulmonary disease. *The Journal of allergy and clinical immunology* 1993; 92: 537-548.
114. Keatings VM, Collins PD, Scott DM, Barnes PJ. Differences in interleukin-8 and tumor necrosis factor-alpha in induced sputum from patients with chronic obstructive pulmonary disease or asthma. *American journal of respiratory and critical care medicine* 1996; 153: 530-534.
115. Di Stefano A, Maestrelli P, Roggeri A, Turato G, Calabro S, Potena A, Mapp CE, Ciaccia A, Covacev L, Fabbri LM, Saetta M. Upregulation of adhesion molecules in the bronchial mucosa of subjects with chronic obstructive bronchitis. *American journal of respiratory and critical care medicine* 1994; 149: 803-810.
116. Majo J, Ghezze H, Cosio MG. Lymphocyte population and apoptosis in the lungs of smokers and their relation to emphysema. *The European respiratory journal* 2001; 17: 946-953.
117. Zeid NA, Muller HK. Tobacco smoke induced lung granulomas and tumors: association with pulmonary Langerhans cells. *Pathology* 1995; 27: 247-254.
118. Givi ME, Peck MJ, Boon L, Mortaz E. The role of dendritic cells in the pathogenesis of cigarette smoke-induced emphysema in mice. *European journal of pharmacology* 2013; 721: 259-266.
119. Stoll P, Heinz AS, Bratke K, Bier A, Garbe K, Kuepper M, Virchow JC, Lommatzsch M. Impact of smoking on dendritic cell phenotypes in the airway lumen of patients with COPD. *Respiratory research* 2014; 15: 48.
120. Hayflick L. The Limited in Vitro Lifetime of Human Diploid Cell Strains. *Experimental cell research* 1965; 37: 614-636.
121. Karrasch S, Holz O, Jorres RA. Aging and induced senescence as factors in the pathogenesis of lung emphysema. *Respiratory medicine* 2008; 102: 1215-1230.
122. Vogelmeier C, Bals R. Chronic obstructive pulmonary disease and premature aging. *American journal of respiratory and critical care medicine* 2007; 175: 1217-1218.

123. Alder JK, Guo N, Kembou F, Parry EM, Anderson CJ, Gorgy AI, Walsh MF, Sussan T, Biswal S, Mitzner W, Tudor RM, Armanios M. Telomere length is a determinant of emphysema susceptibility. *American journal of respiratory and critical care medicine* 2011; 184: 904-912.
124. Muller KC, Welker L, Paasch K, Feindt B, Erpenbeck VJ, Hohlfeld JM, Krug N, Nakashima M, Branscheid D, Magnussen H, Jorres RA, Holz O. Lung fibroblasts from patients with emphysema show markers of senescence in vitro. *Respiratory research* 2006; 7: 32.
125. Aoshiba K, Nagai A. Senescence hypothesis for the pathogenetic mechanism of chronic obstructive pulmonary disease. *Proceedings of the American Thoracic Society* 2009; 6: 596-601.
126. Tsuji T, Aoshiba K, Nagai A. Alveolar cell senescence in patients with pulmonary emphysema. *American journal of respiratory and critical care medicine* 2006; 174: 886-893.
127. Tsuji T, Aoshiba K, Nagai A. Cigarette smoke induces senescence in alveolar epithelial cells. *American journal of respiratory cell and molecular biology* 2004; 31: 643-649.
128. Dimri GP, Lee X, Basile G, Acosta M, Scott G, Roskelley C, Medrano EE, Linskens M, Rubelj I, Pereira-Smith O, et al. A biomarker that identifies senescent human cells in culture and in aging skin in vivo. *Proceedings of the National Academy of Sciences of the United States of America* 1995; 92: 9363-9367.
129. Holz O, Zuhlke I, Jaksztat E, Muller KC, Welker L, Nakashima M, Diemel KD, Branscheid D, Magnussen H, Jorres RA. Lung fibroblasts from patients with emphysema show a reduced proliferation rate in culture. *The European respiratory journal* 2004; 24: 575-579.
130. Baker DJ, Perez-Terzic C, Jin F, Pitel KS, Niederlander NJ, Jeganathan K, Yamada S, Reyes S, Rowe L, Hiddinga HJ, Eberhardt NL, Terzic A, van Deursen JM. Opposing roles for p16Ink4a and p19Arf in senescence and ageing caused by BubR1 insufficiency. *Nature cell biology* 2008; 10: 825-836.
131. Dagouassat M, Gagliolo JM, Chrusciel S, Bourin MC, Duprez C, Caramelle P, Boyer L, Hue S, Stern JB, Validire P, Longrois D, Norel X, Dubois-Rande JL, Le Gouvello S, Adnot S, Boczkowski J. The cyclooxygenase-2-prostaglandin E2 pathway maintains senescence of chronic obstructive pulmonary disease fibroblasts. *American journal of respiratory and critical care medicine* 2013; 187: 703-714.
132. Shapiro SD, Ingenito EP. The pathogenesis of chronic obstructive pulmonary disease: advances in the past 100 years. *American journal of respiratory cell and molecular biology* 2005; 32: 367-372.
133. Krishnamurthy J, Torrice C, Ramsey MR, Kovalev GI, Al-Regaiey K, Su L, Sharpless NE. Ink4a/Arf expression is a biomarker of aging. *The Journal of clinical investigation* 2004; 114: 1299-1307.
134. Aoshiba K, Zhou F, Tsuji T, Nagai A. DNA damage as a molecular link in the pathogenesis of COPD in smokers. *The European respiratory journal* 2012; 39: 1368-1376.
135. Donmez G, Guarente L. Aging and disease: connections to sirtuins. *Aging cell* 2010; 9: 285-290.
136. Rajendrasozhan S, Yang SR, Kinnula VL, Rahman I. SIRT1, an antiinflammatory and antiaging protein, is decreased in lungs of patients with chronic obstructive pulmonary disease. *American journal of respiratory and critical care medicine* 2008; 177: 861-870.
137. Yao H, Chung S, Hwang JW, Rajendrasozhan S, Sundar IK, Dean DA, McBurney MW, Guarente L, Gu W, Ronty M, Kinnula VL, Rahman I. SIRT1 protects against emphysema via FOXO3-mediated reduction of premature senescence in mice. *The Journal of clinical investigation* 2012; 122: 2032-2045.
138. Kao CL, Chen LK, Chang YL, Yung MC, Hsu CC, Chen YC, Lo WL, Chen SJ, Ku HH, Hwang SJ. Resveratrol protects human endothelium from H₂O₂-induced oxidative stress and senescence via SirT1 activation. *Journal of atherosclerosis and thrombosis* 2010; 17: 970-979.
139. Yildirim AO, Muyal V, John G, Muller B, Seifart C, Kasper M, Fehrenbach H. Palifermin induces alveolar maintenance programs in emphysematous mice. *American journal of respiratory and critical care medicine* 2010; 181: 705-717.

140. Vanoirbeek JA, Rinaldi M, De Vooght V, Haenen S, Bobic S, Gayan-Ramirez G, Hoet PH, Verbeken E, Decramer M, Nemery B, Janssens W. Noninvasive and invasive pulmonary function in mouse models of obstructive and restrictive respiratory diseases. *American journal of respiratory cell and molecular biology* 2010; 42: 96-104.
141. Gross P, Pfitzer EA, Tolker E, Babyak MA, Kaschak M. Experimental Emphysema: Its Production with Papain in Normal and Silicotic Rats. *Archives of environmental health* 1965; 11: 50-58.
142. Janoff A. Elastases and emphysema. Current assessment of the protease-antiprotease hypothesis. *The American review of respiratory disease* 1985; 132: 417-433.
143. Kuhn C, Yu SY, Chraplyvy M, Linder HE, Senior RM. The induction of emphysema with elastase. II. Changes in connective tissue. *Laboratory investigation; a journal of technical methods and pathology* 1976; 34: 372-380.
144. Houghton AM, Quintero PA, Perkins DL, Kobayashi DK, Kelley DG, Marconcini LA, Mecham RP, Senior RM, Shapiro SD. Elastin fragments drive disease progression in a murine model of emphysema. *The Journal of clinical investigation* 2006; 116: 753-759.
145. Stone PJ, Pereira W, Jr., Biles D, Snider GL, Kagan HM, Franzblau C. Studies on the fate of pancreatic elastase in the hamster lung: 14C-guanidinated elastase. *The American review of respiratory disease* 1977; 116: 49-56.
146. Starcher BC. Elastin and the lung. *Thorax* 1986; 41: 577-585.
147. Hogg JC, Chu F, Utokaparch S, Woods R, Elliott WM, Buzatu L, Cherniack RM, Rogers RM, Sciurba FC, Coxson HO, Pare PD. The nature of small-airway obstruction in chronic obstructive pulmonary disease. *The New England journal of medicine* 2004; 350: 2645-2653.
148. Kobayashi S, Fujinawa R, Ota F, Kobayashi S, Angata T, Ueno M, Maeno T, Kitazume S, Yoshida K, Ishii T, Gao C, Ohtsubo K, Yamaguchi Y, Betsuyaku T, Kida K, Taniguchi N. A single dose of lipopolysaccharide into mice with emphysema mimics human chronic obstructive pulmonary disease exacerbation as assessed by micro-computed tomography. *American journal of respiratory cell and molecular biology* 2013; 49: 971-977.
149. Hens G, Raap U, Vanoirbeek J, Meyts I, Callebaut I, Verbinnen B, Vanaudenaerde BM, Cadot P, Nemery B, Bullens DM, Ceuppens JL, Hellings PW. Selective nasal allergen provocation induces substance P-mediated bronchial hyperresponsiveness. *American journal of respiratory cell and molecular biology* 2011; 44: 517-523.
150. Dhami R, Gilks B, Xie C, Zay K, Wright JL, Churg A. Acute cigarette smoke-induced connective tissue breakdown is mediated by neutrophils and prevented by alpha1-antitrypsin. *American journal of respiratory cell and molecular biology* 2000; 22: 244-252.
151. Wright JL, Churg A. Cigarette smoke causes physiologic and morphologic changes of emphysema in the guinea pig. *The American review of respiratory disease* 1990; 142: 1422-1428.
152. Stevenson CS, Docx C, Webster R, Battram C, Hynx D, Giddings J, Cooper PR, Chakravarty P, Rahman I, Marwick JA, Kirkham PA, Charman C, Richardson DL, Nirmala NR, Whittaker P, Butler K. Comprehensive gene expression profiling of rat lung reveals distinct acute and chronic responses to cigarette smoke inhalation. *American journal of physiology Lung cellular and molecular physiology* 2007; 293: L1183-1193.
153. Guerassimov A, Hoshino Y, Takubo Y, Turcotte A, Yamamoto M, Ghezzi H, Triantafillopoulos A, Whittaker K, Hoidal JR, Cosio MG. The development of emphysema in cigarette smoke-exposed mice is strain dependent. *American journal of respiratory and critical care medicine* 2004; 170: 974-980.
154. Leberl M, Kratzer A, Taraseviciene-Stewart L. Tobacco smoke induced COPD/emphysema in the animal model-are we all on the same page? *Frontiers in physiology* 2013; 4: 91.
155. John-Schuster G, Hager K, Conlon TM, Irmeler M, Beckers J, Eickelberg O, Yildirim AO. Cigarette smoke-induced iBALT mediates macrophage activation in a B cell-dependent manner in COPD. *American journal of physiology Lung cellular and molecular physiology* 2014; 307: L692-706.

156. Farley AR, Link AJ. Identification and quantification of protein posttranslational modifications. *Methods in enzymology* 2009; 463: 725-763.
157. Bedford MT, Richard S. Arginine methylation an emerging regulator of protein function. *Molecular cell* 2005; 18: 263-272.
158. Tapiero H, Mathe G, Couvreur P, Tew KD. I. Arginine. *Biomedicine & pharmacotherapy = Biomedecine & pharmacotherapie* 2002; 56: 439-445.
159. Rogers GE. Occurrence of citrulline in proteins. *Nature* 1962; 194: 1149-1151.
160. Rogers GE, Simmonds DH. Content of citrulline and other amino-acids in a protein of hair follicles. *Nature* 1958; 182: 186-187.
161. Slade DJ, Subramanian V, Fuhrmann J, Thompson PR. Chemical and biological methods to detect post-translational modifications of arginine. *Biopolymers* 2014; 101: 133-143.
162. Paik WK, Kim S. Protein methylation. New York ; Chichester: Wiley; 1980.
163. Paik WK, Kim S. Enzymatic methylation of protein fractions from calf thymus nuclei. *Biochemical and biophysical research communications* 1967; 29: 14-20.
164. Gary JD, Clarke S. RNA and protein interactions modulated by protein arginine methylation. *Progress in nucleic acid research and molecular biology* 1998; 61: 65-131.
165. Mostaqul Huq MD, Gupta P, Tsai NP, White R, Parker MG, Wei LN. Suppression of receptor interacting protein 140 repressive activity by protein arginine methylation. *The EMBO journal* 2006; 25: 5094-5104.
166. Gary JD, Lin WJ, Yang MC, Herschman HR, Clarke S. The predominant protein-arginine methyltransferase from *Saccharomyces cerevisiae*. *The Journal of biological chemistry* 1996; 271: 12585-12594.
167. Henry MF, Silver PA. A novel methyltransferase (Hmt1p) modifies poly(A)⁺-RNA-binding proteins. *Molecular and cellular biology* 1996; 16: 3668-3678.
168. Wolf SS. The protein arginine methyltransferase family: an update about function, new perspectives and the physiological role in humans. *Cellular and molecular life sciences : CMLS* 2009; 66: 2109-2121.
169. Cheng X, Collins RE, Zhang X. Structural and sequence motifs of protein (histone) methylation enzymes. *Annual review of biophysics and biomolecular structure* 2005; 34: 267-294.
170. Bedford MT, Clarke SG. Protein arginine methylation in mammals: who, what, and why. *Molecular cell* 2009; 33: 1-13.
171. Wei H, Mundade R, Lange KC, Lu T. Protein arginine methylation of non-histone proteins and its role in diseases. *Cell cycle* 2014; 13: 32-41.
172. Bedford MT. Arginine methylation at a glance. *Journal of cell science* 2007; 120: 4243-4246.
173. Lee YH, Stallcup MR. Minireview: protein arginine methylation of nonhistone proteins in transcriptional regulation. *Molecular endocrinology* 2009; 23: 425-433.
174. Najbauer J, Johnson BA, Young AL, Aswad DW. Peptides with sequences similar to glycine, arginine-rich motifs in proteins interacting with RNA are efficiently recognized by methyltransferase(s) modifying arginine in numerous proteins. *The Journal of biological chemistry* 1993; 268: 10501-10509.
175. Cheng D, Cote J, Shaaban S, Bedford MT. The arginine methyltransferase CARM1 regulates the coupling of transcription and mRNA processing. *Molecular cell* 2007; 25: 71-83.
176. Bedford MT, Reed R, Leder P. WW domain-mediated interactions reveal a spliceosome-associated protein that binds a third class of proline-rich motif: the proline glycine and methionine-rich motif. *Proceedings of the National Academy of Sciences of the United States of America* 1998; 95: 10602-10607.
177. Bachand F. Protein arginine methyltransferases: from unicellular eukaryotes to humans. *Eukaryotic cell* 2007; 6: 889-898.
178. Sayegh J, Clarke SG. Hsl7 is a substrate-specific type II protein arginine methyltransferase in yeast. *Biochemical and biophysical research communications* 2008; 372: 811-815.

179. Zurita-Lopez CI, Sandberg T, Kelly R, Clarke SG. Human protein arginine methyltransferase 7 (PRMT7) is a type III enzyme forming omega-NG-monomethylated arginine residues. *The Journal of biological chemistry* 2012; 287: 7859-7870.
180. Fisk JC, Sayegh J, Zurita-Lopez C, Menon S, Presnyak V, Clarke SG, Read LK. A type III protein arginine methyltransferase from the protozoan parasite *Trypanosoma brucei*. *The Journal of biological chemistry* 2009; 284: 11590-11600.
181. Niewmierzycka A, Clarke S. S-Adenosylmethionine-dependent methylation in *Saccharomyces cerevisiae*. Identification of a novel protein arginine methyltransferase. *The Journal of biological chemistry* 1999; 274: 814-824.
182. McBride AE, Zurita-Lopez C, Regis A, Blum E, Conboy A, Elf S, Clarke S. Protein arginine methylation in *Candida albicans*: role in nuclear transport. *Eukaryotic cell* 2007; 6: 1119-1129.
183. Krause CD, Yang ZH, Kim YS, Lee JH, Cook JR, Pestka S. Protein arginine methyltransferases: evolution and assessment of their pharmacological and therapeutic potential. *Pharmacology & therapeutics* 2007; 113: 50-87.
184. Herrmann F, Bossert M, Schwander A, Akgun E, Fackelmayer FO. Arginine methylation of scaffold attachment factor A by heterogeneous nuclear ribonucleoprotein particle-associated PRMT1. *The Journal of biological chemistry* 2004; 279: 48774-48779.
185. Wang H, Huang ZQ, Xia L, Feng Q, Erdjument-Bromage H, Strahl BD, Briggs SD, Allis CD, Wong J, Tempst P, Zhang Y. Methylation of histone H4 at arginine 3 facilitating transcriptional activation by nuclear hormone receptor. *Science* 2001; 293: 853-857.
186. Pawlak MR, Scherer CA, Chen J, Roshon MJ, Ruley HE. Arginine N-methyltransferase 1 is required for early postimplantation mouse development, but cells deficient in the enzyme are viable. *Molecular and cellular biology* 2000; 20: 4859-4869.
187. Scott HS, Antonarakis SE, Lalioti MD, Rossier C, Silver PA, Henry MF. Identification and characterization of two putative human arginine methyltransferases (HRMT1L1 and HRMT1L2). *Genomics* 1998; 48: 330-340.
188. Lakowski TM, Frankel A. Kinetic analysis of human protein arginine N-methyltransferase 2: formation of monomethyl- and asymmetric dimethyl-arginine residues on histone H4. *The Biochemical journal* 2009; 421: 253-261.
189. Kzhyshkowska J, Schutt H, Liss M, Kremmer E, Stauber R, Wolf H, Dobner T. Heterogeneous nuclear ribonucleoprotein E1B-AP5 is methylated in its Arg-Gly-Gly (RGG) box and interacts with human arginine methyltransferase HRMT1L1. *The Biochemical journal* 2001; 358: 305-314.
190. Qi C, Chang J, Zhu Y, Yeldandi AV, Rao SM, Zhu YJ. Identification of protein arginine methyltransferase 2 as a coactivator for estrogen receptor alpha. *The Journal of biological chemistry* 2002; 277: 28624-28630.
191. Meyer R, Wolf SS, Obendorf M. PRMT2, a member of the protein arginine methyltransferase family, is a coactivator of the androgen receptor. *The Journal of steroid biochemistry and molecular biology* 2007; 107: 1-14.
192. Yoshimoto T, Boehm M, Olive M, Crook MF, San H, Langenickel T, Nabel EG. The arginine methyltransferase PRMT2 binds RB and regulates E2F function. *Experimental cell research* 2006; 312: 2040-2053.
193. Yildirim AO, Bulau P, Zakrzewicz D, Kitowska KE, Weissmann N, Grimminger F, Morty RE, Eickelberg O. Increased protein arginine methylation in chronic hypoxia: role of protein arginine methyltransferases. *American journal of respiratory cell and molecular biology* 2006; 35: 436-443.
194. Tang J, Gary JD, Clarke S, Herschman HR. PRMT 3, a type I protein arginine N-methyltransferase that differs from PRMT1 in its oligomerization, subcellular localization, substrate specificity, and regulation. *The Journal of biological chemistry* 1998; 273: 16935-16945.

195. Bachand F, Silver PA. PRMT3 is a ribosomal protein methyltransferase that affects the cellular levels of ribosomal subunits. *The EMBO journal* 2004; 23: 2641-2650.
196. Swiercz R, Person MD, Bedford MT. Ribosomal protein S2 is a substrate for mammalian PRMT3 (protein arginine methyltransferase 3). *The Biochemical journal* 2005; 386: 85-91.
197. Choi S, Jung CR, Kim JY, Im DS. PRMT3 inhibits ubiquitination of ribosomal protein S2 and together forms an active enzyme complex. *Biochimica et biophysica acta* 2008; 1780: 1062-1069.
198. Swiercz R, Cheng D, Kim D, Bedford MT. Ribosomal protein rpS2 is hypomethylated in PRMT3-deficient mice. *The Journal of biological chemistry* 2007; 282: 16917-16923.
199. Chen D, Ma H, Hong H, Koh SS, Huang SM, Schurter BT, Aswad DW, Stallcup MR. Regulation of transcription by a protein methyltransferase. *Science* 1999; 284: 2174-2177.
200. Pollack BP, Kotenko SV, He W, Izotova LS, Barnoski BL, Pestka S. The human homologue of the yeast proteins Skb1 and Hsl7p interacts with Jak kinases and contains protein methyltransferase activity. *The Journal of biological chemistry* 1999; 274: 31531-31542.
201. Rho J, Choi S, Seong YR, Cho WK, Kim SH, Im DS. Prmt5, which forms distinct homo-oligomers, is a member of the protein-arginine methyltransferase family. *The Journal of biological chemistry* 2001; 276: 11393-11401.
202. Branscombe TL, Frankel A, Lee JH, Cook JR, Yang Z, Pestka S, Clarke S. PRMT5 (Janus kinase-binding protein 1) catalyzes the formation of symmetric dimethylarginine residues in proteins. *The Journal of biological chemistry* 2001; 276: 32971-32976.
203. Meister G, Fischer U. Assisted RNP assembly: SMN and PRMT5 complexes cooperate in the formation of spliceosomal UsnRNPs. *The EMBO journal* 2002; 21: 5853-5863.
204. Dacwag CS, Bedford MT, Sif S, Imbalzano AN. Distinct protein arginine methyltransferases promote ATP-dependent chromatin remodeling function at different stages of skeletal muscle differentiation. *Molecular and cellular biology* 2009; 29: 1909-1921.
205. Frankel A, Yadav N, Lee J, Branscombe TL, Clarke S, Bedford MT. The novel human protein arginine N-methyltransferase PRMT6 is a nuclear enzyme displaying unique substrate specificity. *The Journal of biological chemistry* 2002; 277: 3537-3543.
206. Sgarra R, Lee J, Tessari MA, Altamura S, Spolaore B, Giacotti V, Bedford MT, Manfioletti G. The AT-hook of the chromatin architectural transcription factor high mobility group A1a is arginine-methylated by protein arginine methyltransferase 6. *The Journal of biological chemistry* 2006; 281: 3764-3772.
207. El-Andaloussi N, Valovka T, Toueille M, Hassa PO, Gehrig P, Covic M, Hubscher U, Hottiger MO. Methylation of DNA polymerase beta by protein arginine methyltransferase 1 regulates its binding to proliferating cell nuclear antigen. *FASEB journal : official publication of the Federation of American Societies for Experimental Biology* 2007; 21: 26-34.
208. Boulanger MC, Liang C, Russell RS, Lin R, Bedford MT, Wainberg MA, Richard S. Methylation of Tat by PRMT6 regulates human immunodeficiency virus type 1 gene expression. *Journal of virology* 2005; 79: 124-131.
209. Hyllus D, Stein C, Schnabel K, Schiltz E, Imhof A, Dou Y, Hsieh J, Bauer UM. PRMT6-mediated methylation of R2 in histone H3 antagonizes H3 K4 trimethylation. *Genes & development* 2007; 21: 3369-3380.
210. Miranda TB, Miranda M, Frankel A, Clarke S. PRMT7 is a member of the protein arginine methyltransferase family with a distinct substrate specificity. *The Journal of biological chemistry* 2004; 279: 22902-22907.
211. Karkhanis V, Wang L, Tae S, Hu YJ, Imbalzano AN, Sif S. Protein arginine methyltransferase 7 regulates cellular response to DNA damage by methylating promoter histones H2A and H4 of the polymerase delta catalytic subunit gene, POLD1. *The Journal of biological chemistry* 2012; 287: 29801-29814.

212. Lee J, Sayegh J, Daniel J, Clarke S, Bedford MT. PRMT8, a new membrane-bound tissue-specific member of the protein arginine methyltransferase family. *The Journal of biological chemistry* 2005; 280: 32890-32896.
213. Sayegh J, Webb K, Cheng D, Bedford MT, Clarke SG. Regulation of protein arginine methyltransferase 8 (PRMT8) activity by its N-terminal domain. *The Journal of biological chemistry* 2007; 282: 36444-36453.
214. Cook JR, Lee JH, Yang ZH, Krause CD, Herth N, Hoffmann R, Pestka S. FBXO11/PRMT9, a new protein arginine methyltransferase, symmetrically dimethylates arginine residues. *Biochemical and biophysical research communications* 2006; 342: 472-481.
215. Troffer-Charlier N, Cura V, Hassenboehler P, Moras D, Cavarelli J. Functional insights from structures of coactivator-associated arginine methyltransferase 1 domains. *The EMBO journal* 2007; 26: 4391-4401.
216. Yue WW, Hassler M, Roe SM, Thompson-Vale V, Pearl LH. Insights into histone code syntax from structural and biochemical studies of CARM1 methyltransferase. *The EMBO journal* 2007; 26: 4402-4412.
217. Zhang X, Zhou L, Cheng X. Crystal structure of the conserved core of protein arginine methyltransferase PRMT3. *The EMBO journal* 2000; 19: 3509-3519.
218. Martin JL, McMillan FM. SAM (dependent) I AM: the S-adenosylmethionine-dependent methyltransferase fold. *Current opinion in structural biology* 2002; 12: 783-793.
219. Ingley E, Hemmings BA. Pleckstrin homology (PH) domains in signal transduction. *Journal of cellular biochemistry* 1994; 56: 436-443.
220. Dunker AK, Lawson JD, Brown CJ, Williams RM, Romero P, Oh JS, Oldfield CJ, Campen AM, Ratliff CM, Hipps KW, Ausio J, Nissen MS, Reeves R, Kang C, Kissinger CR, Bailey RW, Griswold MD, Chiu W, Garner EC, Obradovic Z. Intrinsically disordered protein. *Journal of molecular graphics & modelling* 2001; 19: 26-59.
221. Kim D, Lee J, Cheng D, Li J, Carter C, Richie E, Bedford MT. Enzymatic activity is required for the in vivo functions of CARM1. *The Journal of biological chemistry* 2010; 285: 1147-1152.
222. Koh SS, Chen D, Lee YH, Stallcup MR. Synergistic enhancement of nuclear receptor function by p160 coactivators and two coactivators with protein methyltransferase activities. *The Journal of biological chemistry* 2001; 276: 1089-1098.
223. Lee YH, Koh SS, Zhang X, Cheng X, Stallcup MR. Synergy among nuclear receptor coactivators: selective requirement for protein methyltransferase and acetyltransferase activities. *Molecular and cellular biology* 2002; 22: 3621-3632.
224. Pang L, Tian H, Chang N, Yi J, Xue L, Jiang B, Gorospe M, Zhang X, Wang W. Loss of CARM1 is linked to reduced HuR function in replicative senescence. *BMC molecular biology* 2013; 14: 15.
225. Ma H, Baumann CT, Li H, Strahl BD, Rice R, Jelinek MA, Aswad DW, Allis CD, Hager GL, Stallcup MR. Hormone-dependent, CARM1-directed, arginine-specific methylation of histone H3 on a steroid-regulated promoter. *Current biology : CB* 2001; 11: 1981-1985.
226. Yadav N, Cheng D, Richard S, Morel M, Iyer VR, Aldaz CM, Bedford MT. CARM1 promotes adipocyte differentiation by coactivating PPARgamma. *EMBO reports* 2008; 9: 193-198.
227. Zhao X, Benveniste EN. Transcriptional activation of human matrix metalloproteinase-9 gene expression by multiple co-activators. *Journal of molecular biology* 2008; 383: 945-956.
228. Koh SS, Li H, Lee YH, Widelitz RB, Chuong CM, Stallcup MR. Synergistic coactivator function by coactivator-associated arginine methyltransferase (CARM) 1 and beta-catenin with two different classes of DNA-binding transcriptional activators. *The Journal of biological chemistry* 2002; 277: 26031-26035.
229. Covic M, Hassa PO, Sacconi S, Buerki C, Meier NI, Lombardi C, Imhof R, Bedford MT, Natoli G, Hottiger MO. Arginine methyltransferase CARM1 is a promoter-specific regulator of NF-kappaB-dependent gene expression. *The EMBO journal* 2005; 24: 85-96.

230. Schurter BT, Koh SS, Chen D, Bunick GJ, Harp JM, Hanson BL, Henschen-Edman A, Mackay DR, Stallcup MR, Aswad DW. Methylation of histone H3 by coactivator-associated arginine methyltransferase 1. *Biochemistry* 2001; 40: 5747-5756.
231. Daujat S, Bauer UM, Shah V, Turner B, Berger S, Kouzarides T. Crosstalk between CARM1 methylation and CBP acetylation on histone H3. *Current biology : CB* 2002; 12: 2090-2097.
232. Yadav N, Lee J, Kim J, Shen J, Hu MC, Aldaz CM, Bedford MT. Specific protein methylation defects and gene expression perturbations in coactivator-associated arginine methyltransferase 1-deficient mice. *Proceedings of the National Academy of Sciences of the United States of America* 2003; 100: 6464-6468.
233. Xu W, Chen H, Du K, Asahara H, Tini M, Emerson BM, Montminy M, Evans RM. A transcriptional switch mediated by cofactor methylation. *Science* 2001; 294: 2507-2511.
234. Feng Q, Yi P, Wong J, O'Malley BW. Signaling within a coactivator complex: methylation of SRC-3/AIB1 is a molecular switch for complex disassembly. *Molecular and cellular biology* 2006; 26: 7846-7857.
235. Sims RJ, 3rd, Rojas LA, Beck D, Bonasio R, Schuller R, Drury WJ, 3rd, Eick D, Reinberg D. The C-terminal domain of RNA polymerase II is modified by site-specific methylation. *Science* 2011; 332: 99-103.
236. Lee J, Bedford MT. PABP1 identified as an arginine methyltransferase substrate using high-density protein arrays. *EMBO reports* 2002; 3: 268-273.
237. Fujiwara T, Mori Y, Chu DL, Koyama Y, Miyata S, Tanaka H, Yachi K, Kubo T, Yoshikawa H, Tohyama M. CARM1 regulates proliferation of PC12 cells by methylating HuD. *Molecular and cellular biology* 2006; 26: 2273-2285.
238. Reed R. Coupling transcription, splicing and mRNA export. *Current opinion in cell biology* 2003; 15: 326-331.
239. Li H, Park S, Kilburn B, Jelinek MA, Henschen-Edman A, Aswad DW, Stallcup MR, Laird-Offringa IA. Lipopolysaccharide-induced methylation of HuR, an mRNA-stabilizing protein, by CARM1. Coactivator-associated arginine methyltransferase. *The Journal of biological chemistry* 2002; 277: 44623-44630.
240. Calvanese V, Lara E, Suarez-Alvarez B, Abu Dawud R, Vazquez-Chantada M, Martinez-Chantar ML, Embade N, Lopez-Nieva P, Horrillo A, Hmadcha A, Soria B, Piazzolla D, Herranz D, Serrano M, Mato JM, Andrews PW, Lopez-Larrea C, Esteller M, Fraga MF. Sirtuin 1 regulation of developmental genes during differentiation of stem cells. *Proceedings of the National Academy of Sciences of the United States of America* 2010; 107: 13736-13741.
241. Abdelmohsen K, Pullmann R, Jr., Lal A, Kim HH, Galban S, Yang X, Blethrow JD, Walker M, Shubert J, Gillespie DA, Furneaux H, Gorospe M. Phosphorylation of HuR by Chk2 regulates SIRT1 expression. *Molecular cell* 2007; 25: 543-557.
242. Guarente L, Picard F. Calorie restriction--the SIR2 connection. *Cell* 2005; 120: 473-482.
243. Chen QM. Replicative senescence and oxidant-induced premature senescence. Beyond the control of cell cycle checkpoints. *Annals of the New York Academy of Sciences* 2000; 908: 111-125.
244. Feng Q, He B, Jung SY, Song Y, Qin J, Tsai SY, Tsai MJ, O'Malley BW. Biochemical control of CARM1 enzymatic activity by phosphorylation. *The Journal of biological chemistry* 2009; 284: 36167-36174.
245. Higashimoto K, Kuhn P, Desai D, Cheng X, Xu W. Phosphorylation-mediated inactivation of coactivator-associated arginine methyltransferase 1. *Proceedings of the National Academy of Sciences of the United States of America* 2007; 104: 12318-12323.
246. Carascossa S, Dudek P, Cenni B, Briand PA, Picard D. CARM1 mediates the ligand-independent and tamoxifen-resistant activation of the estrogen receptor alpha by cAMP. *Genes & development* 2010; 24: 708-719.

247. Kuhn P, Xu Q, Cline E, Zhang D, Ge Y, Xu W. Delineating *Anopheles gambiae* coactivator associated arginine methyltransferase 1 automethylation using top-down high resolution tandem mass spectrometry. *Protein science : a publication of the Protein Society* 2009; 18: 1272-1280.
248. Kuhn P, Chumanov R, Wang Y, Ge Y, Burgess RR, Xu W. Automethylation of CARM1 allows coupling of transcription and mRNA splicing. *Nucleic acids research* 2011; 39: 2717-2726.
249. Wang L, Charoensuksai P, Watson NJ, Wang X, Zhao Z, Coriano CG, Kerr LR, Xu W. CARM1 automethylation is controlled at the level of alternative splicing. *Nucleic acids research* 2013; 41: 6870-6880.
250. Ito T, Yadav N, Lee J, Furumatsu T, Yamashita S, Yoshida K, Taniguchi N, Hashimoto M, Tsuchiya M, Ozaki T, Lotz M, Bedford MT, Asahara H. Arginine methyltransferase CARM1/PRMT4 regulates endochondral ossification. *BMC developmental biology* 2009; 9: 47.
251. O'Brien KB, Alberich-Jorda M, Yadav N, Kocher O, Diruscio A, Ebralidze A, Levantini E, Sng NJ, Bhasin M, Caron T, Kim D, Steidl U, Huang G, Halmos B, Rodig SJ, Bedford MT, Tenen DG, Kobayashi S. CARM1 is required for proper control of proliferation and differentiation of pulmonary epithelial cells. *Development* 2010; 137: 2147-2156.
252. El Messaoudi S, Fabbriozio E, Rodriguez C, Chuchana P, Fauquier L, Cheng D, Theillet C, Vandel L, Bedford MT, Sardet C. Coactivator-associated arginine methyltransferase 1 (CARM1) is a positive regulator of the Cyclin E1 gene. *Proceedings of the National Academy of Sciences of the United States of America* 2006; 103: 13351-13356.
253. Mann M, Cortez V, Vadlamudi R. PELP1 oncogenic functions involve CARM1 regulation. *Carcinogenesis* 2013; 34: 1468-1475.
254. Hong H, Kao C, Jeng MH, Eble JN, Koch MO, Gardner TA, Zhang S, Li L, Pan CX, Hu Z, MacLennan GT, Cheng L. Aberrant expression of CARM1, a transcriptional coactivator of androgen receptor, in the development of prostate carcinoma and androgen-independent status. *Cancer* 2004; 101: 83-89.
255. Majumder S, Liu Y, Ford OH, 3rd, Mohler JL, Whang YE. Involvement of arginine methyltransferase CARM1 in androgen receptor function and prostate cancer cell viability. *The Prostate* 2006; 66: 1292-1301.
256. Naeem H, Cheng D, Zhao Q, Underhill C, Tini M, Bedford MT, Torchia J. The activity and stability of the transcriptional coactivator p/CIP/SRC-3 are regulated by CARM1-dependent methylation. *Molecular and cellular biology* 2007; 27: 120-134.
257. Ou CY, LaBonte MJ, Manegold PC, So AY, Ianculescu I, Gerke DS, Yamamoto KR, Ladner RD, Kahn M, Kim JH, Stallcup MR. A coactivator role of CARM1 in the dysregulation of beta-catenin activity in colorectal cancer cell growth and gene expression. *Molecular cancer research : MCR* 2011; 9: 660-670.
258. Kim YR, Lee BK, Park RY, Nguyen NT, Bae JA, Kwon DD, Jung C. Differential CARM1 expression in prostate and colorectal cancers. *BMC cancer* 2010; 10: 197.
259. Elakoum R, Gauchotte G, Oussalah A, Wissler MP, Clement-Duchene C, Vignaud JM, Gueant JL, Namour F. CARM1 and PRMT1 are dysregulated in lung cancer without hierarchical features. *Biochimie* 2014; 97: 210-218.
260. Zakrzewicz D, Zakrzewicz A, Preissner KT, Markart P, Wygrecka M. Protein Arginine Methyltransferases (PRMTs): promising targets for the treatment of pulmonary disorders. *International journal of molecular sciences* 2012; 13: 12383-12400.
261. Kim J, Lee J, Yadav N, Wu Q, Carter C, Richard S, Richie E, Bedford MT. Loss of CARM1 results in hypomethylation of thymocyte cyclic AMP-regulated phosphoprotein and deregulated early T cell development. *The Journal of biological chemistry* 2004; 279: 25339-25344.
262. Li J, Zhao Z, Carter C, Ehrlich LI, Bedford MT, Richie ER. Coactivator-associated arginine methyltransferase 1 regulates fetal hematopoiesis and thymocyte development. *Journal of immunology* 2013; 190: 597-604.

263. Lim Y, Lee E, Lee J, Oh S, Kim S. Down-regulation of asymmetric arginine methylation during replicative and H₂O₂-induced premature senescence in WI-38 human diploid fibroblasts. *Journal of biochemistry* 2008; 144: 523-529.
264. Hong E, Lim Y, Lee E, Oh M, Kwon D. Tissue-specific and age-dependent expression of protein arginine methyltransferases (PRMTs) in male rat tissues. *Biogerontology* 2012; 13: 329-336.
265. Vallance P, Leiper J. Cardiovascular biology of the asymmetric dimethylarginine:dimethylarginine dimethylaminohydrolase pathway. *Arteriosclerosis, thrombosis, and vascular biology* 2004; 24: 1023-1030.
266. Teerlink T, Nijveldt RJ, de Jong S, van Leeuwen PA. Determination of arginine, asymmetric dimethylarginine, and symmetric dimethylarginine in human plasma and other biological samples by high-performance liquid chromatography. *Analytical biochemistry* 2002; 303: 131-137.
267. Boger RH. Asymmetric dimethylarginine (ADMA) and cardiovascular disease: insights from prospective clinical trials. *Vascular medicine* 2005; 10 Suppl 1: S19-25.
268. Zakrzewicz D, Eickelberg O. From arginine methylation to ADMA: a novel mechanism with therapeutic potential in chronic lung diseases. *BMC pulmonary medicine* 2009; 9: 5.
269. Brindicci C, Kharitonov SA, Ito M, Elliott MW, Hogg JC, Barnes PJ, Ito K. Nitric oxide synthase isoenzyme expression and activity in peripheral lung tissue of patients with chronic obstructive pulmonary disease. *American journal of respiratory and critical care medicine* 2010; 181: 21-30.
270. Vallance P, Leone A, Calver A, Collier J, Moncada S. Accumulation of an endogenous inhibitor of nitric oxide synthesis in chronic renal failure. *Lancet* 1992; 339: 572-575.
271. Eid HM, Arnesen H, Hjerkin EM, Lyberg T, Seljeflot I. Relationship between obesity, smoking, and the endogenous nitric oxide synthase inhibitor, asymmetric dimethylarginine. *Metabolism: clinical and experimental* 2004; 53: 1574-1579.
272. Maas R, Schulze F, Baumert J, Lowel H, Hamraz K, Schwedhelm E, Koenig W, Boger RH. Asymmetric dimethylarginine, smoking, and risk of coronary heart disease in apparently healthy men: prospective analysis from the population-based Monitoring of Trends and Determinants in Cardiovascular Disease/Kooperative Gesundheitsforschung in der Region Augsburg study and experimental data. *Clinical chemistry* 2007; 53: 693-701.
273. Zhang WZ, Venardos K, Chin-Dusting J, Kaye DM. Adverse effects of cigarette smoke on NO bioavailability: role of arginine metabolism and oxidative stress. *Hypertension* 2006; 48: 278-285.
274. Bulau P, Zakrzewicz D, Kitowska K, Leiper J, Gunther A, Grimminger F, Eickelberg O. Analysis of methylarginine metabolism in the cardiovascular system identifies the lung as a major source of ADMA. *American journal of physiology Lung cellular and molecular physiology* 2007; 292: L18-24.
275. Stoner GD, Kikkawa Y, Kniazeff AJ, Miyai K, Wagner RM. Clonal isolation of epithelial cells from mouse lung adenoma. *Cancer research* 1975; 35: 2177-2185.
276. Furukawa A, Tada-Oikawa S, Kawanishi S, Oikawa S. H₂O₂ accelerates cellular senescence by accumulation of acetylated p53 via decrease in the function of SIRT1 by NAD⁺ depletion. *Cellular physiology and biochemistry : international journal of experimental cellular physiology, biochemistry, and pharmacology* 2007; 20: 45-54.
277. Lucey EC, Goldstein RH, Stone PJ, Snider GL. Remodeling of alveolar walls after elastase treatment of hamsters. Results of elastin and collagen mRNA in situ hybridization. *American Journal of Respiratory Cell and Molecular Biology*.1998 Aug;158(2):555-64.
278. Konigshoff M, Wilhelm A, Jahn A, Sedding D, Amarie OV, Eul B, Seeger W, Fink L, Gunther A, Eickelberg O, Rose F. The angiotensin II receptor 2 is expressed and mediates angiotensin II signaling in lung fibrosis. *American journal of respiratory cell and molecular biology* 2007; 37: 640-650.

279. Tsuji T, Aoshiba K, Nagai A. Alveolar cell senescence exacerbates pulmonary inflammation in patients with chronic obstructive pulmonary disease. *Respiration; international review of thoracic diseases* 2010; 80: 59-70.
280. Tuder RM, Yoshida T, Fijalkowka I, Biswal S, Petrache I. Role of lung maintenance program in the heterogeneity of lung destruction in emphysema. *Proceedings of the American Thoracic Society* 2006; 3: 673-679.
281. Witherden IR, Vanden Bon EJ, Goldstraw P, Ratcliffe C, Pastorino U, Tetley TD. Primary human alveolar type II epithelial cell chemokine release: effects of cigarette smoke and neutrophil elastase. *American journal of respiratory cell and molecular biology* 2004; 30: 500-509.
282. Aoshiba K, Nagai A. Oxidative stress, cell death, and other damage to alveolar epithelial cells induced by cigarette smoke. *Tobacco induced diseases* 2003; 1: 219-226.
283. Rennard SI, Togo S, Holz O. Cigarette smoke inhibits alveolar repair: a mechanism for the development of emphysema. *Proceedings of the American Thoracic Society* 2006; 3: 703-708.
284. Ito K, Barnes PJ. COPD as a disease of accelerated lung aging. *Chest* 2009; 135: 173-180.
285. Morla M, Busquets X, Pons J, Sauleda J, MacNee W, Agusti AG. Telomere shortening in smokers with and without COPD. *The European respiratory journal* 2006; 27: 525-528.
286. Savale L, Chaouat A, Bastuji-Garin S, Marcos E, Boyer L, Maitre B, Sarni M, Housset B, Weitzenblum E, Matrat M, Le Corvoisier P, Rideau D, Boczkowski J, Dubois-Rande JL, Chouaid C, Adnot S. Shortened telomeres in circulating leukocytes of patients with chronic obstructive pulmonary disease. *American journal of respiratory and critical care medicine* 2009; 179: 566-571.
287. Campisi J, Andersen JK, Kapahi P, Melov S. Cellular senescence: a link between cancer and age-related degenerative disease? *Seminars in cancer biology* 2011; 21: 354-359.
288. Sato T, Seyama K, Sato Y, Mori H, Souma S, Akiyoshi T, Kodama Y, Mori T, Goto S, Takahashi K, Fukuchi Y, Maruyama N, Ishigami A. Senescence marker protein-30 protects mice lungs from oxidative stress, aging, and smoking. *American journal of respiratory and critical care medicine* 2006; 174: 530-537.
289. Campisi J. Senescent cells, tumor suppression, and organismal aging: good citizens, bad neighbors. *Cell* 2005; 120: 513-522.
290. Campisi J, d'Adda di Fagagna F. Cellular senescence: when bad things happen to good cells. *Nature reviews Molecular cell biology* 2007; 8: 729-740.
291. Freund A, Orjalo AV, Desprez PY, Campisi J. Inflammatory networks during cellular senescence: causes and consequences. *Trends in molecular medicine* 2010; 16: 238-246.
292. Wright JL, Churg A. Animal models of COPD: Barriers, successes, and challenges. *Pulmonary pharmacology & therapeutics* 2008; 21: 696-698.
293. Rabe KF1, Hurd S, Anzueto A, Barnes PJ, Buist SA, Calverley P, Fukuchi Y, Jenkins C, Rodriguez-Roisin R, van Weel C, Zielinski J; Global Initiative for Chronic Obstructive Lung Disease. Global strategy for the diagnosis, management, and prevention of chronic obstructive pulmonary disease: GOLD executive summary. *American Journal of Respiratory and Critical Care Medicine*. 2007 Sep 15;176(6):532-55.
294. Brusselle GG. Matrix metalloproteinase 12, asthma, and COPD. *The New England journal of medicine* 2009; 361: 2664-2665.
295. Willemse BW, ten Hacken NH, Rutgers B, Lesman-Leegte IG, Postma DS, Timens W. Effect of 1-year smoking cessation on airway inflammation in COPD and asymptomatic smokers. *The European respiratory journal* 2005; 26: 835-845.
296. Jobse BN, McCurry CA, Morissette MC, Rhem RG, Stampfli MR, Labiris NR. Impact of inflammation, emphysema, and smoking cessation on V/Q in mouse models of lung obstruction. *Respiratory research* 2014; 15: 42.

297. Nakamaru Y, Vuppusetty C, Wada H, Milne JC, Ito M, Rossios C, Elliot M, Hogg J, Kharitonov S, Goto H, Bemis JE, Elliott P, Barnes PJ, Ito K. A protein deacetylase SIRT1 is a negative regulator of metalloproteinase-9. *FASEB journal : official publication of the Federation of American Societies for Experimental Biology* 2009; 23: 2810-2819.
298. Sasaki T, Maier B, Bartke A, Scrable H. Progressive loss of SIRT1 with cell cycle withdrawal. *Aging cell* 2006; 5: 413-422.
299. Arunachalam G, Yao H, Sundar IK, Caito S, Rahman I. SIRT1 regulates oxidant- and cigarette smoke-induced eNOS acetylation in endothelial cells: Role of resveratrol. *Biochemical and biophysical research communications* 2010; 393: 66-72.
300. Chang BD, Watanabe K, Broude EV, Fang J, Poole JC, Kalinichenko TV, Roninson IB. Effects of p21Waf1/Cip1/Sdi1 on cellular gene expression: implications for carcinogenesis, senescence, and age-related diseases. *Proceedings of the National Academy of Sciences of the United States of America* 2000; 97: 4291-4296.
301. Wang W, Furneaux H, Cheng H, Caldwell MC, Hutter D, Liu Y, Holbrook N, Gorospe M. HuR regulates p21 mRNA stabilization by UV light. *Molecular and cellular biology* 2000; 20: 760-769.
302. Mondal AM, Horikawa I, Pine SR, Fujita K, Morgan KM, Vera E, Mazur SJ, Appella E, Vojtesek B, Blasco MA, Lane DP, Harris CC. p53 isoforms regulate aging- and tumor-associated replicative senescence in T lymphocytes. *The Journal of clinical investigation* 2013; 123: 5247-5257.
303. Luo J, Nikolaev AY, Imai S, Chen D, Su F, Shiloh A, Guarente L, Gu W. Negative control of p53 by Sir2alpha promotes cell survival under stress. *Cell* 2001; 107: 137-148.
304. Vaziri H, Dessain SK, Ng Eaton E, Imai SI, Frye RA, Pandita TK, Guarente L, Weinberg RA. hSIR2(SIRT1) functions as an NAD-dependent p53 deacetylase. *Cell* 2001; 107: 149-159.
305. Debacq-Chainiaux F, Erusalimsky JD, Campisi J, Toussaint O. Protocols to detect senescence-associated beta-galactosidase (SA-beta-gal) activity, a biomarker of senescent cells in culture and in vivo. *Nature protocols* 2009; 4: 1798-1806.
306. Nyunoya T, Monick MM, Klingelutz A, Yarovinsky TO, Cagley JR, Hunninghake GW. Cigarette smoke induces cellular senescence. *American journal of respiratory cell and molecular biology* 2006; 35: 681-688.
307. Zhou F, Onizawa S, Nagai A, Aoshiba K. Epithelial cell senescence impairs repair process and exacerbates inflammation after airway injury. *Respiratory research* 2011; 12: 78.
308. Marconett CN, Zhou B, Rieger ME, Selamat SA, Dubourd M, Fang X, Lynch SK, Stueve TR, Siegmund KD, Berman BP, Borok Z, Laird-Offringa IA. Integrated transcriptomic and epigenomic analysis of primary human lung epithelial cell differentiation. *PLoS genetics* 2013; 9: e1003513.
309. Flozak AS, Lam AP, Russell S, Jain M, Peled ON, Sheppard KA, Beri R, Mutlu GM, Budinger GR, Gottardi CJ. Beta-catenin/T-cell factor signaling is activated during lung injury and promotes the survival and migration of alveolar epithelial cells. *The Journal of biological chemistry* 2010; 285: 3157-3167.

6. ABBREVIATION

AP	Alkaline phosphatase
ATCC	American type culture collection
AAT	Alpha1-antitrypsin
ATI	Alveolar epithelial type I
ATII	Alveolar epithelial type II
ANOVA	One-way analysis of variance
BAL	Bronchoalveolar lavage
cDNA	Complementary DNA
COPD	Chronic obstructive pulmonary disease
Ct	Cycle threshold
CAST	Computer assisted stereological toolbox
CARM1	Co-activator associated arginine methyltransferase
DNA	Deoxyribonucleic acid
dNTP	Deoxynucleotide triphosphates mix
ELISA	Enzyme-linked immunosorbent assay
HPRT1	hypoxanthine phosphoribosyltransferase 1
PBS	Phosphate buffered saline
kDa	Kilo Dalton
L(p)	Length per point
MCL	Mean chord length
MMPs	Matrix metalloproteinases
mRNA	Messenger RNA
PFA	Paraformaldehyde

PCR	Polymerase chain reaction
pH	Potential of hydrogen
PPE	Porcine pancreatic elastase
PVDF	Polyvinylidene fluoride
WT	Wild type
Het	Heterozygous
RNA	Ribonucleic acid
ROS	Reactive oxygen species
RT	Reverse transcription
Rtase	Reverse transcriptase
SDS	Sodium dodecylsulfate
SP-C	Surfactant protein-C
WHO	World Health Organization
SIRT1	Sirtuin1 (silent mating type information regulation 2 homolog 1)
DAPI	4',6-diamidino-2-phenylindole
ΔC_t	Delta cycle threshold
μg	Microgram
μl	Microlitre
μm	Micrometer
DMF	Dimethylformamide
HIER	Heat Induced Epitope Retrieval
NEA	Non-essential amino acids
VFR	Vulcan fast red
RIPA	Radioimmunoprecipitation assay
TBS	Tris-buffered saline
MEF	Mouse embryonic fibroblast
DMEM	Dulbecco's Modified Eagle's Medium

RPMI medium	Roswell Park Memorial Institute medium
FBS	Fetal bovine serum
BSA	Bovine serum albumin
siRNA	Small interfering RNA
PCNA	Proliferating cell nuclear antigen
Cyc E1	Cyclin E1
FVC	Forced Expiratory Volume
FRC	Functional Residual Capacity
TLC	Total Lung Capacity
Cdyn	Dynamic compliance
BW	Body weight
E	Elastance
H&E	Hematoxylin and eosin
NTC	Non template control
BCA assay	Bicinchoninic acid assay
HRP	Horseradish peroxidase
CSE	Cigarette smoke extract
AdoMet	S-adenosyl-L-methionine
ADMA	Asymmetric ω -NG, NG-dimethylarginine
PRMT	Protein arginine methyltransferases
GAR	Glycine- and arginine-
PGM	Proline-, glycine-, methionine-
MMA	ω -NG-monomethyl arginine
SDMA	symmetric ω -NG, N'G-dimethylarginine
NOS	Nitric oxide synthase

7. APPENDIX

7.1 ACKNOWLEDGEMENT

Firstly, my heartiest gratitude goes to my direct supervisor Dr. Ali Önder Yildirim for his cordial help, relentless support and advice throughout my 4-year long PhD life. I have deep respect and admiration for his great mentoring skill that acted as a driving force for me to carry out my current thesis project.

I would also like to sincerely thank my Doctor Father Prof. Dr. Oliver Eickelberg for his invaluable constructive criticism and encouragements. I want to specially thank Prof. Dr. Heinz Fehrenbach, Division of Experimental Pneumology Research Center Borstel for his patient monitoring of the progress of my work. Last but not least, I am humbly grateful to all of them as they have been a strong support and positive influence on my project by acting as my thesis committee.

I would like to thank Dr. Melanie Königshoff and Prof. Dr. Oliver Eickelberg for providing their support for facilitating few techniques at their labs. I also thank Dr. Gerald Burgstaller and Dr. Kathrin Mutze and for providing expertise in immunofluorescence and isolated ATII cell culture and, respectively.

I would like to cordially thank Dr. Gerrit John-Schuster for his support during the writing and compilation of this thesis. I also acknowledge the input of Dr. Thomas Mark Conlon for his helpful discussions. I express my cordial gratitude for Alexander Bhola for giving me a detail overview and framework at the beginning of this project. I deeply acknowledge the help of my dear fellow lab mates Katrin Hager, Jie Jia and our technician Christine Hollauer.

Lastly, I am grateful to my family and to my husband for all their support and inspiration.

7.2 CURRICULUM VITAE

PERSONAL INFORMATION

Name: Rim Sabrina Jahan Sarker

Date of Birth: 20.08.1986

Country of citizenship: Bangladesh

Home address: 77, Shah Makhdum Road, Uttara- 1230, Dhaka, Bangladesh

Current residence: 70A, Thalkirchner Strasse, Munich-80337, Germany

CONTACT INFORMATION

Phone (office): +880-2-9661900~73, Office Ex- 7816

Phone (personal): +880-1775842162

Email: rim.sabrina@yahoo.com, rim.sarker@helmholtz-muenchen.de

ACADEMIC QUALIFICATION

Lecturer, Department of Genetic Engineering & Biotechnology, University of Dhaka, Dhaka-1000, Bangladesh (Aug 2014-to date)

PhD student, lab: Immunopathology of COPD; supervisor: Dr. Ali Önder Yildirim (Dec 2010-Nov 2014)

DEGREES

Degree	Department	Institution	Passing year	Division/Class/ GPA/percentage
M.Sc.	Genetic Engineering & Biotechnology	University of Dhaka	2010	1st class; Percentage: 73.17%
B.Sc. (Hons.)	Genetic Engineering & Biotechnology	University of Dhaka	2009	1st class; Percentage: 71%
Higher-secondary School Certificate	Science	Viqarunnisa Noon College	2003	Grade: A; GPA: 4.5 out of 5
Secondary School Certificate	Science	Udayan Higher Secondary School	2001	Grade: A; GPA: 4.88 out of 5

AWARDS and HONOURS

- International Trainee Travel Award (1000 \$), American Thoracic Society (ATS) International Conference in San Diego, California, USA, 2014
- Travel grant (1500 €), HELENA-Helmholtz Graduate School Environmental Health, 2012
- Curriculum competition certificate, CPC Research School "Lung Biology and Disease", 2012
- PhD Scholarship, International Graduate Program "Lung Biology and Disease", Comprehensive Pneumology Center, 2010-2014
- Dean's Award, Biological Faculty, University of Dhaka, 2010
- 2nd prize, poster competition at International Symposium on Cancer and Developmental Biology, Dhaka, Bangladesh, 2010
- Duke of Edinburgh Award (DofE), Bronze level 2010
- 1st prize, M.Sc. Thesis Research Fellowship grant, Ministry of Science and Information and Technology (MOSCIT), Government of Bangladesh, 2009
- Post Graduation Scholarship at B.Sc. level, University of Dhaka, Bangladesh, 2009
- Pre Graduation Scholarship at B.Sc. level, University of Dhaka, Bangladesh, 2008
- All Bangladesh Junior Government Scholarship at class VIII, 1998
- Jainul Smriti Scholarship at class VI, 1996
- Jainul Smriti Scholarship at class V, 1995

CONFERENCES

Presentations:

- Annual INSERM-CPC retreat, Fürstfeldbruck, Germany, 2012
- National conference on lung disease, Homburg, Germany, 2011: "**Critical role of bronchial epithelial cells in the pathogenesis of COPD**"

Posters:

- American Thoracic Society (ATS), San Diego, USA, May 16-21, 2014 (to be held). Nominated as the best abstract: Reduced CARM1 expression enhances susceptibility to emphysema by accelerating alveolar senescence
- DZL Annual Meeting, Heidelberg, Germany, 2014
- Annual INSERM-CPC retreat, Tours, France, 2013: Role of CARM1 in regulation of lung epithelial cell repair and regeneration.
- Munich Lung Conference (MLC), 2013

- ERS International Congress, Barcelona, Spain, 2013:
- Munich Lung Conference (MLC), 2012
- Lung Science Conference (LSC), Estoril, Portugal, 2012
- International Symposium on Cancer and Developmental Biology, Dhaka, Bangladesh, 2010: Arsenic-mediated induction of hyperplasia in mice is accompanied by changes in various blood parameters.

ADMINISTRATIVE SKILLS:

- Student representative, CP research school, 2011-12
- Former managing editor of “Biogen”, a magazine published by the Department Genetic Engineering and Biotechnology, University of Dhaka

AFFILIATIONS:

- Trainee member, American Thoracic Society (ATS)
- Life member, Bangladesh Women Scientists' Association
- Member, Young Biotechnologist of Bangladesh (Young BB)
- Member, Genetic Engineering and Biotechnology Club (GEBC) of Department of Genetic Engineering and Biotechnology, University of Dhaka
- University Sports Club (USC) Karate Munich

LANGUAGE SKILL:

- German language course, A1/A2, Helmholtz Zentrum Language Course, 2012
- IELTS Score: Overall Band: **7.5**; Speaking: **8.5**, British Council, Dhaka, 2009
- French language course, Modern Language Institute, University of Dhaka, 2003
- English language course, British Council, Dhaka, 2001
- English language course, British Council, Dhaka, 1998

COMPUTATIONAL SKILLS

Biostatistics (GraphPad Prism, MS Excel)

PERSONAL INTEREST

Writing:

Articles:

- Leather Biotechnology-Prospects in Bangladesh, 2008 (Biogen)
- RNAi: A silent revolution in medical science, 2007 (Biogen)
- The Golden Death of Cancer, 2006 (The Daily Star)

<http://www.thedailystar.net/campus/2006/11/04/mfeature.htm>

- Making Biology Fun and Simple, 2006 (The Daily Star)

<http://www.thedailystar.net/campus/2006/09/01/academic.htm>

- When a Gene Gets Cranky, 2006 (The Daily Independent)

- Waterproof Rice, 2006 (The Daily Independent)

- Nanotech kills the cancer!, 2006 (The Daily Independent)

<http://www.bdnewsarchive.com/news/odetails.php?id=189373>

OTHER ACTIVITIES

Karate: Brown belt; (Honors: Gold Medal, Karate Competition; Bangladesh Karate-Do Renmei, 1997; Silver Medal, Karate Competition; Bangladesh Karate -Do & B.T.A. Competition 1997 All Bangladesh)

7.3 EIDESSTATTLICHE VERSICHERUNG

Sarker, Rim Sabrina Jahan

Name, Vorname

Ich erkläre hiermit an Eides statt,
dass ich die vorliegende Dissertation mit dem Thema

"Role of CARM1 in regulation of alveolar epithelial senescence and emphysema susceptibility"

selbständig verfasst, mich außer der angegebenen keiner weiteren Hilfsmittel bedient und alle Erkenntnisse, die aus dem Schrifttum ganz oder annähernd übernommen sind, als solche kenntlich gemacht und nach ihrer Herkunft unter Bezeichnung der Fundstelle einzeln nachgewiesen habe.

Ich erkläre des Weiteren, dass die hier vorgelegte Dissertation nicht in gleicher oder in ähnlicher Form bei einer anderen Stelle zur Erlangung eines akademischen Grades eingereicht wurde.

Munich, 4.12.2014

Rim Sabrina Jahan Sarker

Ort, Datum

Unterschrift Doktorandin/Doktorand

7.4 LIST of PUBLICATIONS

- **Sarker RS**, John-Schuster G, Bohla A, Mutze K, Burgstaller G, Bedford MT, Königshoff M, Eickelberg O, Yildirim ÖA. Reduced CARM1 expression enhances susceptibility to emphysema by accelerating alveolar senescence. *American Journal of Respiratory Cell and Molecular Biology*, 2015 Apr 23. [Epub ahead of print]. PMID: 25906418.
- Dau T, **Sarker RS**, Yildirim AÖ, Eickelberg O, Jenne DE. Autoprocessing of neutrophil elastase near its active site reduces the efficiency of natural and synthetic elastase inhibitors. *Nature Communications*, 2015 Apr 10;6:6722. PMID: 25857284.
- **Sarker RS**, Ahsan N, Hossain K, Ghosh PK, Ahsan CR, Akhand AA. Reduction of sodium arsenite-mediated adverse effects in mice using dietary supplementation of water hyacinth (*Eichornia crassipes*) root powder. *Avicenna J Med Biotechnol*. 2012 Jul; 4(3):148-54. PMID: 23407303.
- **Sarker RS**, Ahsan N, Akhand AA. Sodium arsenite induced systemic organ damage and changes in various blood parameters in mice. *Dhaka University Journal of Pharmacological Science*, 2012 Dec;11(2):169-172.

7.5 RE-PRINT PERMISSION

Reprinted with permission of the American Thoracic Society. Copyright © 2015 American Thoracic Society.

Author(s): Sarker RS, John-Schuster G, Bohla A, Mutze K, Burgstaller G, Bedford MT, Königshoff M, Eickelberg O, Yildirim AÖ

Year: 2015

Title: CARM1 Regulates Alveolar Epithelial Senescence and Elastase-induced Emphysema Susceptibility

Journal title: American Journal of Respiratory Cell and Molecular Biology

Volume/Pages: Epub ahead of print.

First published online 23 Apr 2015 as DOI:10.1165/rcmb.2014-0216OC

The *American Journal of Respiratory Cell and Molecular Biology* is an official journal of the American Thoracic Society.